Calhoun: The NPS Institutional Archive

DSpace Repository

Theses and Dissertations 1. Thesis and Dissertation Collection, all items

1975

A computer analysis for the determination of electrode voltage losses in magnetohydrodynamic-generator plasmas.

Dolson, Richard Charles

Monterey, California. Naval Postgraduate School

http://hdl.handle.net/10945/20785

This publication is a work of the U.S. Government as defined in Title 17, United States Code, Section 101. Copyright protection is not available for this work in the United States.

Downloaded from NPS Archive: Calhoun

Calhoun is the Naval Postgraduate School's public access digital repository for research materials and institutional publications created by the NPS community. Calhoun is named for Professor of Mathematics Guy K. Calhoun, NPS's first appointed -- and published -- scholarly author.

Dudley Knox Library / Naval Postgraduate School
411 Dyer Road / 1 University Circle
Monterey, California USA 93943

http://www.nps.edu/library

A COMPUTER ANALYSIS FOR THE
DETERMINATION OF ELECTRODE
VOLTAGE LOSSES IN
MAGNETOHYDRO-
DYNAMIC-GENERATOR
PLASMAS

Richard Charles Dolson

DUDLEY KNOX LIBRARY
NAVAL POSTGRADUATE SCHOOL
MONTEREY, CALIFORNIA 93940

NAVAL POSTGRADUATE SCHOOL
Monterey, California

THESIS

A COMPUTER ANALYSIS FOR THE DETERMINATION
OF ELECTRODE VOLTAGE LOSSES
IN MAGNETOHYDRODYNAMIC-GENERATOR PLASMAS

by

Richard Charles Dolson

December 1975

Thesis Advisor: O. Biblarz

Approved for public release; distribution unlimited.

T170837

REPORT DOCUMENTATION PAGE		READ INSTRUCTIONS BEFORE COMPLETING FORM
1. REPORT NUMBER	2. GOVT ACCESSION NO.	3. RECIPIENT'S CATALOG NUMBER
4. TITLE (and Subtitle) A Computer Analysis for the Determination of Electrode Voltage Losses in Magnetohydrodynamic-Generator Plasmas		5. TYPE OF REPORT & PERIOD COVERED Ph.D. Dissertation; December 1975
		6. PERFORMING ORG. REPORT NUMBER
7. AUTHOR(s) Richard Charles Dolson		8. CONTRACT OR GRANT NUMBER(s)
9. PERFORMING ORGANIZATION NAME AND ADDRESS Naval Postgraduate School Monterey, California 93940		10. PROGRAM ELEMENT, PROJECT, TASK AREA & WORK UNIT NUMBERS
11. CONTROLLING OFFICE NAME AND ADDRESS Naval Postgraduate School Monterey, California 93940		12. REPORT DATE December 1975
		13. NUMBER OF PAGES 150
14. MONITORING AGENCY NAME & ADDRESS(if different from Controlling Office)		15. SECURITY CLASS. (of this report) Unclassified
		15a. DECLASSIFICATION/DOWNGRADING SCHEDULE

16. DISTRIBUTION STATEMENT (of this Report)

Approved for public release; distribution unlimited.

17. DISTRIBUTION STATEMENT (of the abstract entered in Block 20, if different from Report)

18. SUPPLEMENTARY NOTES

Supported in part by the Air Force Office of Scientific Research

19. KEY WORDS (Continue on reverse side if necessary and identify by block number)

Plasmas	Anodes
Magnetohydrodynamics	Conducting Gases
Electrodes	Plasma Sheath

20. ABSTRACT (Continue on reverse side if necessary and identify by block number)

This work investigates the nature and extent of the voltage drops in the vicinity of MHD non-emitting electrodes, especially the losses attributable to the sheath. The non-existence of a one-dimensional sheath solution is proved and a computer model with two-dimensional, periodic active sites representing a flat plate electrode is developed. The sheath and ambipolar regions evolve from the same set of equations in

(20. ABSTRACT Continued)

a self-consistent way, obviating the requirement to match boundary conditions between the regions. With this model the effects of a magnetic field and Joule heating are studied. Results are compared with experimental observations. To supplement the sheath investigation a peripheral study of the boundary layer voltage losses has been made and a relatively simple technique for determining these losses is presented.

A Computer Analysis for the Determination of Electrode Voltage Losses in Magnetohydrodynamic-Generator Plasmas

by

Richard Charles Dolson
Lieutenant, United States Navy
B.S., Purdue University, 1966
M.S., Naval Postgraduate School, 1973

Submitted in partial fulfillment of the
requirements for the degree of

DOCTOR OF PHILOSOPHY

from the
NAVAL POSTGRADUATE SCHOOL
December 1975

DUDLEY KNOX LIBRARY
NAVAL POSTGRADUATE SCHOOL
MONTEREY, CALIFORNIA 93940

ABSTRACT

This work investigates the nature and extent of the voltage drops in the vicinity of MHD non-emitting electrodes, especially the losses attributable to the sheath. The non-existence of a one-dimensional sheath solution is proved and a computer model with two-dimensional, periodic active sites representing a flat plate electrode is developed. The sheath and ambipolar regions evclve from the same set of equations in a self-consistent way, obviating the requirement to match boundary conditions between the regions. With this model the effects of a magnetic field and Joule heating are studied. Results are compared with experimental observations. To supplement the sheath investigation a peripheral study of the boundary layer voltage losses has been made and a relatively simple technique for determining these losses is presented.

TABLE OF CONTENTS

I. INTRODUCTION.............................. 16

A. BACKGROUND.............................. 16

B. REVIEW OF PREVIOUS WORK.................. 18

C. PHYSICAL MODELING........................ 20

D. OBJECTIVES OF THE PRESENT WORK........... 22

E. ORGANIZATION............................. 24

II. ANALYSIS OF THE SHEATH AND AMBIPOLAR REGIONS. 25

A. THE SHEATH ENVIRONMENT................... 25

B. CONTROLLING EQUATIONS.................... 26

1. Basic Equations....................... 26

2. Non-Dimensional Parameters........... 28

3. Poisson's Equation.................... 29

4. Energy Equation....................... 29

5. Species Equations with Magnetic Field Effects and Negligible Joule Heating.... 32

6. Species Equations with Non-Constant Electron Temperature.................... 34

C. BOUNDARY CONDITIONS...................... 34

III. METHOD OF SOLUTION......................... 39

A. INTRODUCTION............................. 39

B. NON-LINEARITY CONSIDERATIONS............. 39

C. GRID SIZE AND COMPUTATIONAL SEQUENCE..... 40

D. CONTROLLING EQUATIONS.................... 42

E. BOUNDARY CONDITIONS........................ 43

F. EVOLUTION OF THE MODEL AND PRIOR ATTEMPTS. 45

IV. RESULTS................................. 48

A. PROCEDURE AND CONVERGENCE CRITERIA....... 48

B. NEGLIGIBLE JOULE HEATING AND NO MAGNETIC FIELD.................................... 49

1. Potential Distributions............... 58

2. Charged Particle Distributions....... 59

C. NON-CONSTANT ELECTRON TEMPERATURE........ 60

D. EFFECT OF EQUILIBRIUM DENSITY............ 63

E. EFFECT OF THE NUMBER OF ELEMENTS IN THE ARRAY AND ELECTRODE POSITIONING.......... 66

F. MAGNETIC FIELD EFFECTS................... 68

G. CURRENT PROFILES......................... 77

V. CONCLUSIONS AND RECOMMENDATIONS............... 84

A. PHYSICAL CONCLUSIONS..................... 84

1. Sheath Formation and Charge Density Profiles................................ 85

2. Current Density Distributions........ 86

3. Comparisons With Experiment.......... 89

B. NUMERICAL CONCLUSIONS.................... 91

C. RECOMMENDATIONS FOR FURTHER STUDY........ 92

APPENDIX A. A SIMPLIFIED TECHNIQUE FOR DETERMINING THE BOUNDARY LAYER VOLTAGE DROP IN MHD GENERATORS........................... 94

APPENDIX B. PROOF OF THE NON-EXISTENCE OF A ONE-DIMENSIONAL SHEATH SOLUTION............. 110

APPENDIX C. DIMENSIONAL AND FRACTIONAL ANALYSES OF THE SHEATH EQUATIONS...................... 113

COMPUTER PROGRAMS.............................. 120

BIBLIOGRAPHY................................... 145

INITIAL DISTRIBUTION LIST...................... 149

LIST OF FIGURES

Figure No. Title Page

1. Anode Model with Periodic Current Constriction Nodes.... 23
2. Arrangement of Electrodes and Boundary Conditions for Computational Array.... 38
3. Potential and Charge Density Profile, $\hat{\phi}=5.80$, $\gamma=0$, $\beta=0$, $\hat{n}=10^{-3}$, array size=500L, 51x51 grid... 50
4. Potential and Charge Density Profile, $\hat{\phi}=17.4$, $\gamma=0$, $\beta=0$, $\hat{n}=10^{-3}$, array size=500L, 51x51 grid... 50
5. Potential and Charge Density Profile, $\hat{\phi}=29.0$, $\gamma=0$, $\beta=0$, $\hat{n}=10^{-3}$, array size=500L, 51x51 grid... 51
6. Potential Contour Plot, $\hat{\phi}=5.80$, $\gamma=0$, $\beta=0$, $\hat{n}=10^{-3}$, array size=500L, 51x51 grid.... 51
7. Potential Contour Plot, $\hat{\phi}=17.4$, $\gamma=0$, $\beta=0$, $\hat{n}=10^{-3}$, array size=500L, 51x51 grid.... 52
8. Potential Contour Plot, $\hat{\phi}=29.0$, $\gamma=0$, $\beta=0$, $\hat{n}=10^{-3}$, array size=500L, 51x51 grid.... 52
9. Electron Density Contour Plot, $\hat{\phi}=5.80$, $\gamma=0$, $\beta=0$, $\hat{n}=10^{-3}$, array size=500L, 51x51 grid.... 53
10. Electron Density Contour Plot, $\hat{\phi}=17.4$, $\gamma=0$, $\beta=0$, $\hat{n}=10^{-3}$, array size=500L, 51x51 grid.... 53
11. Electron Density Contour Plot, $\hat{\phi}=29.0$, $\gamma=0$, $\beta=0$, $\hat{n}=10^{-3}$, array size=500L, 51x51 grid.... 54
12. Ion Density Contour Plot, $\hat{\phi}=5.80$, $\gamma=0$, $\beta=0$, $\hat{n}=10^{-3}$, array size=500L, 51x51 grid.... 54
13. Ion Density Contour Plot, $\hat{\phi}=17.4$, $\gamma=0$, $\beta=0$, $\hat{n}=10^{-3}$, array size=500L, 51x51 grid.... 55
14. Ion Density Contour Plot, $\hat{\phi}=29.0$, $\gamma=0$, $\beta=0$, $\hat{n}=10^{-3}$, array size=500L, 51x51 grid.... 55
15. Potential and Charge Density Profile, $\hat{\phi}=29.0$, $\gamma=0$, $\beta=0$, $\hat{n}=10^{-3}$, array size=1000L, 51x51 grid.. 56
16. Potential Contour Plot, $\hat{\phi}=29.0$, $\gamma=0$, $\beta=0$, $\hat{n}=10^{-3}$, array size=1000L, 51x51 grid.... 56

17. Electron Density Contour Plot, $\hat{\phi}$=29.0, γ=0, β=0, $\hat{n}=10^{-3}$, array size=1000L, 51x51 grid............ 57

18. Ion Density Contour Plot, $\hat{\phi}$=29.0, γ=0, β=0, $\hat{n}=10^{-3}$, array size=1000L, 51x51 grid............ 57

19. Potential and Charge Density Profile, $\hat{\phi}$=5.80, γ=100, β=0, $\hat{n}=10^{-3}$, array size=500L, 51x51 grid.. 61

20. Potential Contour Plot, $\hat{\phi}$=5.80, γ=100, β=0, $\hat{n}=10^{-3}$, array size=500L, 51x51 grid............. 61

21. Potential and Charge Density Profile, $\hat{\phi}$=29.0, γ=100, β=0, $\hat{n}=10^{-3}$, array size=500L, 51x51 grid.. 62

22. Potential Contour Plot, $\hat{\phi}$=29.0, γ=100, β=0, $\hat{n}=10^{-3}$, array size=500L, 51x51 grid............. 62

23. Potential and Charge Density Profile, $\hat{\phi}$=5.80, γ=1000, β=0, $\hat{n}=10^{-3}$, array size=500L, 51x51 grid.. 64

24. Potential Contour Plot, $\hat{\phi}$=5.80, γ=1000, β=0, $\hat{n}=10^{-3}$, array size=500L, 51x51 grid............. 64

25. Electron Temperature Profile, $\hat{\phi}$=5.80, γ=100, β=0, $\hat{n}=10^{-3}$, array size=500L, 51x51 grid............. 65

26. Potential and Charge Density Profile, $\hat{\phi}$=5.80, γ=0, β=0, $\hat{n}$=1, array size=25L, 51x51 grid....... 67

27. Potential and Charge Density Profile, $\hat{\phi}$=17.4, γ=0, β=0, $\hat{n}$=1, array size=25L, 51x51 grid....... 67

28. Potential and Charge Density Profile, $\hat{\phi}$=11.6, γ=0, β=0, $\hat{n}$=1, array size=20L, 41x41 grid....... 69

29. Potential and Charge Density Profile, $\hat{\phi}$=11.6, γ=0, β=0, $\hat{n}$=1, array size=25L, 41x41 grid....... 69

30. Potential and Charge Density Profile, $\hat{\phi}$=11.6, γ=0, β=0, $\hat{n}$=1, array size=35L, 41x41 grid....... 70

31. Potential Contour Plot, $\hat{\phi}$=29.0, γ=0, β=0, $\hat{n}$=1, array size=50L, 41x41 grid........................ 70

32. Space Charge Plot ($\hat{n}_i-\hat{n}_e$) for multiple electrodes, $\hat{\phi}$=29.0, γ=0, β=0, $\hat{n}$=1, array size=50L, 41x41 grid............................ 71

33. Total Charge Plot ($\hat{n}_i+\hat{n}_e$) for multiple electrodes, $\hat{\phi}$=29.0, γ=0, β=0, $\hat{n}$=1, array size=50L, 41x41 grid.................................. 71

34. Potential and Charge Density Profile, $\hat{\phi}$=5.80, γ=0, β=1, $\hat{n}$=10^{-3}, array size=500L, 51x51 grid... 72

35. Potential Contour Plot, $\hat{\phi}$=5.80, γ=0, β=1, $\hat{n}$=10^{-3}, array size=500L, 51x51 grid........................ 72

36. Electron Density Contour Plot, $\hat{\phi}$=5.80, γ=0, β=1, $\hat{n}$=10^{-3}, array size=500L, 51x51 grid............. 73

37. Ion Density Contour Plot, $\hat{\phi}$=5.80, γ=0, β=1, $\hat{n}$=10^{-3}, array size=500L, 51x51 grid............. 73

38. Potential and Charge Density Profile, $\hat{\phi}$=29.0, γ=0, β=1, $\hat{n}$=10^{-3}, array size=500L, 51x51 grid... 74

39. Potential Contour Plot, $\hat{\phi}$=29.0, γ=0, β=1, $\hat{n}$=10^{-3}, array size=500L, 51x51 grid........................ 74

40. Electron Density Contour Plot, $\hat{\phi}$=29.0, γ=0, β=1, $\hat{n}$=10^{-3}, array size=500L, 51x51 grid............. 75

41. Ion Density Contour Plot, $\hat{\phi}$=29.0, γ=0, β=1, $\hat{n}$=10^{-3}, array size=500L, 51x51 grid............. 75

42. Potential and Charge Density Profile, $\hat{\phi}$=5.80, γ=0, β=2, $\hat{n}$=1, array size=25L, 51x51 grid....... 76

43. Potential Contour Plot, $\hat{\phi}$=5.80, γ=0, β=2, $\hat{n}$=1, array size=25L, 51x51 grid........................ 76

44. Current Density Contour Plot, $\hat{\phi}$=5.80, γ=0, β=0, $\hat{n}$=10^{-3}, array size=500L, 51x51 grid............. 78

45. Current Density Contour Plot, $\hat{\phi}$=5.80, γ=0, β=1, $\hat{n}$=10^{-3}, array size=500L, 51x51 grid............. 79

46. Current-Voltage Diagram, $\hat{n}$=10^{-3},51x51 grid...... 81

47. Current-Voltage Diagram, $\hat{n}$=1, 41x41 grid........ 82

48. Current-Voltage Diagram, $\hat{n}$=1, 51x51 grid........ 83

APPENDIX A

A.1 Three Representations of Voltage Losses in the MHD Generator.................................... 95

A.2 Conductivity for Stochiometric Mixture of Toluene and Oxygen with Two Percent Cesium Seed at 0.3 Atmospheres.................................... 100

A.3 Effect of Weighting Function on Two Programs for Resistivity of Toluene/Oxygen/Cesium Plasma Using 1/7th-power Law and Varying C_p 102

A.4 Non-dimensional Voltage Drop ϕ Versus Wall Temperature and free Stream Temperature for Cesium Seed, Constant C_p 104

A.5 Non-dimensional Voltage Drop ϕ Versus Wall Temperature and Free Stream Temperature for Cesium Seed, Varying C_p 105

A.6 Observed Transverse Voltage Distributions....... 106

A.7 Sidewall Probe Potential, Core Temperature = 2700°K.. 108

TABLE OF SYMBOLS

A	any variable to be finite-differenced
B	magnetic field
c	average thermal velocity
C	constant defined in Appendix B
C_p	specific heat at constant pressure
D	channel dimension, electrode wall distance
$D_{e,i}$	electron, ion diffusion coefficient
e	electron charge, or exponential
E	electric field
G	G-factor, see Ref. 31
h	specific enthalpy, or grid step size
j	non-dimensional current density
J	current density, conventional direction
k	Boltzmann's constant
ℓ	mean free path
L	characteristic length
L_d	diffusion length
L_j	conduction length
L_r	ionization/recombination length
m	particle mass
n	particle density
N	number of elements across grid
n_o	characteristic charge density
p	pressure
Q	collision cross-section
T	temperature
T_o	characteristic temperature

U	velocity
V	electric potential
w	successive over-relaxation parameter
W	weighting function
x	coordinate
x_k	partial pressure of species k
y	coordinate
y_{cl}	distance from electrode in characteristic lengths L
y_o	critical y-coordinate defined in Appendix B
Z	atomic weight
α	coefficient = $\nu_{es}\delta_s m_e/m_s$, or = $\epsilon_I/2kT_o$
β	Hall parameter
γ	Joule heating parameter defined by Eq. 18
Γ	non-dimensional space charge = $\hat{n}_i-\hat{n}_e$
δ	thermal boundary layer thickness
δ_{es}	energy loss factor
ϵ	error term as defined in Eq. 44
ϵ_I	seed ionization potential
ϵ_o	permittivity of a vaccuum
θ	temperature ratio T_e/T_o, or T/T_o
λ_s	sheath thickness
μ	mobility
ν_{es}	collision frequency
ξ	non-dimensional total charge = $\hat{n}_i+\hat{n}_e$
σ	conductivity
τ_c	convection time
τ_j	conduction time
τ_r	ionization/recombination time

ϕ	electric potential
ϕ_{bl}	non-dimensional boundary layer voltage drop
ψ	defined by Eq. 30

Subscripts and Superscripts

$\hat{}$	non-dimensional term
$\bar{}$	average term
∞	conditions at infinity
bl	boundary layer
c	core value
e	electron
i	ion, or finite difference index
j	finite difference index
k	summation index
n	neutral species
o	characteristic parameter
s	species i or e
Saha	value predicted at Saha equilibrium
w	wall condition
x	flow direction coordinate
y	cross channel coordinate

ACKNOWLEDGEMENTS

The author gratefully acknowledges the help and guidence of my thesis advisor, Professor Oscar Biblarz, without whose kind and expert assistance this work would not be possible. I also wish to thank Professor Robert Ball for his advice and counsel on computer techniques, and Drs. Robert Kessler and Richard Rosa of AVCO Everett Research Laboratory for their contribution to my education in MHD research.

The operators of the IBM 360/67 computer at the Naval Postgraduate School provided me and other students with courteous and professional service including assistance with special problems. It is with deepest gratitude that I cite them by name: Andy Anderson, Kris Butler, Ed Donnellan, Doris Goodwin, Jim Powers, Jimmy Shaffer, Mick Sholley and Duffy Tegtmeier.

Finally, I wish to express my thanks and devotion to my family, Amy, Stacy, and Alice, who, while competing with the computer for my attentions, provided the necessary moral support to complete the job.

This work was supported in part by the Air Force Office of Scientific Research.

I. INTRODUCTION

A. BACKGROUND

A Magnetohydrodynamic (MHD) generator is a device for converting the energy of a flowing gas, or of a liquid metal, directly into electrical energy. As with conventional electrical generators, the conducting medium crosses a magnetic field; however, MHD deals with conducting fluids instead of solid moving parts. Anticipated efficiencies are far above those of conventional generators because of the higher temperatures in the conversion channel. The thermal energy of flowing gases is changed directly to electrical energy, eliminating the mechanical energy step of the conventional generator which means that there are fewer parts to wear out.

Although MHD power generation has been studied for nearly 30 years, financing of MHD research waned in the 1960's. Interest is now being rekindled because of a new "energy consciousness" of government, industry, and the military. MHD offers an attractive alternative energy transformation means which is relevant to the pursuit of clean ways of using the vast coal reserves in the United States and making more efficient use of dwindling petroleum resources. MHD promises to fulfill the requirements for a light-weight, high-power source for military use. For example, the Navy, recognizing its energy requirements and dependency on world fossil-fuel supplies[1], is sponsoring research on practical MHD devices with large power outputs and high efficiencies[2]. The Air Force is interested in power sources for airborn weapons systems.

The basic MHD device consists of a channel through which

ionized gas or liquid metal flows. A magnetic field is imposed perpendicular to the flow direction; as a result, an electric field is induced and power is tapped by means of electrodes. Principal concern is with ionized gas (hereafter refered to as plasma) devices since with these the combustion energy can be more directly changed to electrical power.

A major problem involved in the performance of MHD generators is the high voltage loss in the vicinity of the electrodes. Accurate performance predictions in the design of MHD devices require a realistic determination of these voltage losses. This research investigates the nature of electrode voltage drops and computer models are developed to describe the physical phenomena involved. With the results from this investigation, appropriate steps may be taken to minimize the losses.

The principal voltage loss mechanisms in the MHD generator can be divided into two main classes, ohmic and sheath losses. Ohmic drops are those that occur because of the finite conductivity of a real plasma. Thermal boundary layers, degree and kinetics of ionization, and Joule heating are factors affecting the ohmic resistivity of the plasma. Sheath drops occur as the result of the Debye shielding which forms a non-neutral layer adjacent to the electrode and results in a space charge field. Material problems restrict the temperatures at which the electrodes can operate. In many cases cooling of the electrodes is required since the plasma, in order to maintain a high ionization, must be hotter than the working temperatures of most materials. This temperature difference between the electrodes and the plasma further aggravates the voltage losses because of the presence of the thermal boundary layers. As will be shown, voltages losses can be as much as 50% or more of the total power output, with sheath drops

accounting for a non-negligible fraction of the drop and boundary layer losses the rest.

B. REVIEW OF PREVIOUS WORK

Analyses and experiments on boundary layer phenomena in MHD generators are numerous. It is not the purpose of this work to further add to the literature on the boundary layer losses, but, as will be explained in Part C of this section, this phase of the problem was treated as a necessary appendage to the problem of the sheath drop. Consequently a short review of boundary layer work is presented here: High and Felderman[3] as well as Argyropoulos, Demetriades, and Lackner[4] studied the problem of the turbulent boundary layer and several descriptions of the nature of the temperature field. Doss, Dwyer and Hoffman[5] investigated the boundary layer and used a rudimentary collisionless sheath as an "inside" boundary condition. Kessler and Eustis[6] reported on experiments with electrode temperature effects on turbulent boundary layers, and Rubin and Eustis[7] extended Kessler's work to include the effects of electrode size. Wu et al.[8] and Oliver and Mitchner[9] investigated non-uniformities of current distributions within the boundary layer.

Although the existence of the sheath is well understood, its effects have been investigated to a much lesser extent than those of the boundary layer. This is principally because this loss is described by a relatively complicated set of coupled, non-linear, partial differential equations that present considerable difficulty for numerical solutions. There is no known exact solution for these equations.

Most work on sheath phenomena is embodied in "probe" theory investigations, that is in the mutual effects on a

quiescent plasma which is disturbed by the presence of an electric probe. Such work is relevant to MHD electrodes since the anode is essentially a heavily biased probe in contact with a plasma, which is quiescent within the sheath region (see Part C of this section). The cathode, which is an electron emitter, has some of the same characteristics as the anode, but is more complicated to represent analytically. The description of the cathode will not be attempted here.

Necessary simplifications limit existing probe solutions to special cases as can be seen by sampling the literature regarding plasma probes. Lam[10] solves a sheath problem by matching the boundaries of "inner" and "outer" solutions and discusses their dimensionality. Stahl and Su[11] use the same approach of separating the sheath, ambipolar region and free stream. Additionally, they prove the existence of a sheath on a flat probe. Cohen[12] criticizes this approach of separate regions on mathematical grounds saying that quantities are forced to fit and some derivatives tend to be discontinuous. McKee and Mitchner[13] deal with a collisionless sheath $(\ell \geq \lambda_s)$ but include ionization and recombination in the ambipolar region. Bailey and Touryan[14] investigate a sheath that is large enough to be of the same order of magnitude as the boundary layer, and take advantage of Blasius' similitude co-ordinates to reduce the problem to one dimension.

Several solutions are available for spherical probes including Kiel[15], Barad and Cohen[16], Su and Lam[17], and Cohen[12]. Kiel ignored diffusion while Barad and Cohen neglected ionization and recombination. Su and Lam, and Cohen were the first to use a systematic analysis of probes in collision-dominated plasmas. Lengyel[18], by dropping diffusion, was able to modify the elliptic equations in such

a way as to solve them by the method of characteristics as one might do with hyperbolic equations.

Chung, Talbot, and Touryan[19], in a rather extensive review of probe work, state that no general solution is available for determining charge density and species temperature for probes small relative to boundary layer thicknesses. The work of this thesis may help to fill that void because the model of the anode is that of an array of point or line probes immersed in the non-convective portion of a boundary layer. Results of this work may also be useful to other fields such as arc-discharges and lasers.

C. PHYSICAL MODELING

Both theoretical and experimental results indicate that in the MHD environment, where pressures are near atmospheric, the sheath lies well within the boundary layer (about 10^{-5} m for the sheath thickness or three orders of magnitude less than the boundary layer). Additionally, the sheath is only about one or two orders of magnitude larger than the electron mean-free-path for combustion gases. It becomes apparent then, that convection plays little or no role in the behavior of the sheath other than to modify the gross temperatures encountered near the wall. Consequently, the boundary layer or ohmic problem can be divorced from the sheath and treated separately[20]. The boundary layer, as well as the wall conditions, determines the gas temperature for the sheath region. Thus, the boundary layer voltage drop can be added to the sheath drop to give the total loss due to electrode effects.

As mentioned earlier, analyses of boundary layer effects in MHD have been developed, but they tend to be complicated and difficult to use. In order to have a complete picture

of electrode drops and to assist in interpreting data, a simplified method for determining the voltage drop across a thermal boundary layer has been devised. It has the capability of rendering quick results with little computer space and time. It does not pretend to be a complete analysis, but through appropriate assumptions and simplifications it gives the drop as a function of temperature only. Appendix A gives the details of the method along with its limitations.

An investigation of the nature of the controlling equations for the sheath shows that a one-dimensional solution does not exist except for very special cases. This investigation resulted in the publication of Ref. 21, and a summary of that paper may be found in Appendix B. It provides a basis for many of the assumptions used in this work. The following conclusions which appear in Ref. 21 helped to shape the model chosen for this work: Current density must decrease away from the electrode by whatever means possible. The mechanisms of geometry, current constrictions at the electrode, or ionization/recombination can effect this decrease singly or jointly. A two-dimensional flat plate in the absence of ionization/recombination would be at least partially one-dimensional away from the edges and is therefore not a workable model.

Since previous solutions have been obtained with spherical probes, it appears that a geometrical decrease of current density is a proper means of satisfying the nature of the equations. Chen[22] used ionization/recombination to extract a strictly one-dimensional solution for the sheath. What remains then is to study the features that result from current constrictions at discrete periodic sites rather than uniform current density across the electrode surface.

D. OBJECTIVES OF THE PRESENT WORK

In this work, a two-dimensional, flat plate, non-emitting electrode is modeled. Here, the current has only discrete points through which to flow on the electrode surface (See Fig. 1). These points are assumed to be periodic. The points simulate the current constriction at the electrode which may be there because of temperature irregularities or surface roughness. A collection of these points or nodes might represent the anode spots observed by Biblarz[23] and Kimblin[24]. In a two-dimensional representation the point is actually a "wire" of unit depth. The spacing of the active sites must be greater than the sheath thickness in order to avoid one-dimensional effects, and small enough to be compatible with a two-dimensional computational field. It must be emphasized here that this work does not consider the phenomenon of arc discharge, which is the result of thermal instabilites[25]. Rather it looks at the current constriction required to satisfy continuity of charge, Ohm's law, and Poisson's equation.

The primary objective of this work is to present a mathematical model of a two-dimensional (Cartesian geometry) electrode in a quiescent MHD plasma. The controlling equations are solved for the potential, the current, and the charge density distributions in the vicinity of the electrode. The additional effects of a magnetic field and Joule heating are investigated. It appears that this is the first investigation of the magnetic field within the sheath. The resulting program generates sheath and ambipolar regions in a self-consistent way using the same set of equations throughout the field, obviating the need to match layers. The size of the sheath and the voltage drop attributable to its shielding effects are investigated.

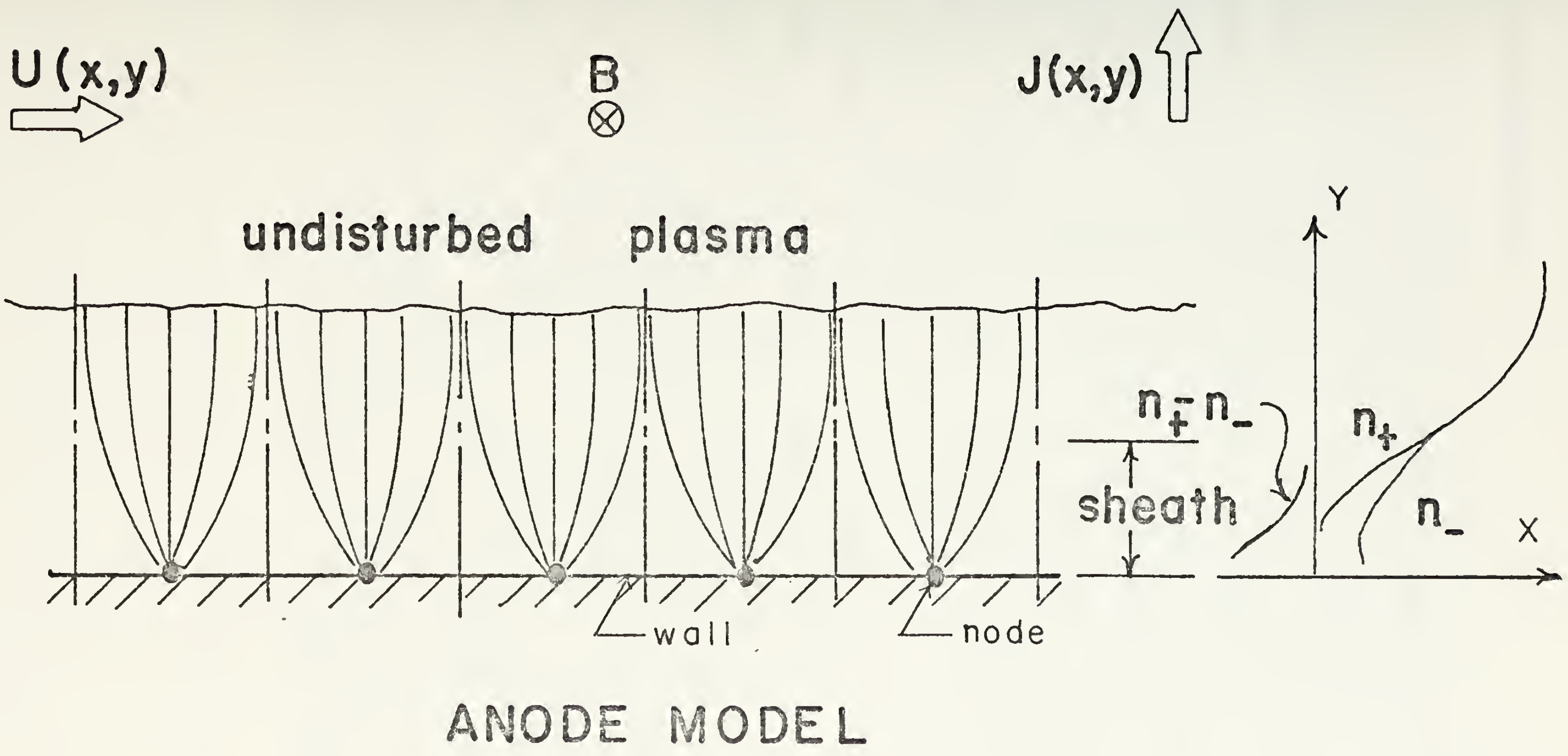

Figure 1. Anode model with periodic current constriction.

E. ORGANIZATION

In Section II the physical concepts and the controlling and boundary equations are developed. The equations are cast into a form for use in the computer in Section III. It includes a description of the numerical methods which produced successful results, as well as a short chronology of techniques that failed to work. A summary of the results of potential and charge distributions, and current and temperature plots for all the cases studied is included in Section IV. Section V lists the conclusions reached from both a physical and numerical point of view and gives examples on the use of the results.

Appendix A shows the technique for determining the boundary layer losses. Appendix B is a condensation of Ref. 21 proving the non-existence of a one-dimensional solution for the limit of the non-reacting flux of charges in a collision-dominated plasma. A dimensional analysis which derives a set of independent non-dimensional variables for the controlling equations is found in Appendix C. Additionally, Appendix C contains a fractional analysis of these and other equations to estimate the significance of certain physical effects. Finally, the computer programs used in this work are included in the section "Computer Programs", with explanations as to their use.

II. ANALYSIS OF THE SHEATH AND AMBIPOLAR REGIONS

A. THE SHEATH ENVIRONMENT

A sheath is a non-neutral region which lies adjacent to the electrode or insulator surface. The strict definition of a plasma requires charge neutrality, thus the sheath is not part of the plasma since a space charge exists. For example, the anode is positive, which means that it attracts electrons and repels positive ions. As the electrons collect at the anode surface, the anode potential is partially shielded from the rest of the plasma by the space-charge potential drop.

Between the sheath and the free stream lies the ambipolar region. As the name implies, it has an equal number of positive and negative charges. In this transition region the electrons are slowed by heavier ions, and strong concentration gradients exist. The electrodes themselves are usually metallic, and may be pins, wires, or flat plates separated by ceramic insulator wall segments (segmented electrodes). The surface of the electrodes, even when highly polished have roughnesses of the order of the sheath thickness, and in addition exchange material with the flowing plasma, further adding to the irregularities. These irregularities increase the tendency for the current to constrict by providing active sites for the current to flow along minimum energy paths.

The size of the sheath in MHD generators is about 10^{-5} m, putting it well within the boundary layer which is about 10^{-2} m. The flow is therefore essentially stagnated in the sheath region. Though the ambipolar region extends further into the boundary layer, a fractional analysis

(Appendix C) on convection shows that the characteristic length for convection in most flows is much greater than the conduction or diffusion lengths within the sheath and ambipolar regions. Consequently, convection may be entirely assigned to the ohmic study of electrode losses (see Appendix A). The boundary layer lies within the undisturbed plasma. That is, it lies beyond the ambipolar region, there is charge neutrality, and electron/ion concentrations are as would be predicted by the Saha equation[26] for plasmas at local equilibrium.

In the model presented here, the following assumptions are made:

1) Steady state,
2) Chemical equilibrium in the boundary layer, but frozen flow in the sheath,
3) No induced magnetic field, i.e., low Magnetic Reynolds number,
4) Negligible ion slip,
5) $J_i << J_e$,
6) No continuum radiation losses in the energy equation,
7) No ion emission, and
8) Neutral and ion particle temperature is T_o, unaffected by Joule heating and uniform within the domain of the sheath.

B. CONTROLLING EQUATIONS

1. Basic Equations

For some MHD plasmas the mean-free-path is small enough that the sheath can be treated as a continuum. A set of collisional equations is then used to describe the sheath, ambipolar, and adjacent free stream regions. No

matching between these regions is necessary since they are generated in a self-consistent way within the computational array. The equations used are a combination of the conservation equations and Maxwell's equations. Specifically, they are expressions of conservation of charge, momentum and energy, as well as Gauss' law.

A special representation of the electron momentum equation is embodied in a generalized Ohm's law and may be written [Ref. 26, p. 363]

$$J_s = -\mu_s n_s e \nabla\phi - \frac{\beta_s}{|B|}(J_s \times B) \pm D_s e \nabla n_s \quad (1)$$

where the + sign applies to the electrons and - is for ions. The first term on the right-hand-side represents conduction, the second is due to the magnetic JXB current and the third term represents diffusion. The term β_s is the Hall parameter and gives the relative effect of the magnetic field in the plasma. The equation for species continuity can be written as

$$\nabla \cdot J_s = \dot{n}_s e \quad (2)$$

Appendix C shows that the characteristic length for ionization/recombination is much larger than the sheath or ambipolar region lengths. Under these conditions Eq. 2 becomes

$$\nabla \cdot J_s = 0 \quad (3)$$

Poisson's equation comes from Gauss' law for the divergence of an electric field and is given in potential form as

$$\nabla^2\phi = -(n_i - n_e)\, e/\varepsilon_o \quad (4)$$

Another equation that will be useful later and which

applies under local equilibrium is the Einstein relation.

$$D_s/\mu_s = kT_s/e \tag{5}$$

Electrons absorb energy at the rate of $J_e \cdot E$ per unit volume from the electric field. Because of their relatively small mass, the electrons are inefficient in transfering energy to the other particles. For that reason much of this energy goes into raising the electron temperature above that of the heavier particles. Collisions with these particles, both elastic and inelastic, tend to limit the energy retained by the electrons. In a quiescent plasma an expression accounting for the electron energy balance is (Ref. 26, p. 240-243)

$$J_e \cdot E = 3n_e k(T_e - T) \sum_s \nu_{es} \frac{\delta_s m_e}{m_s} \tag{6}$$

2. Non-Dimensional Parameters

The non-dimensional parameters developed in Appendix C are repeated here for use in this section.

$$\begin{array}{lll} \hat{n}_i = n_i/n_o & \hat{n}_e = n_e/n_o & \hat{\phi} = \phi/\phi_o \\ \hat{\nabla} = L\nabla & \hat{x} = x/L & \hat{y} = y/L \end{array} \tag{7}$$

where:

$\phi_o = kT_o/e$ $\quad$ $L = e^2/(\varepsilon_o kT_o)$ and $n_o = (kT_o\varepsilon_o/e^2)^3$

T_o is the temperature of the neutral gas which is constant throughout the region of interest, and independent of Joule heating.

Each of the three characteristic parameters ϕ_o, L_o and n_o are functions only of a characteristic energy kT_o. $\hat{n}_e$ now represents a non-dimensional electron charge, or a measure of the deviation from the equilibrium density value in the free stream. $\hat{n}_i$ is a non-dimensional ion charge density, and within the sheath $\hat{n}_i \neq \hat{n}_e$, whereas within the ambipolar region $\hat{n}_e = \hat{n}_i$ and $\hat{n}_e < \hat{n}_{Saha}$ and in the free stream plasma $\hat{n}_e = \hat{n}_i = \hat{n}_{Saha}$. In fact, for purposes of this work, the edge of the sheath will be where $\hat{n}_e$ approaches $\hat{n}_i$ within 1 %, and the edge of the ambipolar region will be where $\hat{n}_e$ approaches $\hat{n}_{Saha}$ within 1%.

3. Poisson's Equation

Using the non-dimensionalizing scheme on Poisson's equation, Eq. 3 becomes

$$\hat{\nabla}^2 \hat{\phi} = \hat{n}_e - \hat{n}_i \qquad (8)$$

4. Energy Equation

Applying the non-dimensional parameters of Eq. 7 to $E = -\nabla\phi$ gives the following result:

$$E = -\frac{(kT_o)^2 \varepsilon_o}{e^3} \hat{\nabla}\hat{\phi} \qquad (9)$$

In the current equation, account must be taken of the effect of varying electron temperature. Since $J_e >> J_i$ the current is essentially an electron current. Neglecting magnetic field effects and using Einstein's relation, the current is written as

$$J_e = -\mu_e e\ [n_e\nabla\phi - \frac{kT_o}{e}\frac{T_e}{T_o}\ \nabla n_e] \qquad (10)$$

With the introduction of a dimensionless temperature, $\theta = T_e/T_o$, the non-dimensionalized current equation becomes

$$J_e = \frac{\mu_e(kT_o)^5\ \varepsilon_o^4}{e^8} \qquad (11)$$

where

$$j = -\hat{n}_e\hat{\nabla}\hat{\phi} + \theta\hat{\nabla}\hat{n}_e \qquad (12)$$

Equation 11 will contain the term $(1+\beta^2)$ in the denominator of the coefficient when magnetic field effects are included. The dot product of Eqs. 9 and 11 yields

$$J_e\cdot E = -\frac{\mu_e(kT_o)^7\varepsilon_o^5}{e^{11}}\ j\cdot\hat{\nabla}\hat{\phi} \qquad (13)$$

Non-dimensionalizing n_e and letting $\alpha = \sum_s \nu_{es}\delta_s\frac{m_e}{m_s}$ in Eq. 6, and introducing Eq. 13 into Eq. 6 results in

$$-\frac{\mu_e(kT_o)^3\varepsilon_o^2}{3\alpha e^5}\ j\cdot\nabla\hat{\phi} = \hat{n}_e(\theta-1) \qquad (14)$$

As the electron temperature increases, the collision frequency with neutral particles increases affecting the terms μ_e and α. Since electron-neutral collisions are by far the most numerous α can be approximated by $\alpha = \nu_{en}\delta_n\frac{m_e}{m_n}$ or

$$\alpha = n_n Q_{en}\delta_n(m_e/m_n)\sqrt{\frac{8kT_o}{\pi m_e}}\ \theta^{1/2} \qquad (15)$$

In the range of interest of the parameters, the collision cross-section changes little with temperature so α depends on $\theta^{1/2}$.

A modification to Compton's equation[27] for small values of E/P gives an electron mobility of the form

$$\mu_e = \frac{e\theta^{-1/2}}{m_e\sqrt{\frac{8kT_o}{\pi m_e}}\;Q_{en}n_n} \tag{16}$$

so that μ_e goes as $\theta^{-1/2}$. Combining Eqs. 14, 15, and 16 and using the perfect gas law results in the form of the energy equation used in this work.

$$\gamma j\cdot\hat{\nabla}\hat{\phi} = -\hat{n}_e(\theta^2-\theta) \tag{17}$$

where

$$\gamma \equiv \frac{0.13(kT_o)^4\,\varepsilon_o^2\,m_n}{p^2Q_{en}^2m_e\delta_n e^4} \tag{18}$$

The value of the coefficient γ appears to dictate the degree of Joule heating in the system. This can best be seen by expanding Eq. 17 and expressing θ implicitely in the form

$$\theta = \frac{(\gamma/\theta)\hat{\nabla}\hat{\phi}\cdot\hat{\nabla}\hat{\phi} + 1}{(\gamma/\theta)\hat{\nabla}\hat{\phi}\cdot\hat{\nabla}\hat{n}_e/\hat{n}_e + 1} \tag{19}$$

For physical reasons it is expected that $\theta \geq 1$. It can be seen from Eq. 19 that for very small values of γ, $\theta \longrightarrow 1$, which is the constant temperature case. Similarly, for γ which is very large, an upper limit for θ is found.

$$\theta = \frac{\hat{n}_e\hat{\nabla}\hat{\phi}\cdot\hat{\nabla}\hat{\phi}}{\hat{\nabla}\hat{\phi}\cdot\hat{\nabla}\hat{n}_e} \quad \text{for} \quad \gamma\rightarrow\infty \tag{20}$$

It is interesting to note that for very large γ, θ becomes independent of γ, which means that it is independent of the chemistry of the plasma.

Now that γ has been described, it will be useful to see what various MHD plasma compositions it represents.

Assuming atmospheric pressure, and the perfect gas law, Eq. 18 can be shown to be

$$\gamma = 10^{-46} \times \frac{T_o^{\,4} Z}{\delta_n Q_{en}^{\,2}} \tag{21}$$

in MKS units where Z is the atomic weight of the principal neutral species, or a mass average of the neutral constituents.

For combustion type gases where the principal constituent might be CO_2, a typical value of γ can be found. From Ref. 26, pages 139 and 148 for a temperature of 1000°K, $Q_{en} = 1.5 \times 10^{-19} m^2$, $\delta_n = 2 \times 10^3$, γ is found to be 98.3. This type of gas has γ values which are low, characteristic of plasmas with high collision cross-sections.

In many inert gas plasmas nitrogen is used to help the plasma reach equilibrium more quickly. The same reference gives typical values of $Q_{es} = 5 \times 10^{-20} m^2$ and $\delta_n = 8$. Then $\gamma = 1.4 \times 10^5$. This is already at the upper limit described by Eq. 20. Even higher values are obtained with argon and cesium seed to the order of 10^9 because of the Ramsauer effect[Ref. 27, p. 31].

5. Species Equations with Magnetic Field Effects and Negligible Joule Heating

When Joule heating is small and collisions between electrons and neutral particles are sufficient for efficient energy exchange, electron temperatures will not differ significantly from the neutrals. Furthermore, ion temperatures will be essentially the same as the neutrals regardless of Joule heating because of their large mass.

That is, the system of equations is stable even when $T_e > T_o$ because it has been assumed that $T_o = T_i$ = a constant which is unaffected by Joule heating. The following expression replaces the energy equation for this case:

$$T_e \cong T_i = T_o \tag{22}$$

Now Eq. 1 is solved for J_x and J_y in a two-dimensional Cartesian system with x and y coordinates.

$$\begin{aligned} J_x = (1+\beta^2)^{-1} \Big[& -\mu_s n_s e \frac{\partial \phi}{\partial x} \pm D_s e \frac{\partial n_s}{\partial x} \\ & - \beta_s \Big(-\mu_s n_s e \frac{\partial \phi}{\partial y} \pm D_s e \frac{\partial n_s}{\partial y} \Big) \Big] \end{aligned} \tag{23}$$

$$\begin{aligned} J_y = (1+\beta^2)^{-1} \Big[& -\mu_s n_s e \frac{\partial \phi}{\partial y} \pm D_s e \frac{\partial n_s}{\partial y} \\ & + \beta_s \Big(-\mu_s n_s e \frac{\partial \phi}{\partial x} \pm D_s e \frac{\partial n_s}{\partial x} \Big) \Big] \end{aligned} \tag{24}$$

Substituting Eqs. 23 and 24 into Eq. 3 and using Eqs. 5 and 22 to help simplify results in

$$-n_s \nabla^2 \phi - \nabla\phi \cdot \nabla n_s \pm (kT_o/e) \nabla^2 n_s + \beta_s \Big(\frac{\partial n_s}{\partial x} \frac{\partial \phi}{\partial y} - \frac{\partial n_s}{\partial y} \frac{\partial \phi}{\partial x} \Big) = 0 \tag{25}$$

Equation 25 represents two equations, one for electrons (+sign) and one for ions (-sign). Now $\beta_i \cong 0$ because of the high ion inertia. Hence the two equations representing species continuity and Ohm's law become

$$-n_e \nabla^2 \phi - \nabla\phi \cdot \nabla n_e + (kT_o/e) \nabla^2 n_e + \beta \Big(\frac{\partial n_e}{\partial x} \frac{\partial \phi}{\partial y} - \frac{\partial n_e}{\partial y} \frac{\partial \phi}{\partial x} \Big) = 0 \tag{26}$$

$$-n_i \nabla^2 \phi - \nabla\phi \cdot \nabla n_i - (kT_o/e) \nabla^2 n_i = 0 \tag{27}$$

Non-dimensionalizing and substituting Eq. 8 into 26 and 27 results in

$$\hat{n}_e(\hat{n}_i-\hat{n}_e) - \hat{\nabla}\hat{\phi}\cdot\hat{\nabla}\hat{n}_e + \hat{\nabla}^2\hat{n}_e + \beta\psi = 0 \tag{28}$$

$$\hat{n}_i(\hat{n}_i-\hat{n}_e) - \hat{\nabla}\hat{\phi}\cdot\hat{\nabla}\hat{n}_i - \hat{\nabla}^2\hat{n}_i = 0 \tag{29}$$

where

$$\psi = \left(\frac{\partial\hat{n}_e}{\partial\hat{x}}\frac{\partial\hat{\phi}}{\partial\hat{y}} - \frac{\partial\hat{n}_e}{\partial\hat{y}}\frac{\partial\hat{\phi}}{\partial\hat{x}}\right) \tag{30}$$

6. Species Equations with Non-Constant Electron Temperature

For the case of significant Joule heating Eqs. 28 and 29 are not descriptive of the species concentration since $T_e \neq T_o$ everywhere in the field. It can be shown that for this case the species equations become

$$\begin{aligned}\theta\hat{n}_e(\hat{n}_i-\hat{n}_e) &- \theta\hat{\nabla}\hat{n}_e\cdot\hat{\nabla}\hat{\phi} + \frac{1}{2}\hat{n}_e\hat{\nabla}\theta\cdot\hat{\nabla}\hat{\phi} + \theta^2\hat{\nabla}^2\hat{n}_e + \frac{1}{2}\theta\hat{\nabla}\theta\cdot\hat{\nabla}\hat{n}_e \\ &+ \beta\Big(-\frac{1}{2}\hat{n}_e\frac{\partial\hat{\phi}}{\partial\hat{y}}\frac{\partial\theta}{\partial\hat{x}} + \frac{1}{2}\hat{n}_e\frac{\partial\hat{\phi}}{\partial\hat{x}}\frac{\partial\theta}{\partial\hat{y}} + \theta\frac{\partial\hat{\phi}}{\partial\hat{y}}\frac{\partial n_e}{\partial\hat{x}} \\ &\quad - \theta\frac{\partial\phi}{\partial\hat{x}}\frac{\partial\hat{n}_e}{\partial\hat{y}} - \frac{1}{2}\theta\frac{\partial\theta}{\partial\hat{x}}\frac{\partial\hat{n}_e}{\partial\hat{y}} + \frac{1}{2}\theta\frac{\partial\theta}{\partial\hat{y}}\frac{\partial\hat{n}_e}{\partial\hat{x}}\Big) = 0\end{aligned} \tag{31}$$

$$\hat{n}_i(\hat{n}_i-\hat{n}_e) - \hat{\nabla}\hat{n}_i\cdot\hat{\nabla}\hat{\phi} - \hat{\nabla}^2\hat{n}_i = 0 \tag{32}$$

Notice that for $\theta = 1$ and $\nabla\theta = 0$ these equations reduce to 28 and 29.

C. BOUNDARY CONDITIONS

Many boundary conditions can be hypothesized for wall, electrode, free stream, and upstream/downstream locations. Free stream conditions are actually those at the edge of the ambipolar region. They are taken to be zero potential and zero space-charge, and a Saha-predicted total charge. The

electrode node potential is a fixed value. Other wall boundary conditions are not so easily determined since they are frequently vague and not well identified in the literature. Also, since this model is new, the boundary conditions used must be compatible with the system that is being represented.

Successful runs have been generated using the following conditions with $T_e = T_o$:

1) Free stream as mentioned above,
2) Periodic electrode nodes allowing periodic conditions at upstream and downstream interfaces (Fig. 1),
3) Line electrode nodes allowing current constrictions (the necessary condition for two dimensions [21]). The potential is fixed and ion and electron concentrations are zero at the node, as dictated by a catalytic surface,
4) The inactive portion of the electrode wall is treated as an "insulated wall". Current perpendicular to this wall is zero, and the wall eliminates space charge and stagnates charge motion.

In reality a small sheath will form along the insulated wall because of the difference between electron and ion mobilites. The analysis of Appendix C shows that the thickness of the sheath goes approximately as the square root of the potential. Since the floating potential will generally be much less than the electrode node potential drop it is expected that the insulated wall sheath will be very much smaller in size than the electrode sheath. Consequently, the hypothetical boundary conditions at the wall specified above are representative.

A closer look at the electrode node boundary conditions is needed. Blue and Ingold[28] point out that though most authors use zero charge density at the electrode surface,

some cases require the modification $n_s = 2J/(e\bar{c})$ for the electrode boundary conditions. Appendix C gives characteristic values for J and $\bar{c}$ of 7×10^4 amps/m^2 and 10^5 m/sec, respectively, at typical temperatures. This results in $n_s = 10^{19}$ particles/m^3 which is of the same order as the charge densities which will be encountered later in this work. The difficulty in the application of this boundary condition comes from the fact that a true "point" electrode node would have an infinite current density. As will be seen later the numerical procedure uses a finite-difference scheme and the electrode is not a true "point". The current density at that location becomes artificially dependent upon the mesh-size. To avoid this problem, either the charge density must be set to zero, or some new non-zero restraint must be found. The use of periodic boundary conditions seems indicated since solutions of Laplace's equation (Poisson's equation in the absence of a space charge) tend to be periodic in two dimensions. As will be seen, several conditions were tried and the results are discussed in later sections.

Other boundary conditions, such as a catalytic insulated wall were attempted with no reasonable results. This is discussed further in the next section.

Figure 2 is a representation of the domain in the vicinity of the electrode, and some boundary conditions that are typical of those used in this work. The domain is represented numerically by a two-dimensional array of equally spaced points which are operated on by finite differencing the controlling equations.

Boundary conditions for $\hat{\Phi}$, $\hat{n}_e$, and $\hat{n}_i$ remain the same as

above for the Joule heating case. Temperature boundary conditions are straightforward. End conditions are again periodic and free stream requires that $\theta = 1$. Since both the electrode node and walls consist of dense materials with which electrons collide, it is assumed that the electrons give up their surplus energy readily to these surfaces. Therefore, $\theta = 1$ along that boundary.

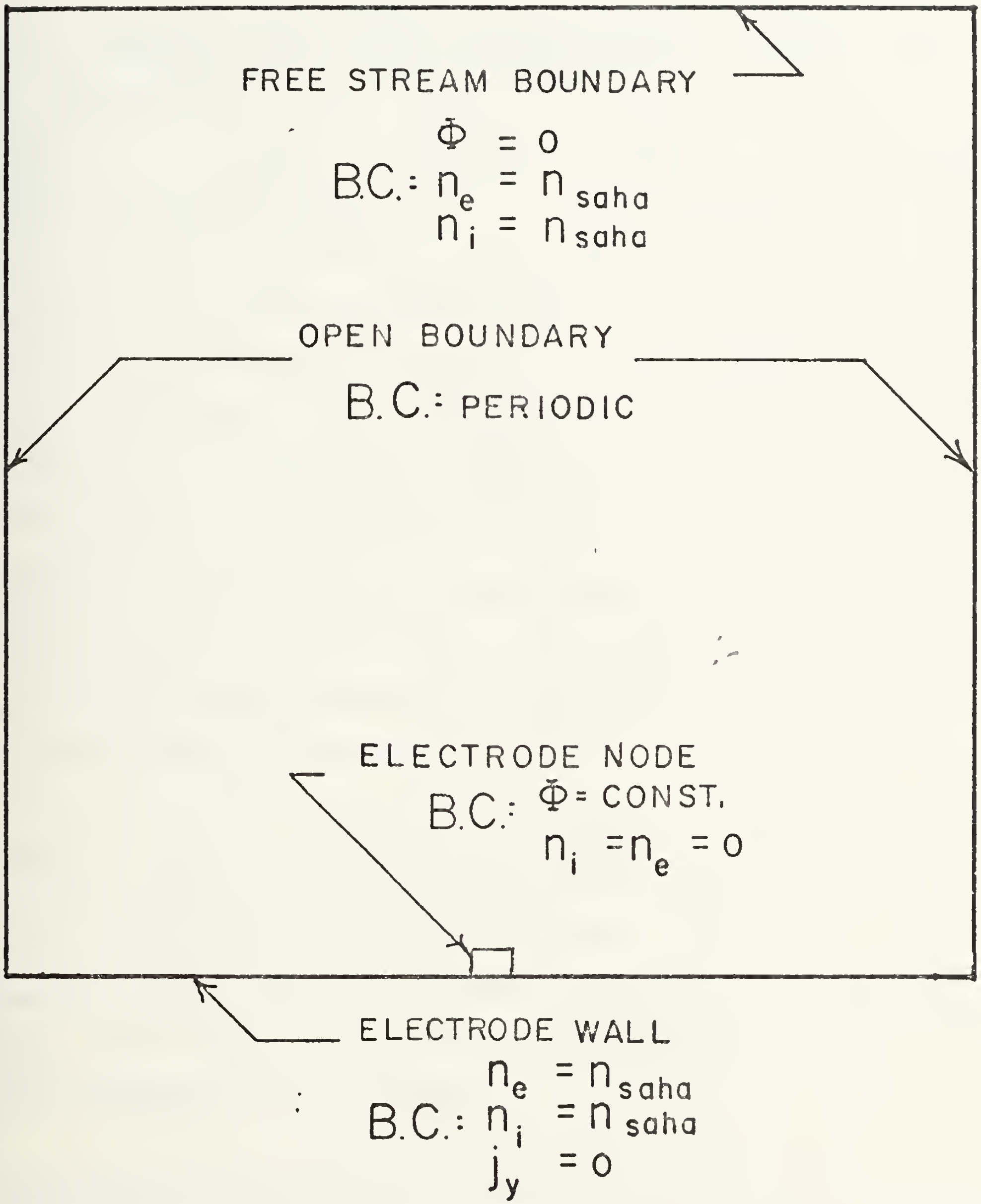

Figure 2. Arrangement of electrodes and boundary conditions for computational array.

III. METHOD OF SOLUTION

A. INTRODUCTION

The governing equations (namely Eqs. 8, 28, and 29) are solved numerically for the parameters $\hat{\phi}$, $\hat{n}_e$, and $\hat{n}_i$ throughout the domain as shown in Fig. 2. Later when the electron energy equation (Eq. 17) is included, a fourth parameter θ is included in the field, with Eqs. 31 and 32 representing the species equations. The method of solution will now be discussed together with the application of the boundary conditions. The system of partial, non-linear, second-order differential equations is basically elliptic and constitutes a boundary value problem. The partial differential equations are replaced by finite difference equations; the technique for solution is discussed below. The non-linear nature of the controlling equations requires rather sophisticated computer techniques, and the boundary conditions present special problems.

There are a number of possible approaches to the numerical analysis of the equations and several were tried before a successful approach evolved. In order to better understand the nature of these complicated equations, this Section also discusses the unsuccessful approaches and probable reasons for failure.

B. NON-LINEARITY CONSIDERATIONS

The two species equations contain the non-linear terms which present special programming problems. One-step techniques for solving this system of three simultaneous, second order, non-linear, partial differential equations are non-existent. One solution procedure in such cases is to

include all non-linear terms on the "right hand side," that is, external to the coefficient matrix, and hope that these non-linear terms change slowly enough with each iteration to render a convergent process. This procedure is known as the Jacobi method[29]. Looking at equations 28 and 29 for the constant termperature case, or 31 and 32 for the Joule heating case, it can be seen that only one term in each, either $\nabla^2 n_e$ or $\nabla^2 n_i$, is linear, and that there is no prescribed "load" on the right hand side. As will be seen in the expansion of these equations later, this leaves a dozen or more non-linear terms for the right hand side. Experience shows that the Jacobi method proves to be unstable.

As a consequence of the failure of the Jacobi method, a quasi-Jacobi method is used. When the product of two variables is encountered, one variable is treated as a constant coefficient for each iteration. This means that the non-linear terms are retained in the coefficient matrix. The "constant" coefficients are updated after every iteration, thus changing the coefficient matrix. Successively higher voltages were calculated in increments allowing small changes to the system.

Had this quasi-Jacobi method not succeeded, the next step would qave been to apply a Newton-Raphsen technique[29] to the equations. Because of the increase in the number of terms and the consequent increase in computer requirements, the Newton-Raphsen method was reserved as a last resort.

C. GRID SIZE AND COMPUTATIONAL SEQUENCE

The number of points required to define a domain sufficiently large to show the sheath and ambipolar regions is critical (See the section on numerical results). For

example, if a two-dimensional field consisting of a square array of 31 x 31 points is desired to be solved simultaneously, then it can be shown that a finite difference scheme will require in excess of 66 million bytes of storage for the coefficient matrix alone. Special storage techniques which take into account the banded structure of the coefficient matrix reduces the storage requirements to 12 million bytes. Even this is about 12 times the core capacity of the IBM 360/67 at the Naval Postgraduate School. Obviously, to have a sufficiently large array and to keep within the core capacity the solution method must consider portions of the array at one time.

This problem is met by using the line iterative method, i.e. by solving one line of the array at a time, sweeping back and forth with successive field iterations. By doing so, the size of the coefficient matrix is reduced to a small fraction of the full matrix. Because the equations are elliptic, and therefore each point affects every other point in the field, it is desirable to reduce the computer time for "information" to move through the field. This is accomplished by rotating the field 90° after every second field iteration such that the line sweeps go forward, then backward, then up and then down. This approach takes considerably less execution time for a converged solution than the usual procedure without alternating directions and rotation.

The final grid size chosen for this line iterative method is 51 x 51. This decision was based upon the time required to reach a converged solution. The time for each run was of the order of four or five hours. The coefficient matrix requires only 51 x 3 x 10 x 8 = 12,240 bytes while the total space needed is 150,000 bytes for the constant temperature case, and 170,000 bytes for Joule heating. This

storage includes program space, variable storage and solution matrices for double precision arithmetic.

To further increase the speed of convergence a method of successive over-relaxation is incorporated similar to that outlined in Ref. [30]. At the end of each line iteration the parameters are subjected to the equation

$$A_{corr} = (1+w)A_{new} - w\,A_{old} \tag{33}$$

where A_{corr} is the corrected value of the parameter, A_{new} is the most recent calculation, A_{old} is the previous A_{corr}, and w is the over-relaxation parameter.

D. CONTROLLING EQUATIONS

The finite difference representation of all terms was expressed to the order of h² when practical, where h is the grid spacing of the square 51 x 51 array. Ketter and Prowell (Ref. 29, p. 226-228) also describe the procedure for setting up finite difference equations. Second derivatives in two-dimensions are given by

$$\nabla^2 A_{i,j} = (A_{i+1,j} + A_{i-1,j} + A_{i,j+1} + A_{i,j-1} - 4A_{i,j})/h^2 \tag{34}$$

First derivatives have the form

$$\frac{\partial A}{\partial x_{i,j}} = (A_{i+1,j} - A_{i-1,j})/(2h) \tag{35}$$

Where a first derivative is required at a boundary it is written as either a forward or backward difference.

$$\frac{\partial A}{\partial x_{i,j}} = (-3A_{i,j} + 4A_{i+1,j} - A_{i+2,j})/(2h) \tag{36}$$

Transforming Eq. 8 into finite differences gives

$$\hat{\phi}_{i+1,j} + \hat{\phi}_{i-1,j} + \hat{\phi}_{i,j+1} + \hat{\phi}_{i,j-1} - 4\hat{\phi}_{i,j} + h^2\hat{n}_{i_{i,j}} - h^2\hat{n}_{e_{i,j}} = 0 \tag{37}$$

This is the simplest of the three controlling equations.

The species equations are considerably more complicated. The finite difference form of Eq. 28 is transformed here to illustrate the use of variables as "constant" coefficients in the non-linear terms.

$$\begin{aligned}
&(\hat\phi_{i,j+1} - \hat\phi_{i,j-1})\left\{\beta(\hat n_{e_{i+1,j}} - \hat n_{e_{i-1,j}}) - \hat n_{e_{i,j+1}} + \hat n_{e_{i,j-1}}\right\}/4h^2 \\
&+ (\hat n_{e_{i,j+1}} + \hat n_{e_{i,j-1}} - 4\hat n_{e_{i,j}})/h^2 \\
&= \hat n_{e_{i,j}}(\hat n_{e_{i,j}} - \hat n_{i_{i,j}}) + (\hat\phi_{i+1,j} - \hat\phi_{i-1,j})\,[\hat n_{e_{i+1,j}} - \hat n_{e_{i-1,j}} \\
&+ \beta(\hat n_{e_{i,j+1}} - \hat n_{e_{i,j-1}})]/4h^2 - (\hat n_{e_{i+1,j}} + \hat n_{e_{i-1,j}})/h^2 \qquad (38)
\end{aligned}$$

This equation corresponds to a line in the y direction. The bracketed terms {} are treated as constant coefficients but are updated with each field iteration. The finite difference version of Eq. 29 resembles Eq. 38, but is considerably simpler since $\beta_i \cong 0$.

When the electron temperature is uniform and equal to the neutral temperature, no energy equation per se is required since the condition $T_e = T_o$ is incorporated in the two species equations. However, for the non-equilibrium case, the energy equation is solved separately from the other three. That is, Eqs. 8, 31, and 32 are solved simultaneously for assumed values of θ. With each iteration θ is updated by solving Eq. 17.

E. BOUNDARY CONDITIONS

Free stream boundary conditions are the simplest. For each case the free stream values are set at $\hat{\phi} = 0$, $\hat{n}_e = \hat{n}_i = \hat{n}_{Saha}$, and $\theta = 1$.

Upstream/downstream conditions are chosen to be periodic. They require that not only the values of the unknowns be the same at periodic points, but also that their derivatives be the same. For example, if the far upstream station is labeled "1" and the far downstream station is "n" the two equations, then

$$A_{n,j} = A_{1,j} \quad \text{and} \; , \tag{39}$$

$$A_{1,j} = A_{2,j} - A_{n,j} + A_{n-1,j} \tag{40}$$

would apply for all parameters $\hat{\phi}$, $\hat{n}_e$, $\hat{n}_i$, and θ.

The insulated wall is hypothesized to be neutral and to equilibrate the charges, therefore, the conditions are numerically set to $\hat{n}_e = \hat{n}_i = \hat{n}_{Saha}$. The wall condition is taken from the restriction that perpendicular current is zero. From a non-dimensional form of Eq. 24 for zero current in the y-direction the boundary condition at the wall is

$$-\hat{n}_e \frac{\partial \hat{\phi}}{\partial \hat{y}} + \frac{\partial \hat{n}_e}{\partial \hat{y}} - \beta \hat{n}_e \frac{\partial \hat{\phi}}{\partial \hat{x}} + \beta \frac{\partial \hat{n}_e}{\partial \hat{x}} = 0 \tag{41}$$

The x-derivative of $\hat{n}_e$ is zero along the wall and $\hat{n}_e = \hat{n}_{Saha}$. So

$$\hat{n}_{saha} \frac{\partial \hat{\phi}}{\partial \hat{y}} = \frac{\partial \hat{n}_e}{\partial \hat{y}} - \beta \hat{n}_{saha} \frac{\partial \hat{\phi}}{\partial \hat{x}} \tag{42}$$

The finite difference expression for Eq. 42 is

$$\begin{aligned}3\hat{n}_{saha}\hat{\phi}_{i,j} - 4\hat{n}_{saha}\hat{\phi}_{i,j+1} - 3\hat{n}_{saha} + 4\hat{n}_{e_{i,j+1}} \\ = -\hat{n}_{saha}\hat{\phi}_{i,j+2} + \hat{n}_{e_{i,j+2}} + \beta\hat{n}_{saha}(\hat{\phi}_{i+1,j} - \hat{\phi}_{i-1,j})\end{aligned} \qquad (43)$$

The boundary conditions at the electrode node consist of the three conditions $\hat{\phi} = \hat{\phi}_o$, $\hat{n}_i = 0$, and $\hat{n}_e = 0$ consistent with catalytic electrodes.

F. EVOLUTION OF THE MODEL AND PRIOR ATTEMPTS

The factors affecting the choice of the calculation procedure and computational model are many. Boundary conditions, array size, electrode placement, choice of coordinate system, and the form of the controlling equations are but a few of the things that had to be considered in modeling the problem. The final successful technique evolved by trial and error. The following paragraphs give a brief account of the evolution including successes and failures.

At the outset a two-dimensional, flat plate, continuous electrode model was proposed. Because of the small thickness of the sheath relative to the electrode size, most areas of the sheath would not experience end effects, and would be effectively one-dimensional. Further investigation led to the proof of the non-existence of a one-dimensional solution presented in Appendix B.

It then became obvious that the key to this problem was in two- or three-dimensional current constriction since the one-dimensional Cartesian geometry offers no natural geometric means to decrease current density away from the electrode. The electrode is then represented by a series of nodes as shown in Fig. 1. An examination of the literature

showed that this mode of current constriction was known and even helps explain the electrode spots which may be present on the anode.

At first the model consisted of both the anode and cathode on opposing sides of a field of computational points, but it was realized that a field of this size could not possibly show all the details of the sheath. Conversely, a field capable of showing the required details could not contain both the electrodes. So the final model consisted of a series of line electrodes (for simplicity, the anode) along an "insulated" wall in a periodic field. The opposite boundary would then represent a free stream conditon. The other two boundaries are upstream/downstream boundaries.

Once the model was chosen, the job of solving the equations was undertaken. Initially, the three controlling equations (the energy equation had not yet been considered) were solved separately for ϕ, n_e, and n_i, respectively, in iterative fashion. The equations were Eqs. 3, 26 and 27 with a Hall parameter of zero. The calculations diverged almost immediately because in the vicinity of the electrode many derivatives are large and values of the parameters changed too rapidly from the initial "guessed" values.

It became apparent then that the three equations would need to be solved simultaneously. Section III.C explains some of the problems of such a technique in terms of overall storage requirements. In the light of this, the line iterative method was chosen.

Armed with a simple set of variables and the line-iterative method a solution was attempted. Convergence was achieved, but very slowly, since it took many iterations

for "information" to cross the array. So the array was rotated 90° at intervals causing the effective sweep to be back and forth, then up and down.

At one time a coordinate transformation was effected putting three of the boundaries at infinity. (The periodicity of the nodes was not yet considered.) This gave no satisfactory solution, and the reason is believed to be the following: Although Eq. 8 is Poisson's equation, it reduces to Laplace's equation in the ambipolar and free stream regions. Since there is no solution in two-dimensions for Laplace's equation satisfying the requirement that ϕ = constant at infinity, then no solution to this problem was forthcoming.

A variable mesh size was also attempted with some success, but since it was determined that the ambipolar region was of the same order of magnitude as the sheath, it was rejected as an unnecessary complication.

Various boundary conditions were tried, but most either did not work or gave physically meaningless results. The most difficult boundary to model is the insulated wall. From the final boundary conditions chosen the system of equations describes a certain physical case.

Once the present technique was successful for various voltages, it proved its versatility by accepting the addition of a magnetic field and the energy equation routinely. While not being the ultimate in possible techniques for solving this system of equations, the present scheme has rendered useful results and promises to be further productive in other cases.

IV. RESULTS

A. PROCEDURE AND CONVERGENCE CRITERIA

The simplest case, which included no magnetic field effects and negligible Joule heating began with the following assumed values:

1. zero potential everywhere except at the electrode,
2. selected non-dimensional potential at the electrode,
3. zero charge density everywhere except at the boundaries, and
4. Saha charge density at the boundaries.

Using these assumed values, iterations for improved values proceeded.

Periodically convergence was checked after many field iterations by comparing the left hand side of Eq. 8 with the right hand side at various locations in the field. This convergence criterion may appear somewhat arbitrary, but was chosen when it was found that Eq. 8 was more difficult to satisfy than Eqs. 28 and 29 and therefore represented stricter convergence criterion. Additionally, Eq. 8 contains all three unknowns providing a check of all parameters.

The error was calculated from the finite difference representation of Eq. 37.

$$\epsilon = 1 - \frac{\hat{\phi}_{i,j+1} + \hat{\phi}_{i,j-1} + \hat{\phi}_{i+1,j} + \hat{\phi}_{i-1,j} - 4\hat{\phi}_{i,j}}{h^2(\hat{n}_{e_{i,j}} - \hat{n}_{i_{i,j}})} \qquad (44)$$

As the calculations converged the error decreased with subsequent iterations, but the rate of convergence slowed as the number of iterations became large. Eventually a point

was reached where further iterations were not cost effective as the additional improvement in the solution required excessive computer time. A second convergence criterion was used in addition to the the first. Certain potential values at critical points in the array were plotted with successive field iterations. If these values approached some assymptotic value, then the procedure was considered convergent.

As discussed earlier, a successive over-relaxation technique was used to increase the rate of convergence. It was found that over-relaxation parameters exceeding 1.1 caused the field to diverge for all but very low voltages. Some improvement of convergence rate was noted for $w = 1.05$ so this value was used for most runs. When attempting to achieve solutions for higher voltages or other conditions which might prove divergent, such as large Hall parameters or Joule heating parameters, a value of $w = 0$ was used in order to put the least possible "stress" on the system of equations.

B. NEGLIGIBLE JOULE HEATING AND NO MAGNETIC FIELD EFFECTS

Convergence for this set of runs was slow. In order to achieve an error of less than 20% ($|\epsilon|<.2$) over 1000 iterations were required, even with a near optimum over-relaxation parameter of 1.05. This equates to about four hours of computer on the IBM 360/67. An additional hour (250 iterations) reduced the error to 16%. Final results shown in Figs. 3-18 were completed with $|\epsilon|<.16$. Further improvement would have required excessive computer time.

Figures 3, 6, 9, and 12 are plots for the case $\hat{\phi} = 5.80$.

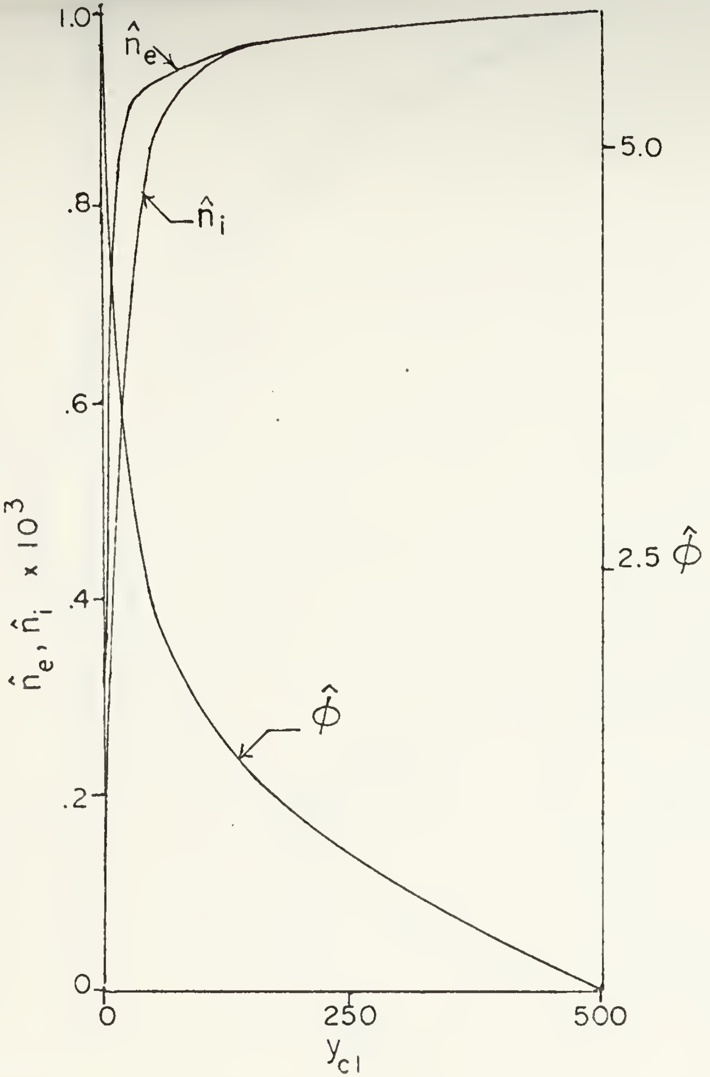

Figure 3. Potential and Charge Density Profile, $\hat{\phi}=5.80, \gamma=0, \beta=0, \hat{n}=10^{-3}$, array size=500L, 51x51 grid.

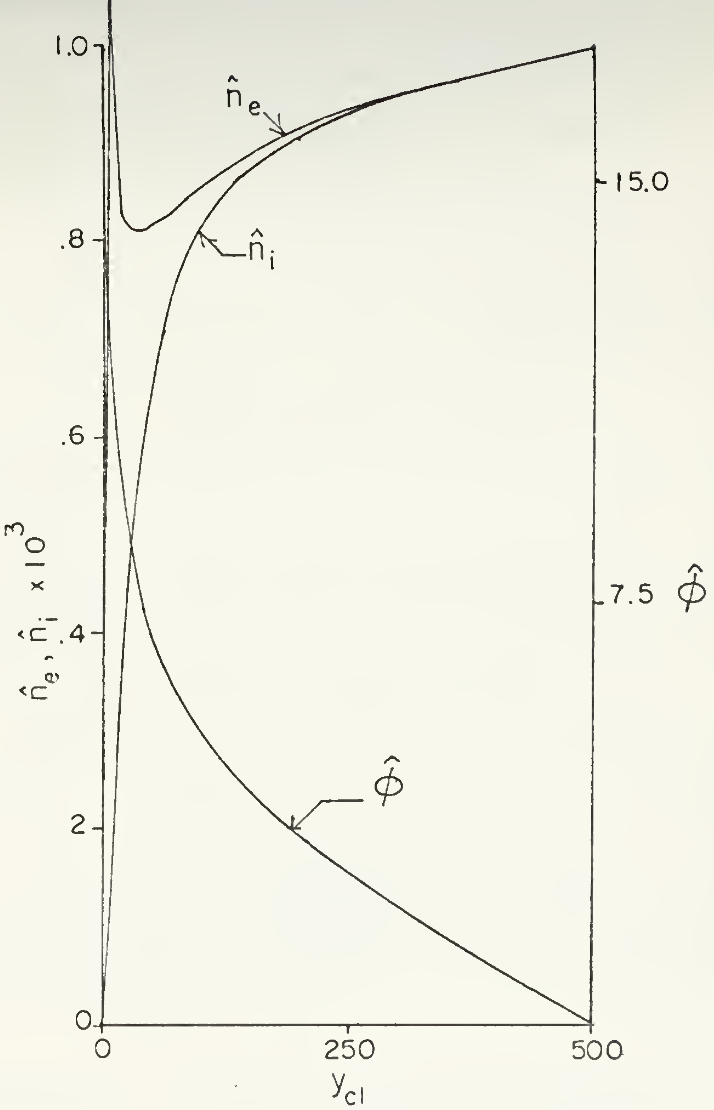

Figure 4. Potential and Charge Density Profile, $\hat{\phi}=17.4, \gamma=0, \beta=0, \hat{n}=10^{-3}$, array size=500L, 51x51 grid.

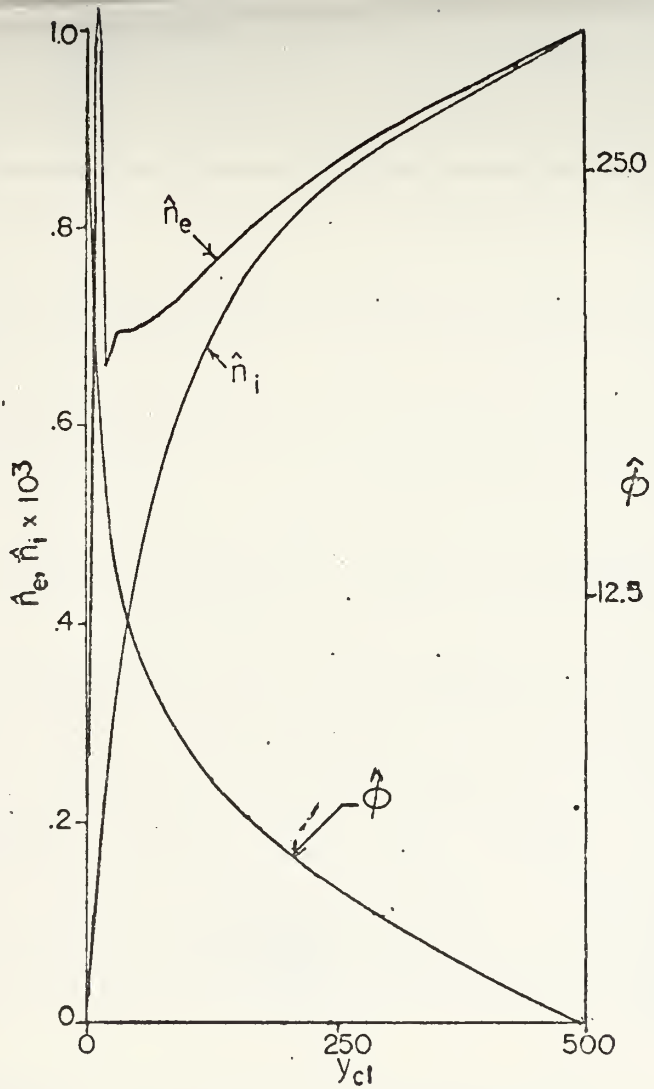

Figure 5. Potential and Charge Density Profile, $\hat{\phi}=29.0, \gamma=0, \beta=0, \hat{n}=10^{-3}$, array size=500L, 51x51 grid.

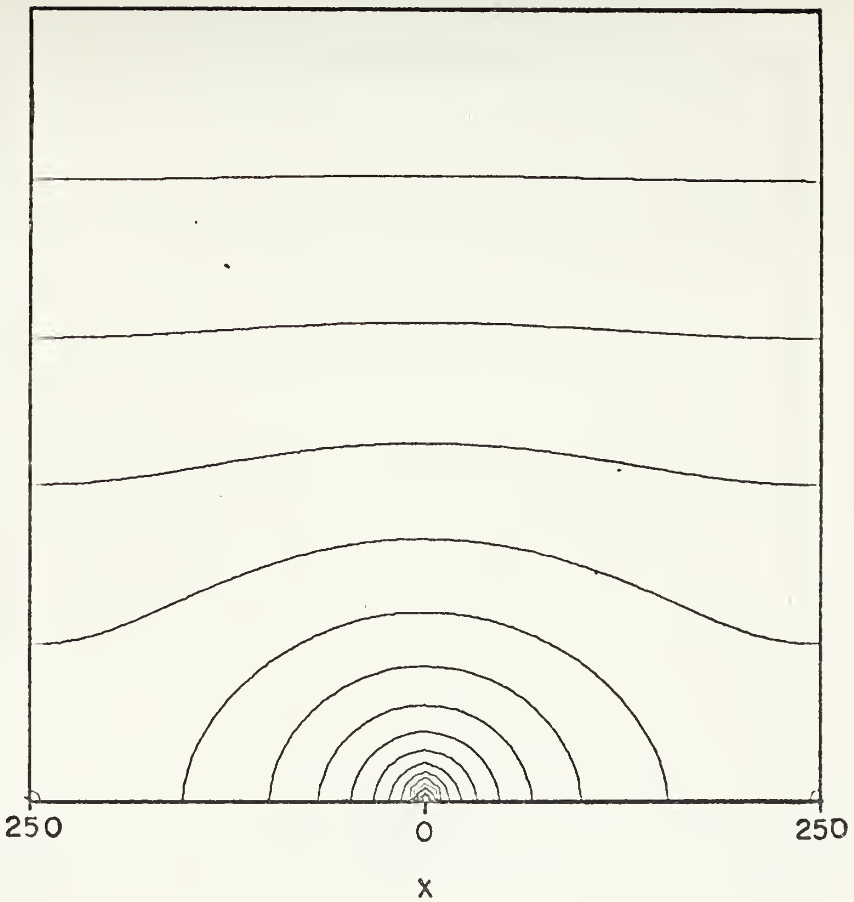

Figure 6. Potential Contour Plot, $\hat{\phi}=5.80$, $\gamma=0, \beta=0, \hat{n}=10^{-3}$, array size = 500L, 51x51 grid.

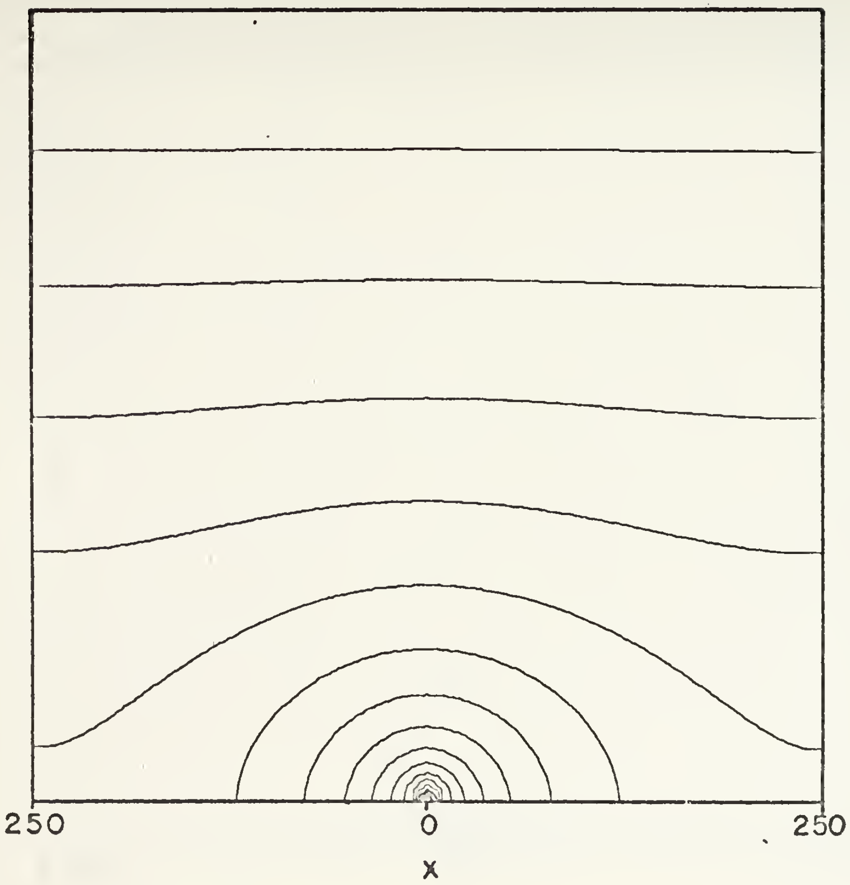

Figure 7. Potential Contour Plot, $\hat{\phi}=17.4$, $\gamma=0, \beta=0$, $\hat{n}=10^{-3}$, array size = 500L, 51x51 grid.

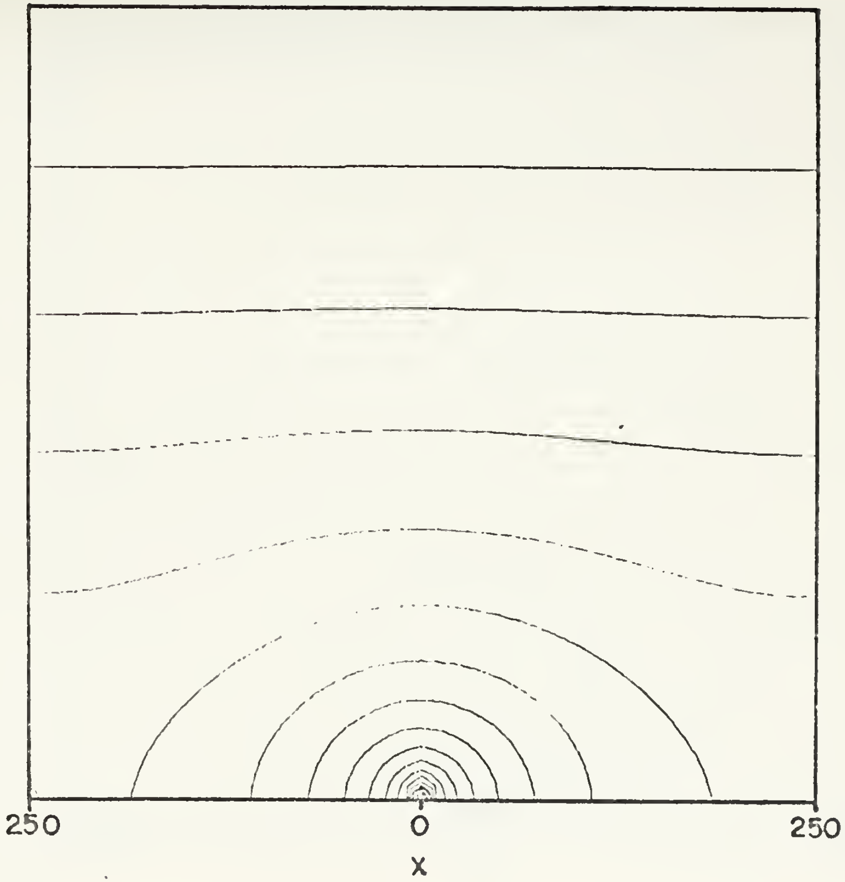

Figure 8. Potential Contour Plot, $\hat{\phi}=29.0$, $\gamma=0, \beta=0$, $\hat{n}=10^{-3}$, array size = 500L, 51x51 grid.

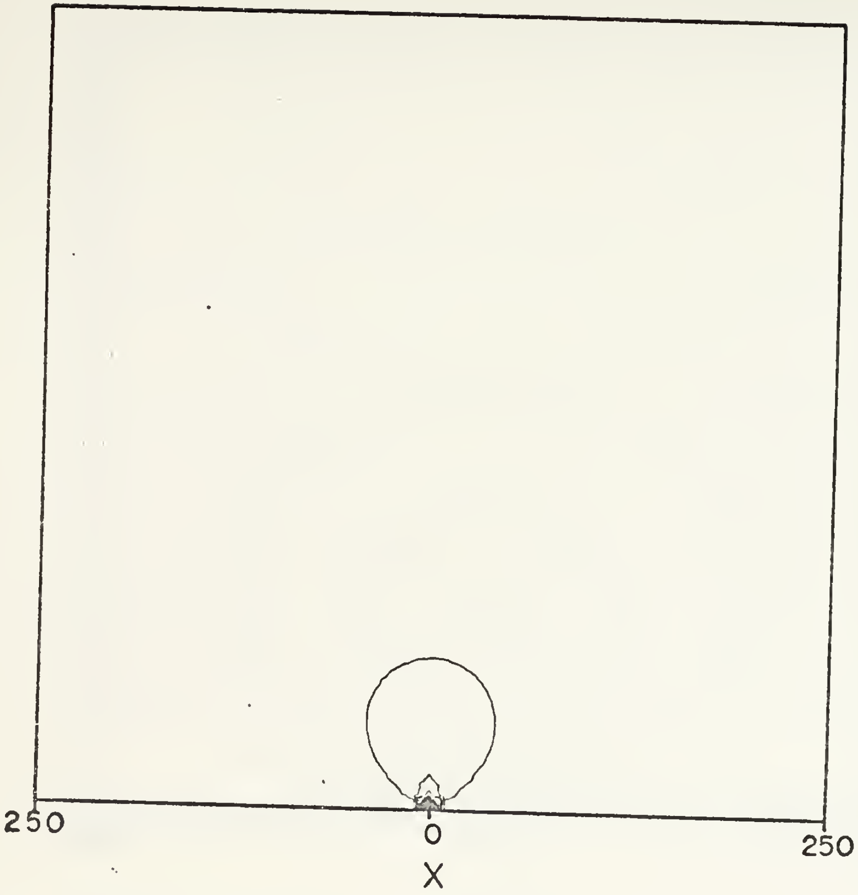

Figure 9. Electron Density Contour Plot, $\hat{\phi}=5.80, \gamma=0, \beta=0, \hat{n}=10^{-3}$, array size=500L, 51x51 grid.

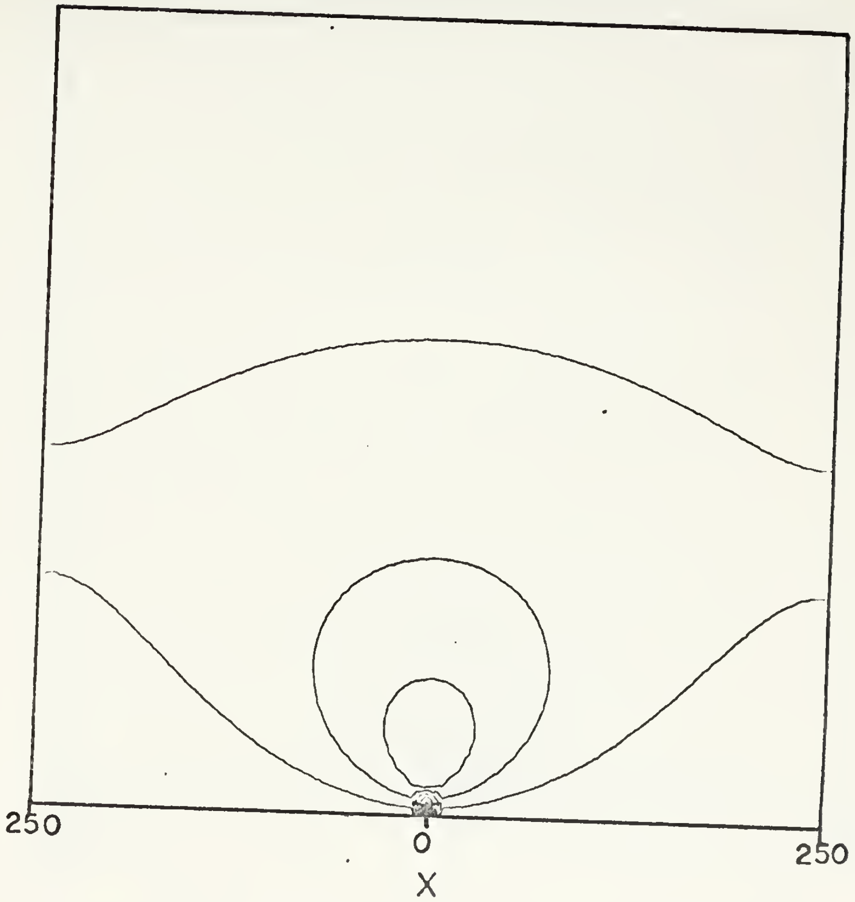

Figure 10. Electron Density Contour Plot, $\hat{\phi}=17.4, \gamma=0, \beta=0, \hat{n}=10^{-3}$, array size=500L, 51x51 grid.

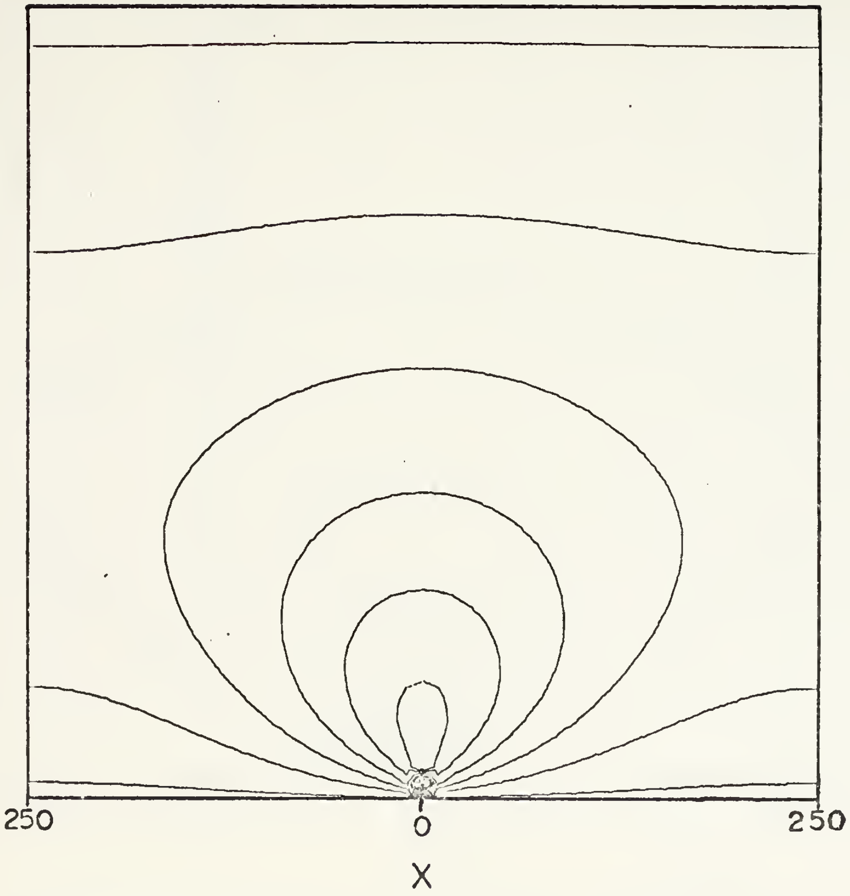

Figure 11. Electron Density Contour Plot, $\hat{\phi}=29.0, \gamma=0, \beta=0, \hat{n}=10^{-3}$, array size=500L, 51x51 grid.

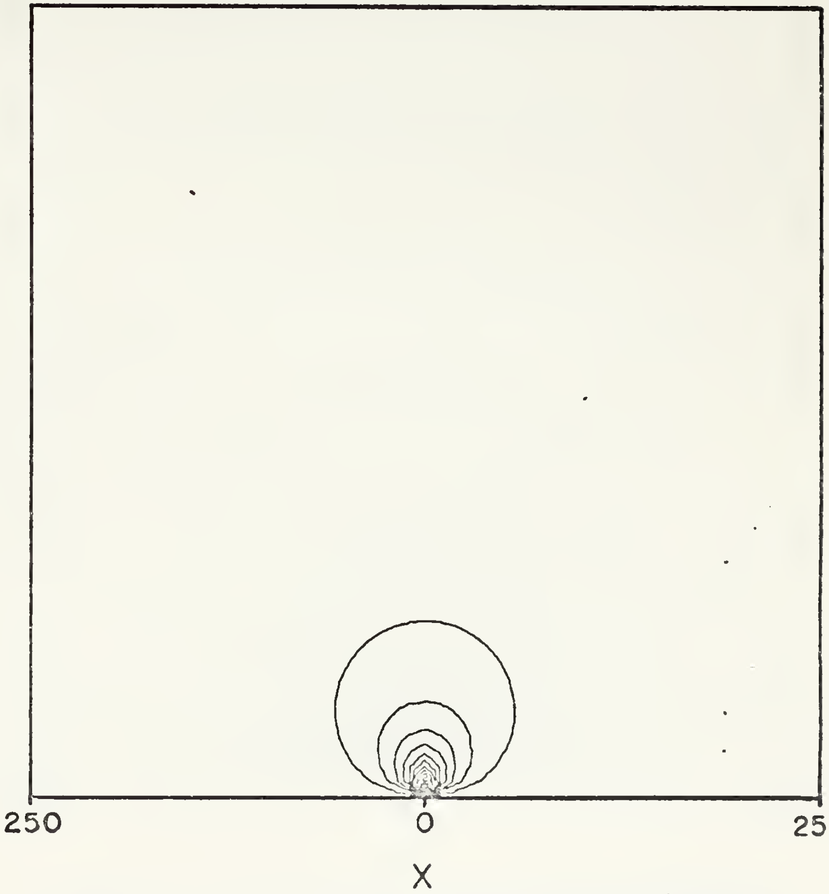

Figure 12. Ion Density Contour Plot, $\hat{\phi}=5.80, \gamma=0, \beta=0, \hat{n}=10^{-3}$, array size=500L, 51x51 grid.

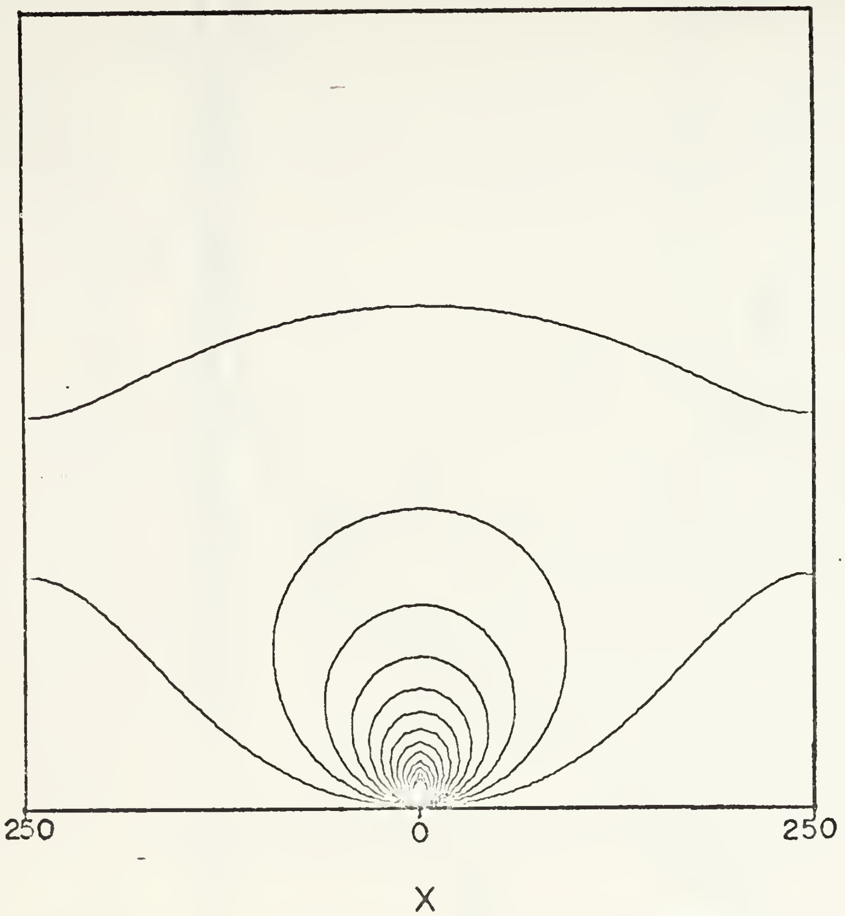

Figure 13. Ion Density Contour Plot, $\hat{\phi}=17.4$, $\gamma=0, \beta=0$, $\hat{n}=10^{-3}$, array size=500L, 51x51 grid.

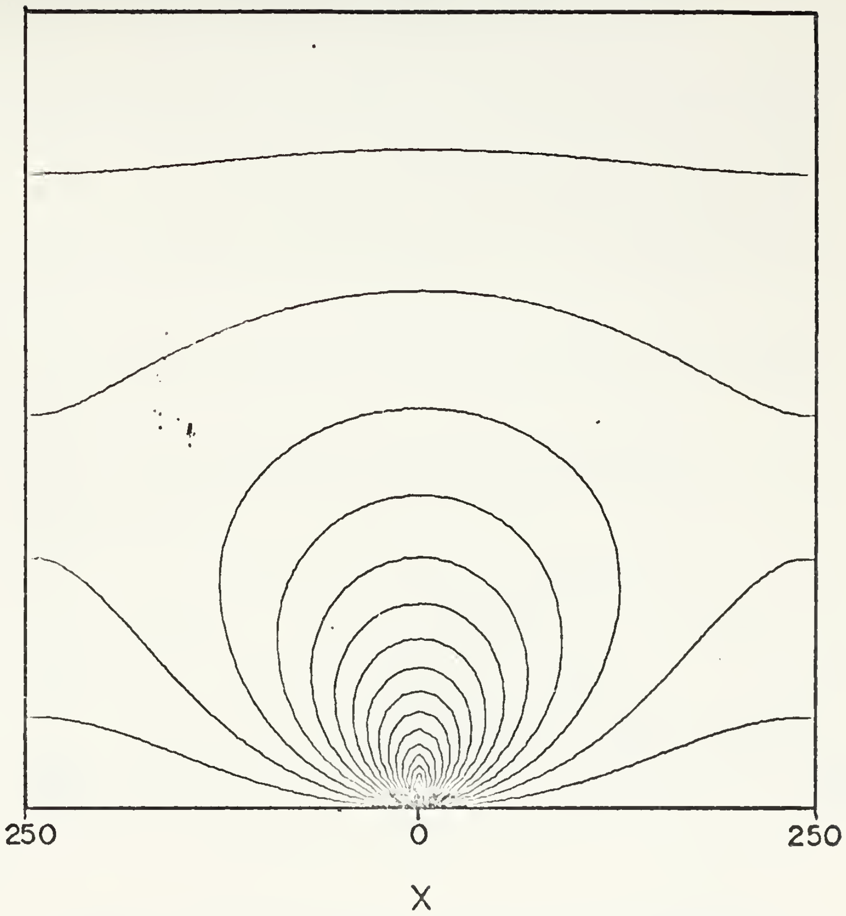

Figure 14. Ion Density Contour Plot, $\hat{\phi}=29.0$, $\gamma=0, \beta=0$, $\hat{n}=10^{-3}$, array size=500L, 51x51 grid.

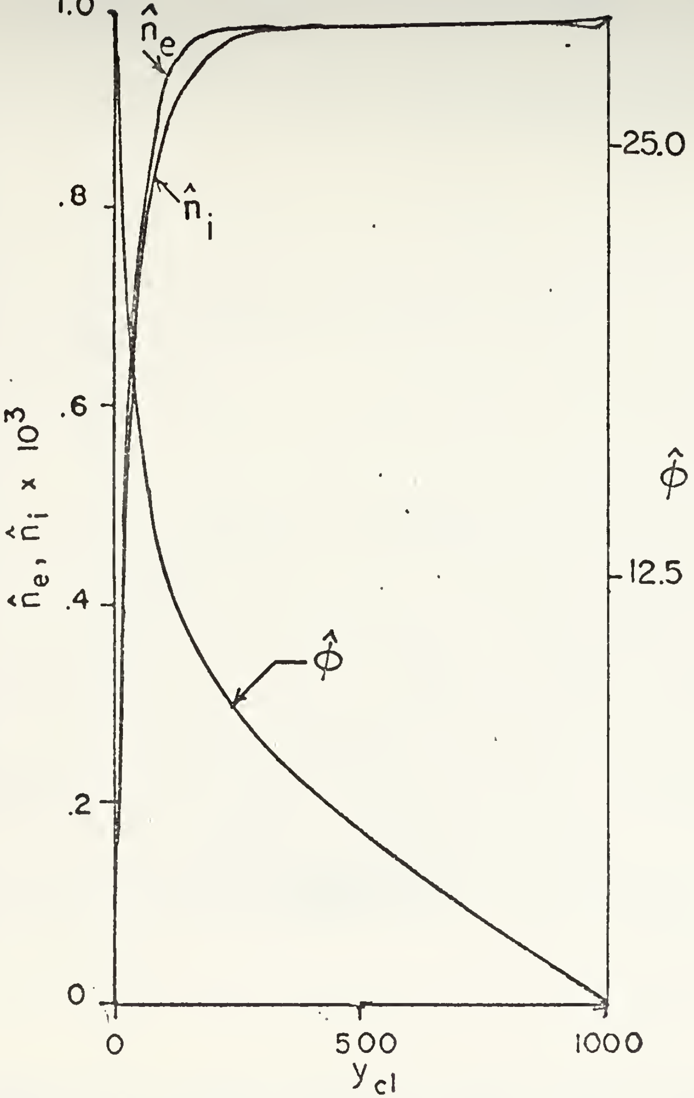

Figure 15. Potential and Charge Density Profile, $\hat{\phi}=29.0$, $\gamma=0$, $\beta=0$, $\hat{n}=10^{-3}$, array size= 1000L, 51x51 grid.

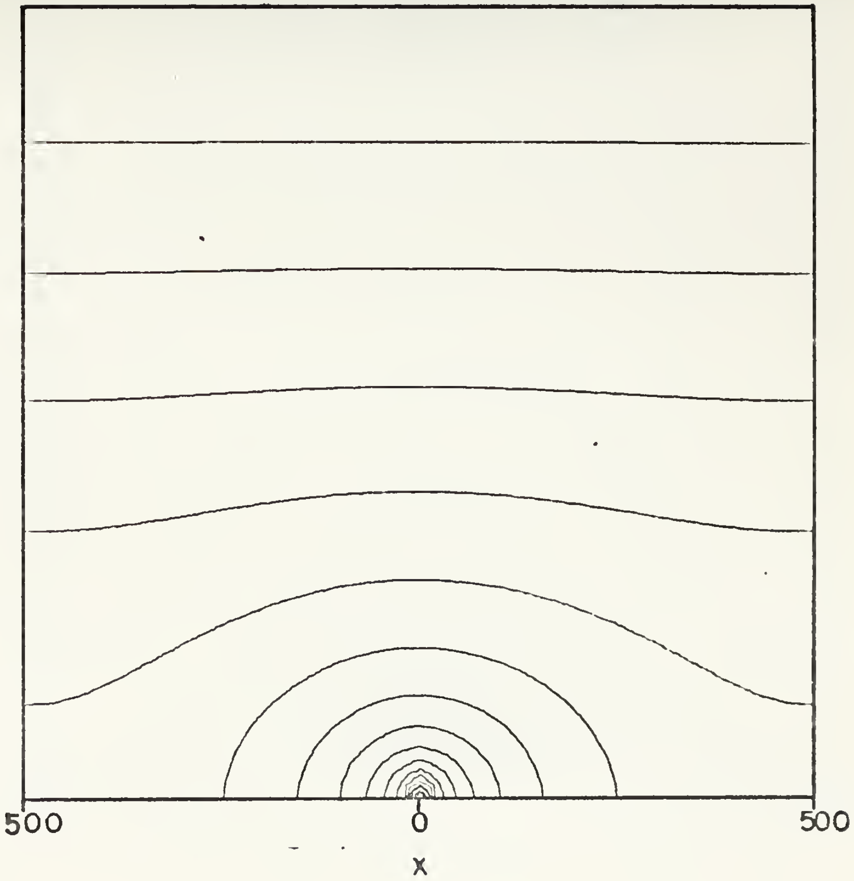

Figure 16. Potential Contour Plot, $\hat{\phi}=29.0$, $\gamma=0$, $\beta=0$, $\hat{n}=10^{-3}$, array size= 1000L, 51x51 grid.

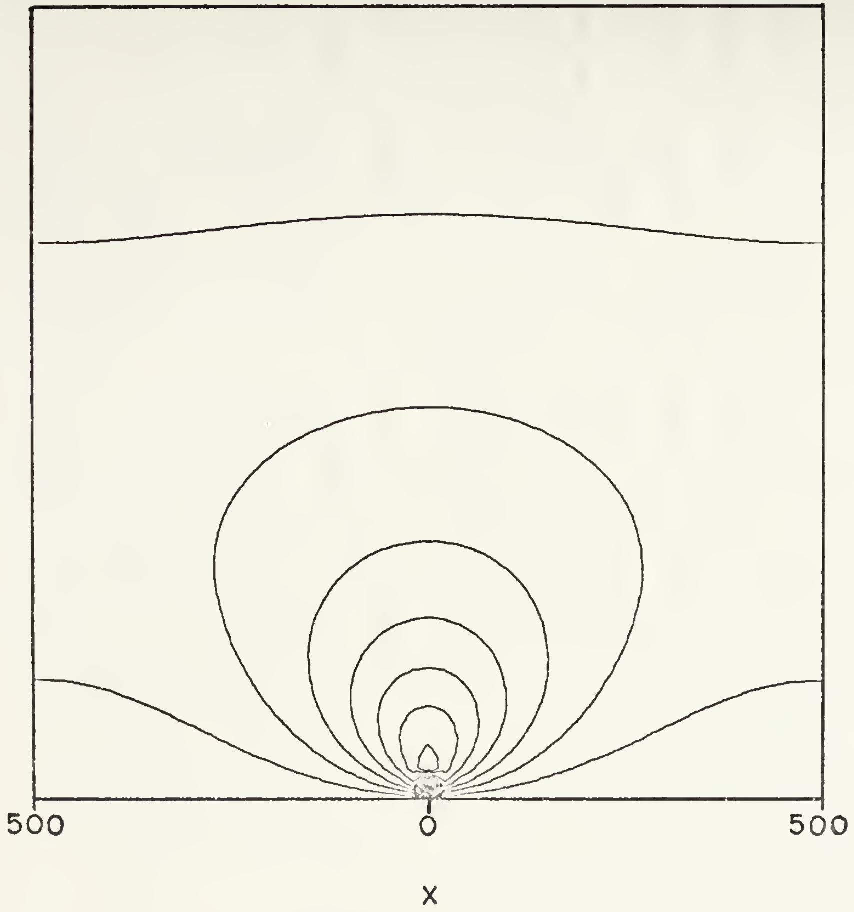

Figure 17. Electron Density Contour Plot, $\hat{\phi}=29.0$, $\gamma=0, \beta=0$, $\hat{n}=10^{-3}$, array size=1000L, 51x51 grid.

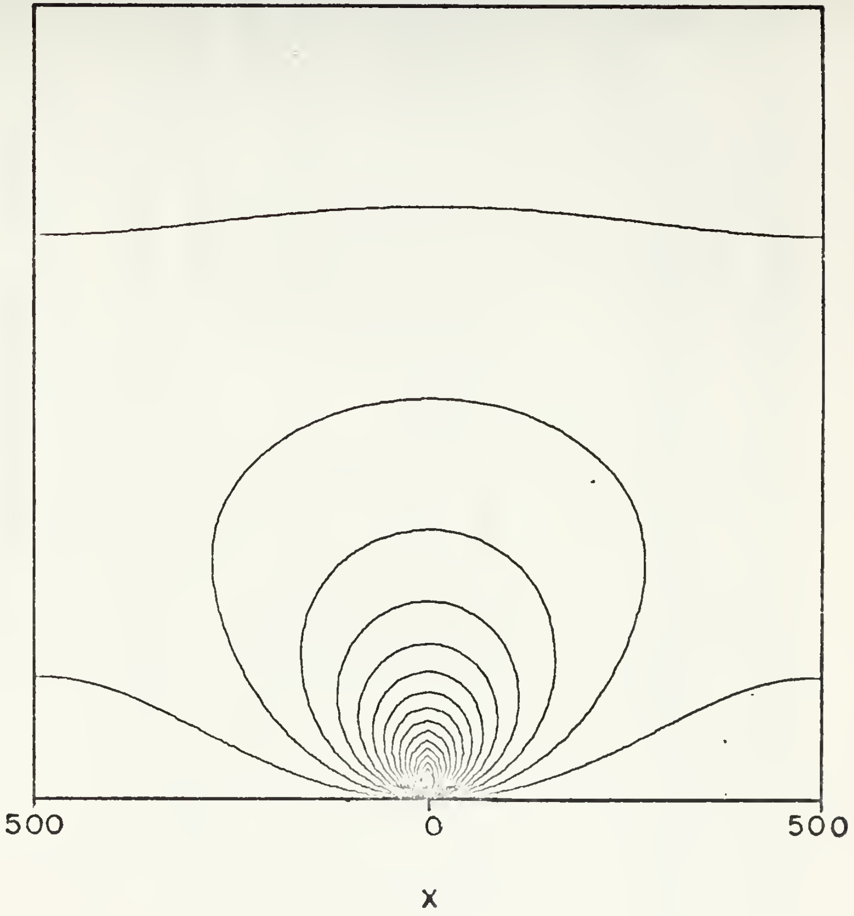

Figure 18. Ion Density Contour Plot, $\hat{\phi}=29.0$, $\gamma=0, \beta=0$, $n=10^{-3}$, array size=1000L, 51x51 grid.

This value represents one volt at T_o=2000°K. Figures 4, 7, 10, and 13 are for $\hat{\phi}$ = 17.41 and Figs. 5, 8, 11, and 14 are for $\hat{\phi}$ = 29.02, representing 3 and 5 volts, respectively, at T_o = 2000°K.

The overall size of the array for each of these runs is 500 times the characteristic length defined in Eq. 7. At 2000°K this means that the dimensions of the square field shown in the figures are 5.25×10^{-5}m on a side. The non-dimensional charge density as determined by the boundary condition is 10^{-3}. This corresponds to 8.6×10^{17} particles/m^3, which is typical of an equilibrium charge density for seeded plasmas at this temperature.

1. Potential Distributions

Figures 3-5 are all one-dimensional profiles of potential and charge density distributions along a line perpendicular to the electrode wall. The abscissa shows distance from the electrode in terms of the characteristic length. Figures 6-8 are two-dimensional contour plots of the potentials for the three voltages. The electrode is located at the bottom center where the contours concentrate. Except for the absolute magnitudes, there is little change noted in the potential plots for the three voltages. As might be expected, the steepest potential slope occurs near the electrode where the greatest electric field exists. At the free boundary the slope of the potential is nearly constant indicating a constant electric field. A constant electric field is a property of two opposing infinite flat-plate electrodes. The plasma spreads the effects of a point or line electrode so that the free stream behaves as if the electrodes were infinite plates.

2. Charged Particle Distributions

Figures 9-11 demonstrate considerable change for the electron densities with increasing voltage as do Figs. 12-14 for ion densities.

An examination of the charge density plots in Figs. 3, 4, and 5 reveal several interesting facts. First, since the edge of the sheath is the line of points where the charge densities are equal, the figures put the sheath length at 35%, 90%, and 100% of the total length of the field. In the following table, the characteristic sheath length as calculated from Eq. C.7 for T_o = 2000°K is shown next to the computer generated sheath length from the extimate of the convergence of the charge density lines in the figures:

$\hat{\Phi}_o$	ϕ_o	characteristic sheath length	computer generated
5.80	1.0 volts	$.800 \times 10^{-5}$ m	1.84×10^{-5} m
17.41	3.0 volts	1.38×10^{-5} m	4.72×10^{-5} m
29.02	5.0 volts	1.79×10^{-5} m	5.25×10^{-5} m

These offer order-of-magnitude comparisons at best, but the predictions of the characteristic sheath length with Eq. C.7 are useful in estimating the size of the field for the computer program.

Notice that the charge density slopes on the right of Figs. 4 and 5 are significantly greater than zero. This means that the field was not sufficiently large to encompass the entire ambipolar region. Since the boundary conditions at the free stream are imposed as constants they are "forced" conditions and probably result in error for these cases. One result of this is the erratic behavior of the charge density close to the electrode. As will be seen

later, this behavior has little effect on the current distribution as long as it occurs in a confined region.

It is evident that the observation of 100% of the field for the sheath length in Fig. 5 is probably low since the convergence of the two charge lines occurs artificially at the boundary. To prove this, and the other observations made above, a run was made for the $\hat{\Phi} = 29.02$ case doubling the field length to 1000 times the characteristic length, or 10.5×10^{-5} m. Figure 15 shows the dramatic result. The erratic behavior of the charge density lines near the electrode is gone and the slope is essentially zero near the free boundary. The sheath length is measured at about 3.94×10^{-5} m, 2.3 times the characteristic predicted value. It is interesting to note that this is about the same ratio as the measured/predicted ratio of the $\hat{\Phi} = 5.80$ case. Figures 16-18 show the two-dimensional plots for this $\hat{\Phi} = 29.02$ case.

C. NON-CONSTANT ELECTRON TEMPERATURE

With the addition of the energy equation the effect of Joule heating on the system was studied. The value $\gamma = 100$ was introduced first to simulate combustion gases. The results are shown in Figs. 19-22 for the cases $\hat{\Phi} = 5.80$ and 29.02. In spite of the earlier discussion showing that the size of the field is inadequate for the higher potential case, it is used here to avoid the complication of changing the electrode spacing when comparing different potentials.

The most obvious change caused by the heating of the electrons is the changed slope of the potential indicating less shielding for the Joule heating case. This is further shown in Figs. 23 and 24 which represent $\hat{\Phi} = 5.80$ and $\gamma = 10^3$. The charge density profiles are relatively

later, this behavior has little effect on the current distribution as long as it occurs in a confined region.

It is evident that the observation of 100% of the field for the sheath length in Fig. 5 is probably low since the convergence of the two charge lines occurs artificially at the boundary. To prove this, and the other observations made above, a run was made for the $\hat{\phi} = 29.02$ case doubling the field length to 1000 times the characteristic length, or 10.5×10^{-5} m. Figure 15 shows the dramatic result. The erratic behavior of the charge density lines near the electrode is gone and the slope is essentially zero near the free boundary. The sheath length is measured at about 3.94×10^{-5} m, 2.3 times the characteristic predicted value. It is interesting to note that this is about the same ratio as the measured/predicted ratio of the $\hat{\phi} = 5.80$ case. Figures 16-18 show the two-dimensional plots for this $\hat{\phi} = 29.02$ case.

C. NON-CONSTANT ELECTRON TEMPERATURE

With the addition of the energy equation the effect of Joule heating on the system was studied. The value $\gamma = 100$ was introduced first to simulate combustion gases. The results are shown in Figs. 19-22 for the cases $\hat{\phi} = 5.80$ and 29.02. In spite of the earlier discussion showing that the size of the field is inadequate for the higher potential case, it is used here to avoid the complication of changing the electrode spacing when comparing different potentials.

The most obvious change caused by the heating of the electrons is the changed slope of the potential indicating less shielding for the Joule heating case. This is further shown in Figs. 23 and 24 which represent $\hat{\phi} = 5.80$ and $\gamma = 10^3$. The charge density profiles are relatively

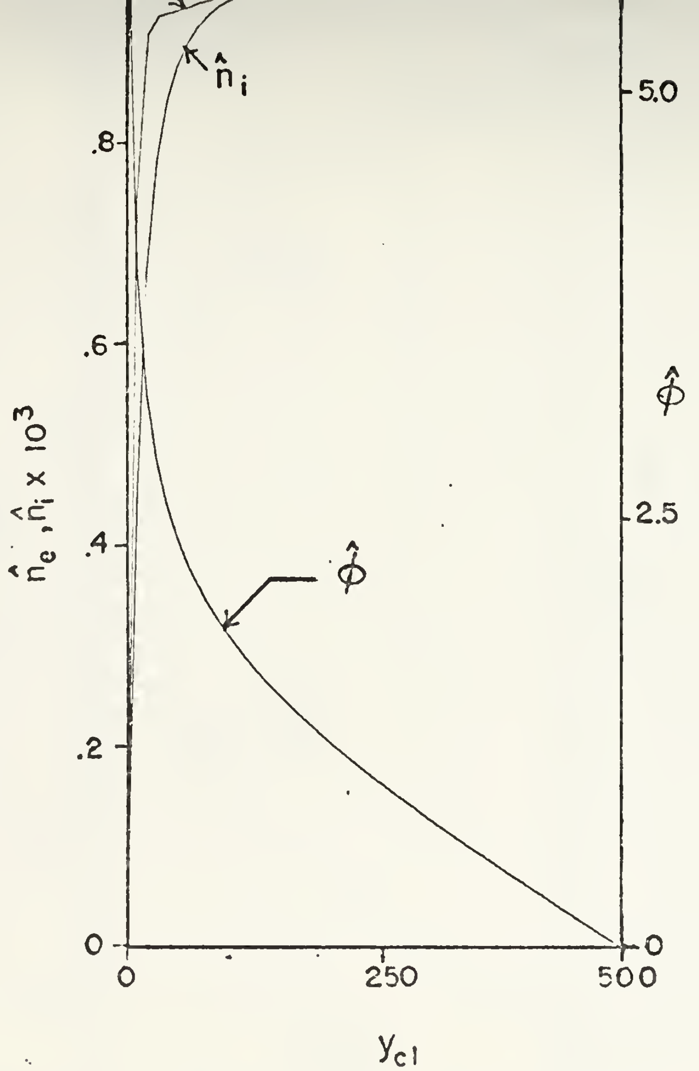

Figure 19. Potential and Charge Density Profile, $\hat{\phi}=5.80$, $\gamma=100$, $\beta=0$, $\hat{n}=10^{-3}$, array size=500L, 51x51 grid.

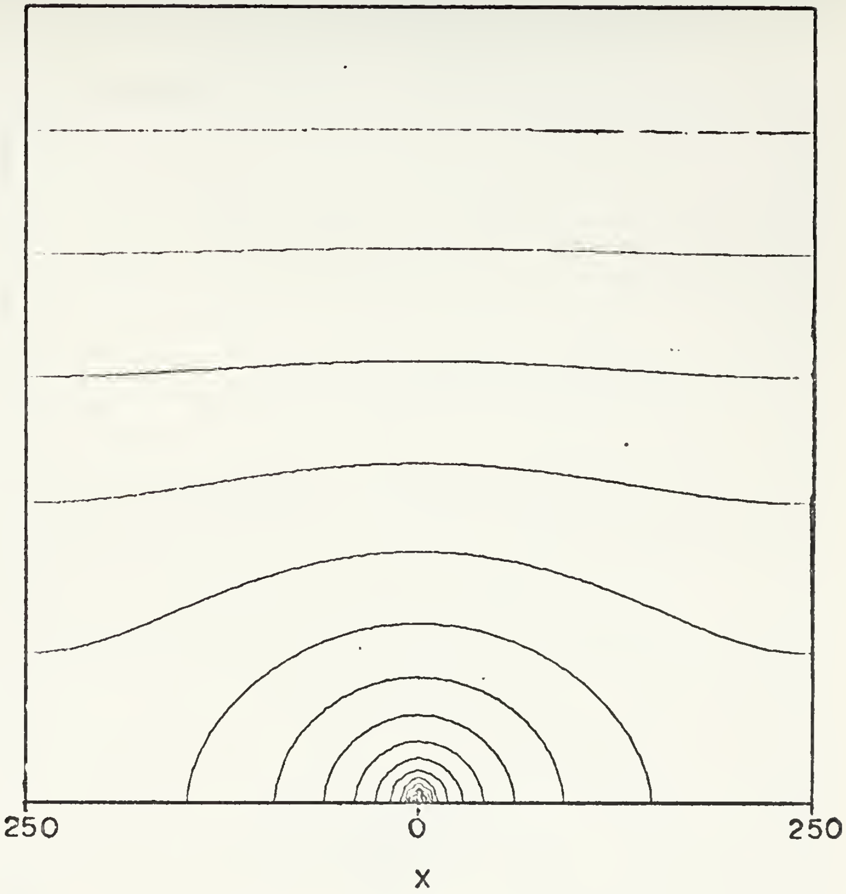

Figure 20. Potential Contour Plot. $\hat{\phi}=5.80$, $\gamma=100$, $\beta=0$, $\hat{n}=10^{-3}$, array size=500L, 51x51 grid.

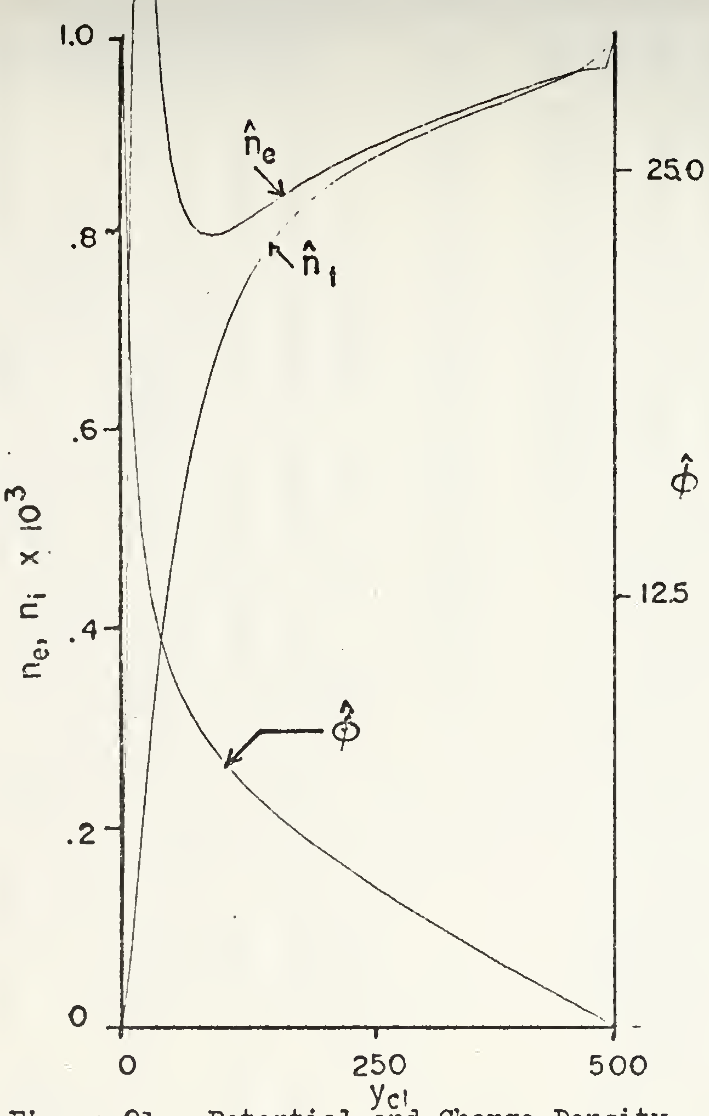

Figure 21. Potential and Charge Density Profile, $\hat{\Phi}=29.0$, $\gamma=100$, $\beta=0$, $n=10^{-3}$, array size=500L, 51x51 grid.

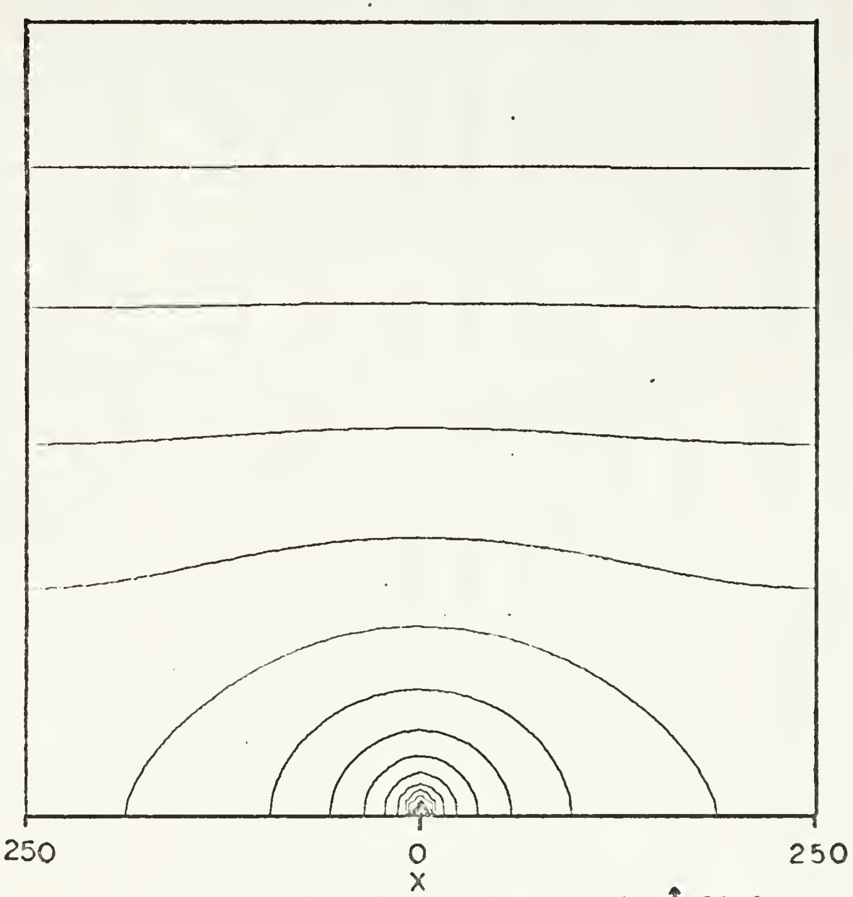

Figure 22. Potential Contour Plot, $\hat{\Phi}=29.0$, $\gamma=100$, $\beta=0$, $\hat{n}=10^{-3}$, array size= 500L, 51x51 grid.

unaffected by the addition of high temperature electrons, in fact there is no observable change in the sheath length.

Figure 25 is the electron temperature profile (T_e/T_o vs. distance from electrode) using the same cut as the previous one-dimensional plots. This plot shows that the majority of the Joule heating occurs very close to the electrode where the largest electric fields exist. There is no noticible electron temperature rise in the ambipolar and free stream regions. This graph is typical of the temperature profiles for the various cases and differs only in the height of the peak near the electrode. This peak appears to be a function of the potential as well as the Joule heating parameter.

From the numerical standpoint, the addition of Joule heating offers a benefit not easily foreseen. Convergence of the system with the addition of the energy equation was accelerated such that errors of less than 2% were achieved in less than 250 iterations. The reason for this improvement is not yet clear but its advantages are obvious. The inclusion of Joule heating is a better approximation for most generators, and provides the bonus of reducing the time of numerical convergence.

D. EFFECT OF EQUILIBRIUM DENSITY

An interesting case is that of increasing the equilibrium charge density to much higher values by changing the boundary value of the electron and ion charge densities. Presented here are the results of setting $\hat{n} = 1$ at the boundary. At a temperature of 2000°K this corresponds to a charge density of 10^{21} particles/m^3. Though not a common case, it serves as an indicator of some of the numerical properties of the method, and a good comparison for the sheath length prediction.

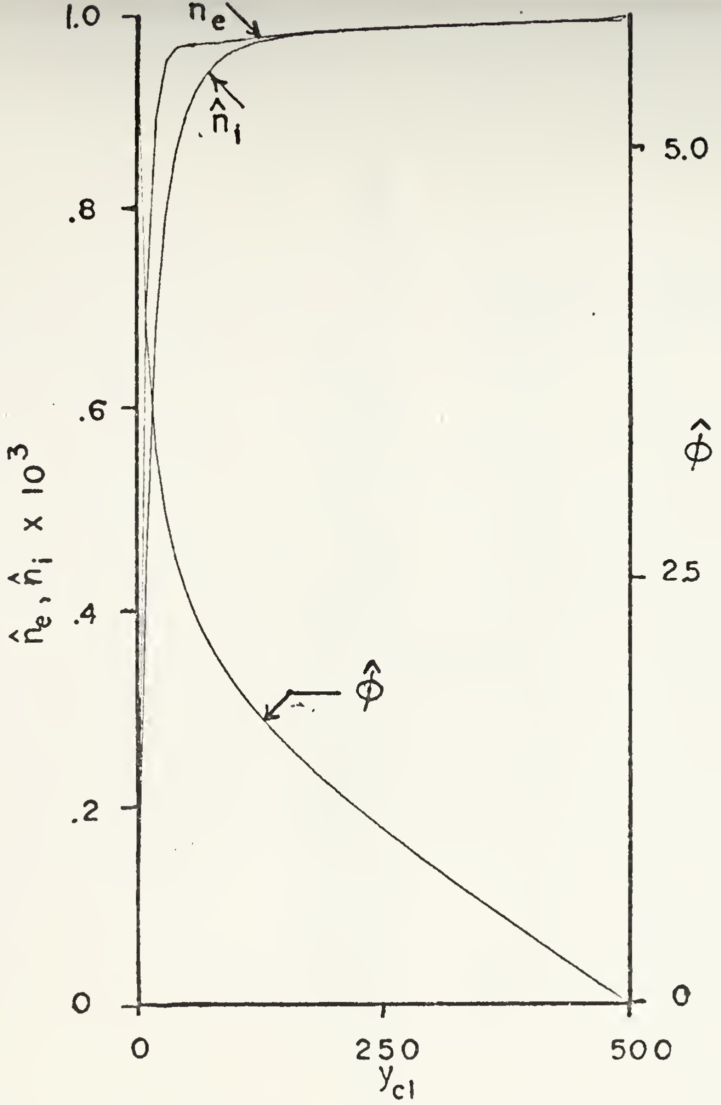

Figure 23. Potential and Charge Density Profile, $\hat{\phi}=5.80$, $\gamma=1000$, $\beta=0$, $\hat{n}=10^{-3}$, array size=500L, 51x51 grid.

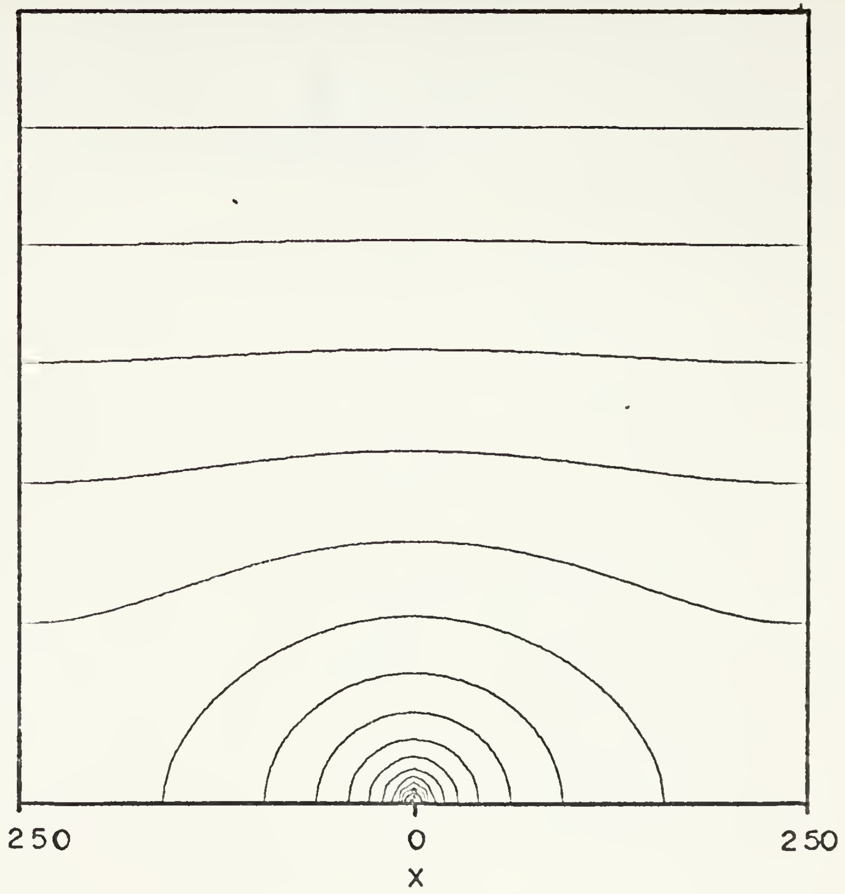

Figure 24. Potential Contour Plot, $\hat{\phi}=5.80$, $\gamma=1000$ $\beta=0$, $\hat{n}=10^{-3}$, array size= 500L, 51x51 grid.

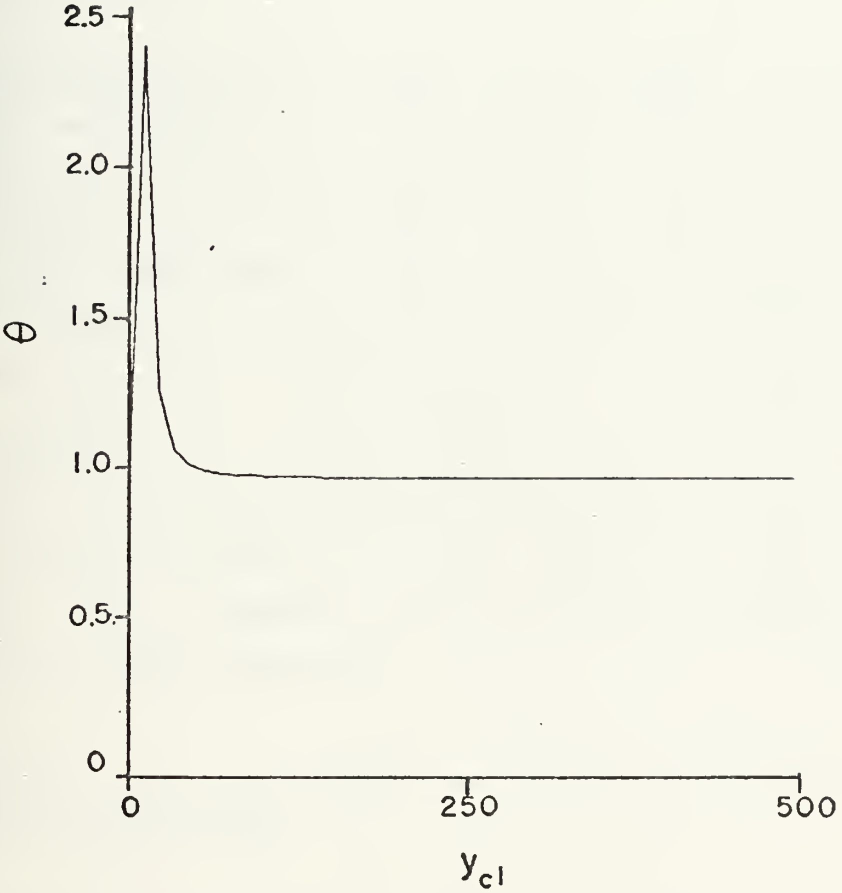

Figure 25. Electron Temperature Profile, $\hat{\phi}$=5.80, γ=100, β=0, $\hat{n}$=10^{-3}, array size=500L, 51x51 grid.

At $T_o = 2000^{o}K$ and for $\hat{\Phi} = 5.80$ and $\hat{n} = 1$ at the boundary, the predicted sheath length from Eq. C.7 is $2.5x10^{-7}$ m. At this same temperature the characteristic length as defined in Eq. 7 is $L = 1.0x10^{-7}$ m. Figures 26 and 27 show the case where the field length is 25L or $2.62x10^{-6}$ m. As expected the sheath length is about 10% of the total field.

The dotted portion of Fig. 27 is drawn to agree with previous arguments on the electrode boundary conditions. Actually, some of these higher density runs were made using a different boundary condition, namely one that attempted to impose a consistent total current through the field. Though erroneous, it was found that this particular boundary condition has little effect on the rest of the field, and that conditions were actually determined by the non-conducting wall surface. The "kinks" seen close to the electrode in several of the one-dimensional plots appear to be a resolution feature of the numerics which tends to override the effects of the charge density boundary condition at the electrode.

E. EFFECT OF THE NUMBER OF ELEMENTS IN THE ARRAY AND ELECTRODE POSITIONING

Earlier trials used a 41x41 array instead of the 51x51 array used later. In general the smaller arrays did not encompass the entire ambipolar region as can be seen in Figs. 28-30 which are for $\hat{n} = 1.0$, $\hat{\phi} = 11.6$, and array size = 20L, 25L, and 35L, respectively, in 41x41 arrays. They seem to lack sufficient room to satisfy the equations even after varying the mesh size.

Figures 28-30 also show the changes that occur when the mesh size is changed. The sheath length appears to be

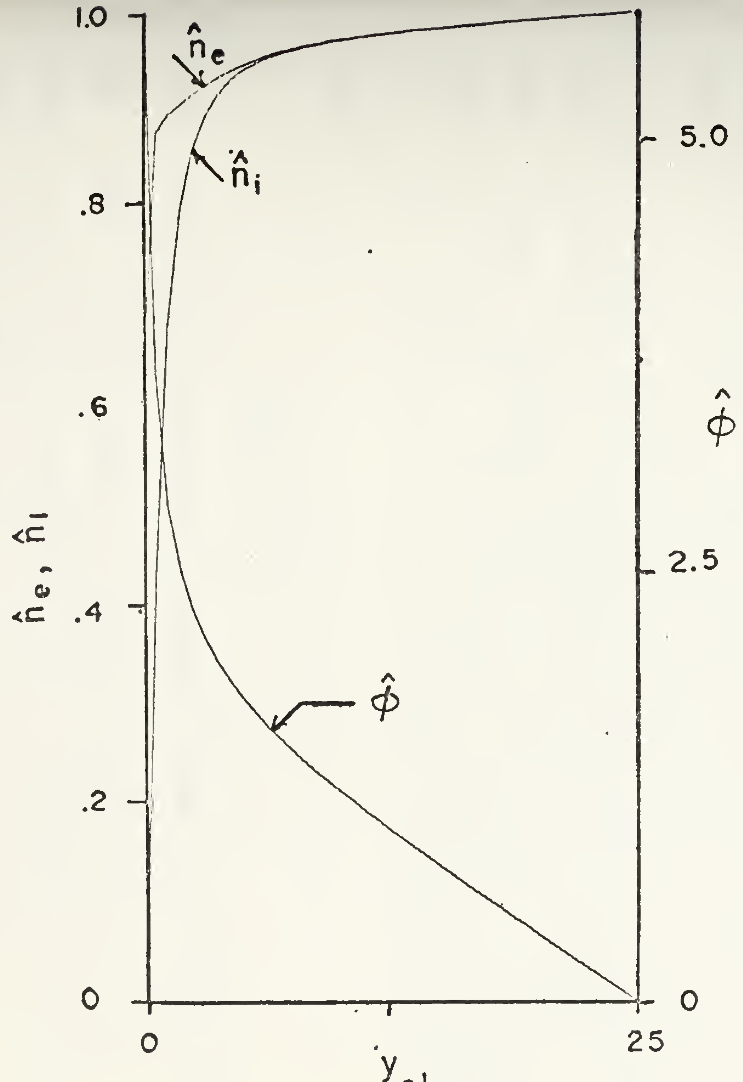

Figure 26. Potential and Charge Density Profile, $\hat{\phi}$=5.80, γ=0, β=0, $\hat{n}$=1, array size=25L, 51x51 grid.

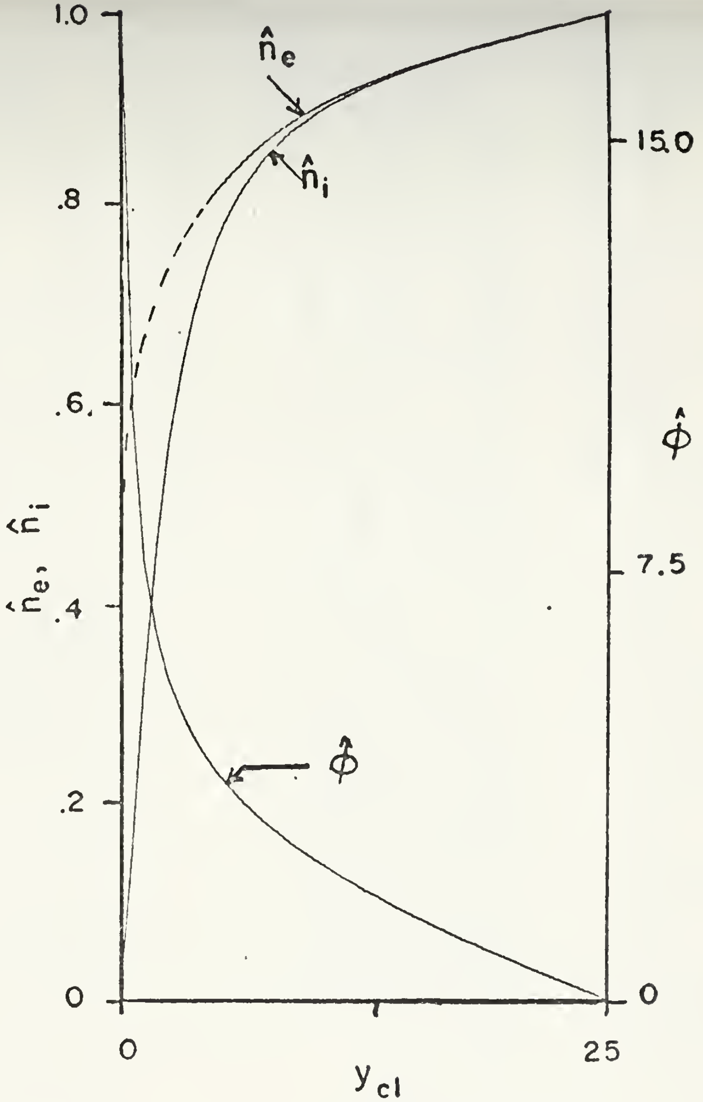

Figure 27. Potential and Charge Density Profile, $\hat{\phi}$=17.4, γ=0, β=0, $\hat{n}$=1, array size=25L, 51x51 grid.

consistent with the scaling, but the ambipolar slope does not appear to change, indicating the inadequacy of mesh-sizing to control the size of the field when the number of elements is too low.

For a qualitative look at a multiple electrode plot, Figs. 31-33 are provided. This scheme allows a current density comparison of this run with one of lower potential and the necessary symmetry in the absence of a magnetic field. Current profiles will be considered later.

F. MAGNETIC FIELD EFFECTS

The introduction of a magnetic field induces the most visible, although not unexpected, effects of all the phenomena discussed so far. As might be anticipated, the symmetry of the field is lost as shown in Figs. 34-43. Notice however, that while the potential shows significant distortion, the charge densities do not, at least for the case of $\hat{\phi} = 5.80$.

The angle of incidence of the potential contours with the insulated wall is approximately the complement of the Hall angle (arctangent β) as can be seen in Fig. 35 (45°) and Fig 43 (27°). This is easily understood by solving Eq. 24 with $J_y = 0$ and considering only conduction effects. The result is

$$\frac{\partial \hat{\phi}}{\partial y} \Bigg/ \frac{\partial \hat{\phi}}{\partial x} = - \beta \qquad (45)$$

This equation says that at points where $J_y = 0$ and diffusion is small, the slope of the potential lines is $-\beta$. In the vicinity of the electrode where diffusion plays a more significant part the slope begins to deviate.

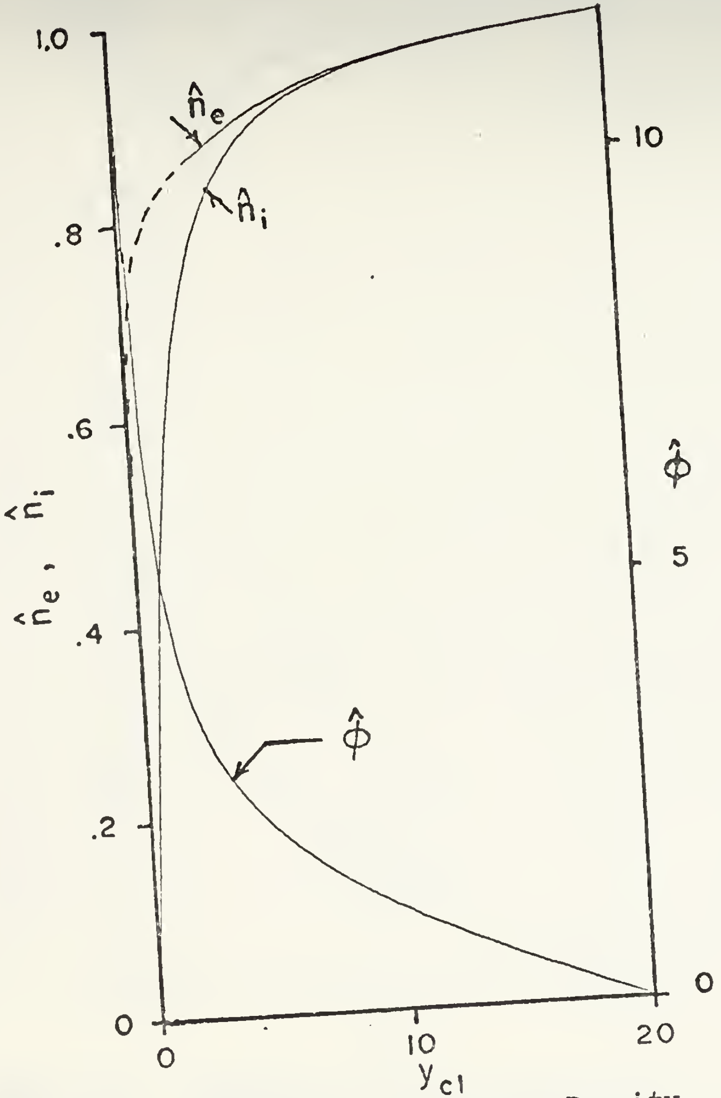

Figure 28. Potential and Charge Density Profile, $\hat{\phi}$=11.6, γ=0, β=0, $\hat{n}$=1, array size=20L, 41x41 grid.

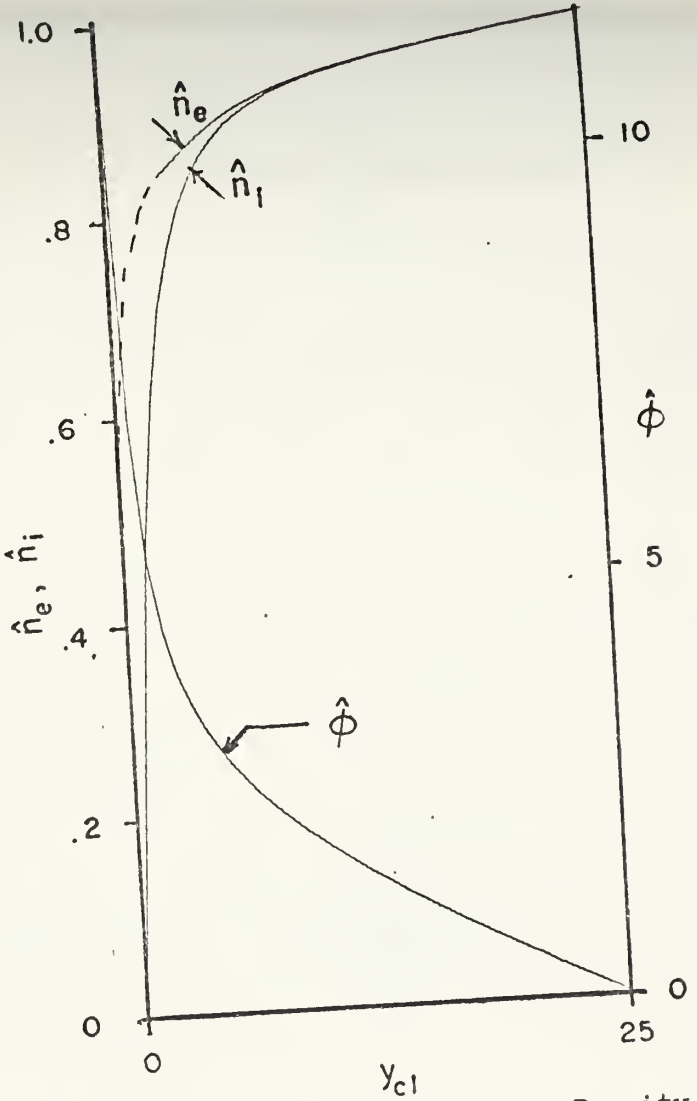

Figure 29. Potential and Charge Density Profile, $\hat{\phi}$=11.6, γ=0, β=0, $\hat{n}$=1, array size=25L, 41x41 grid.

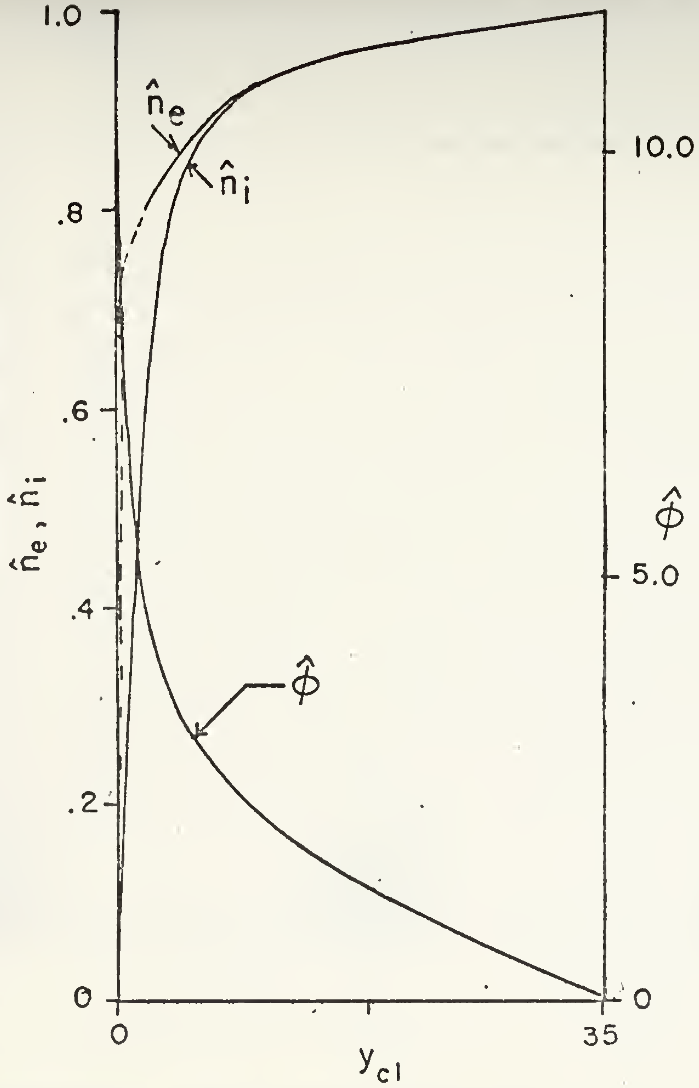

Figure 30. Potential and Charge Density Profile, $\hat{\phi}=11.6$, $\gamma=0$, $\beta=0$, $\hat{n}=1$, array size=35L, 41x41 grid.

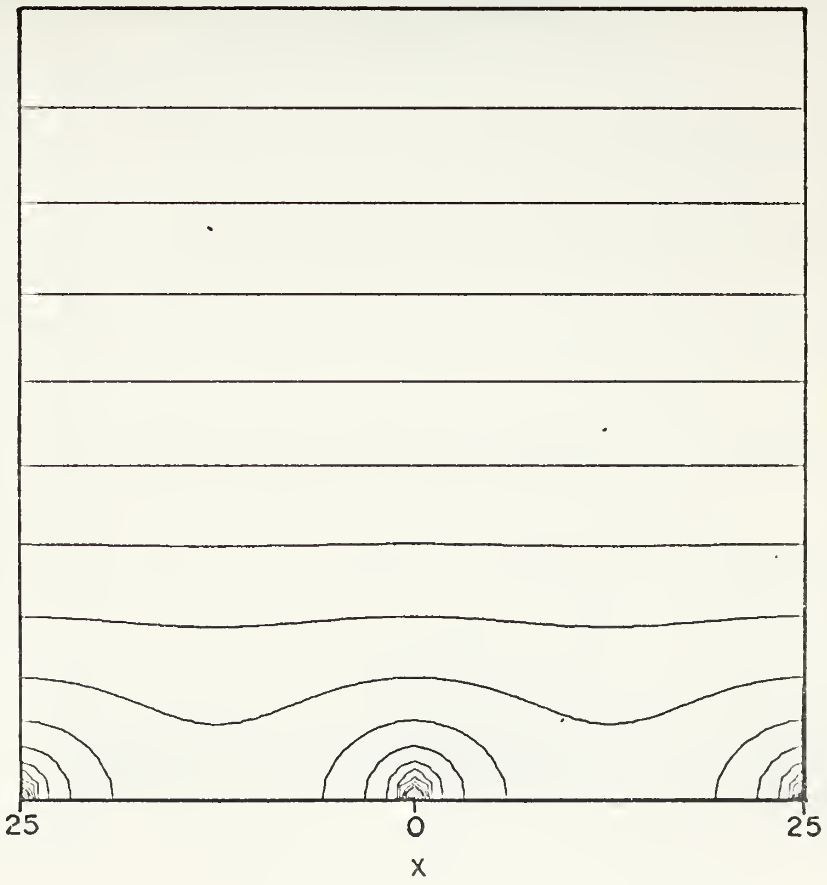

Figure 31. Potential Contour Plot, $\hat{\phi}=29.0$, $\gamma=0$, $\beta=0$, $\hat{n}=1$, array size=50L, 41x41 grid.

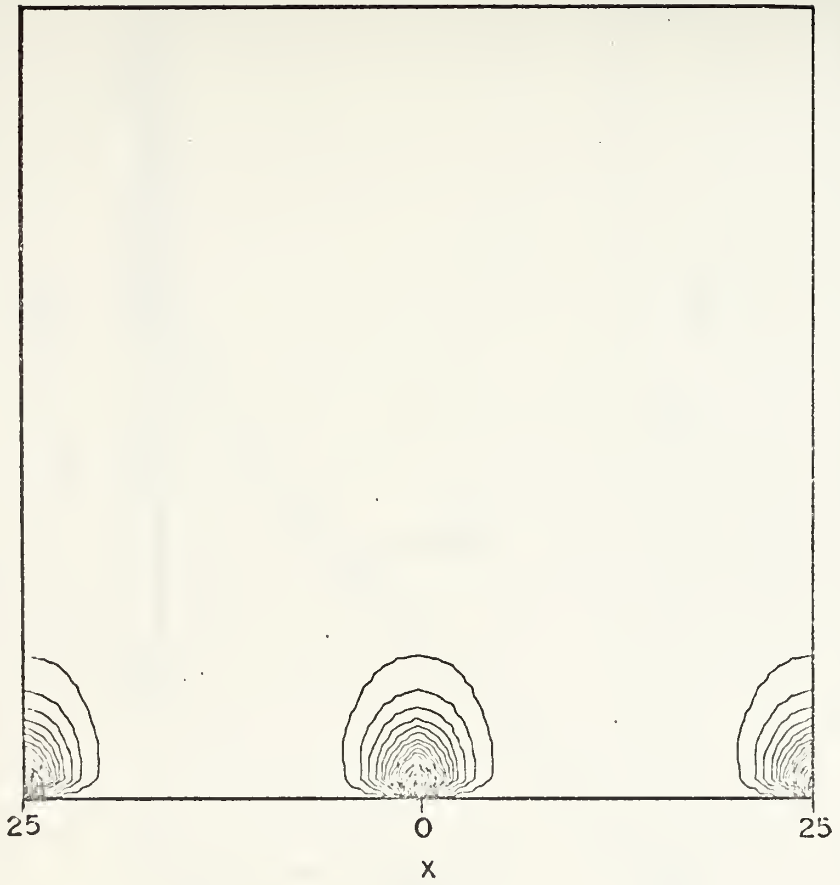

Figure 32. Space Charge Plot ($\hat{n}_i-\hat{n}_e$) for multiple electrodes, $\hat{\Phi}=29.0$, $\gamma=0$, $\beta=0$, $\hat{n}=1$, array size=50L, 41x41 grid.

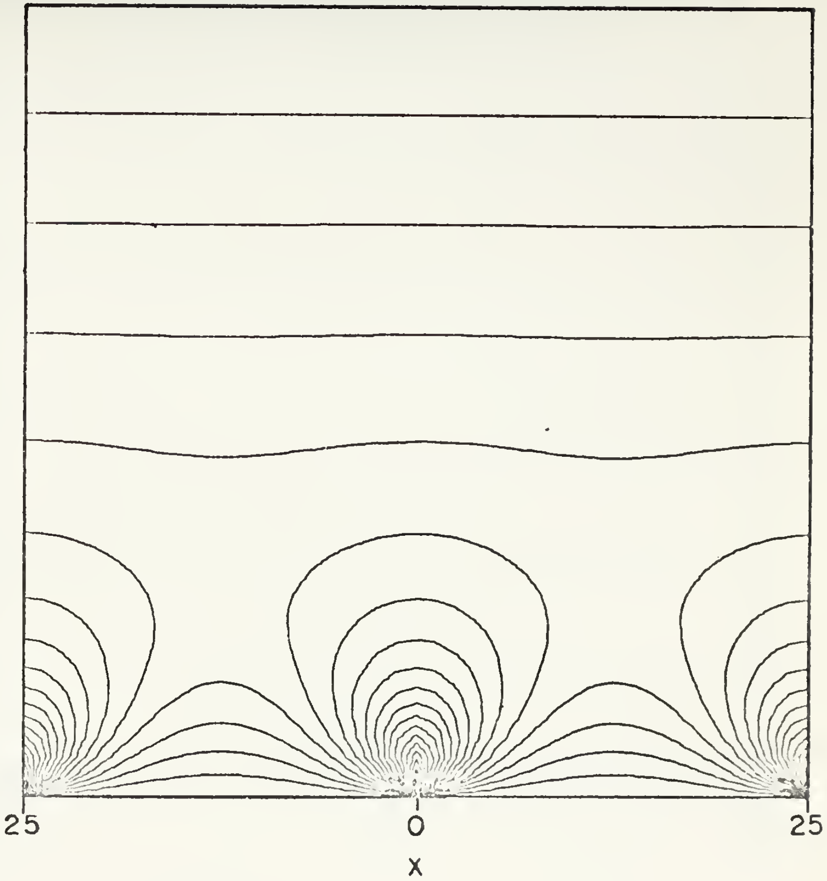

Figure 33. Total Charge Plot ($\hat{n}_i+\hat{n}_e$) for multiple electrodes, $\hat{\Phi}=29.0$, $\gamma=0$, $\beta=0$, $\hat{n}=1$, array size=50L, 41x41 grid.

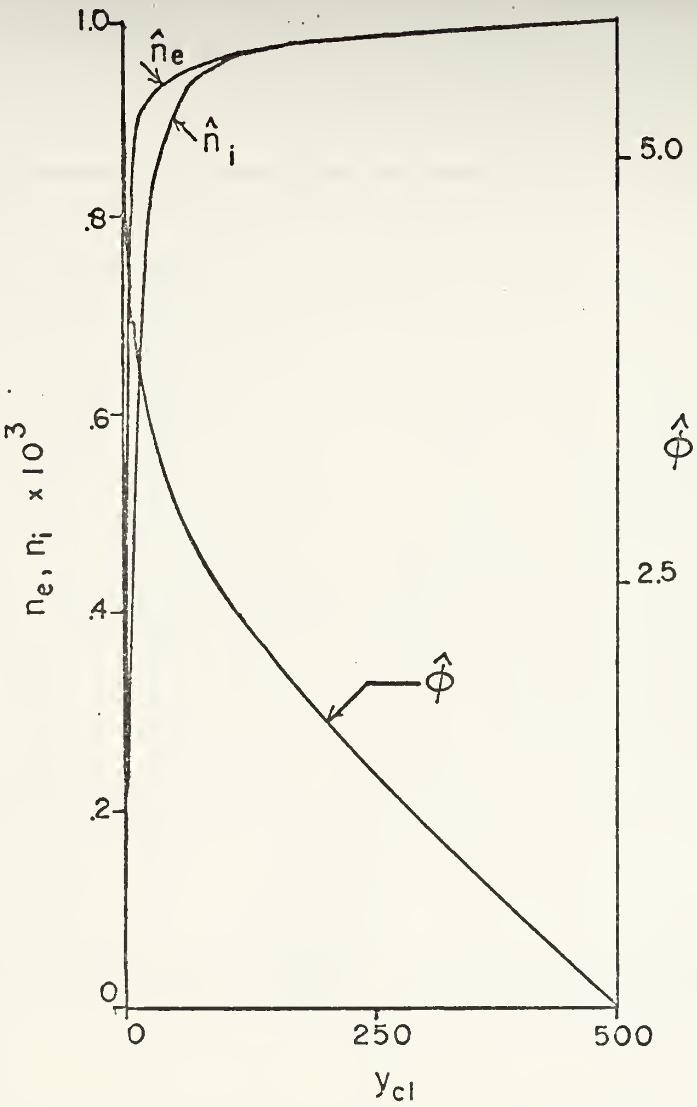

Figure 34. Potential and Charge Density Profile, $\hat{\phi}=5.80$, $\gamma=0$, $\beta=1$, $\hat{n}=10^{-3}$ array size=500L, 51x51 grid.

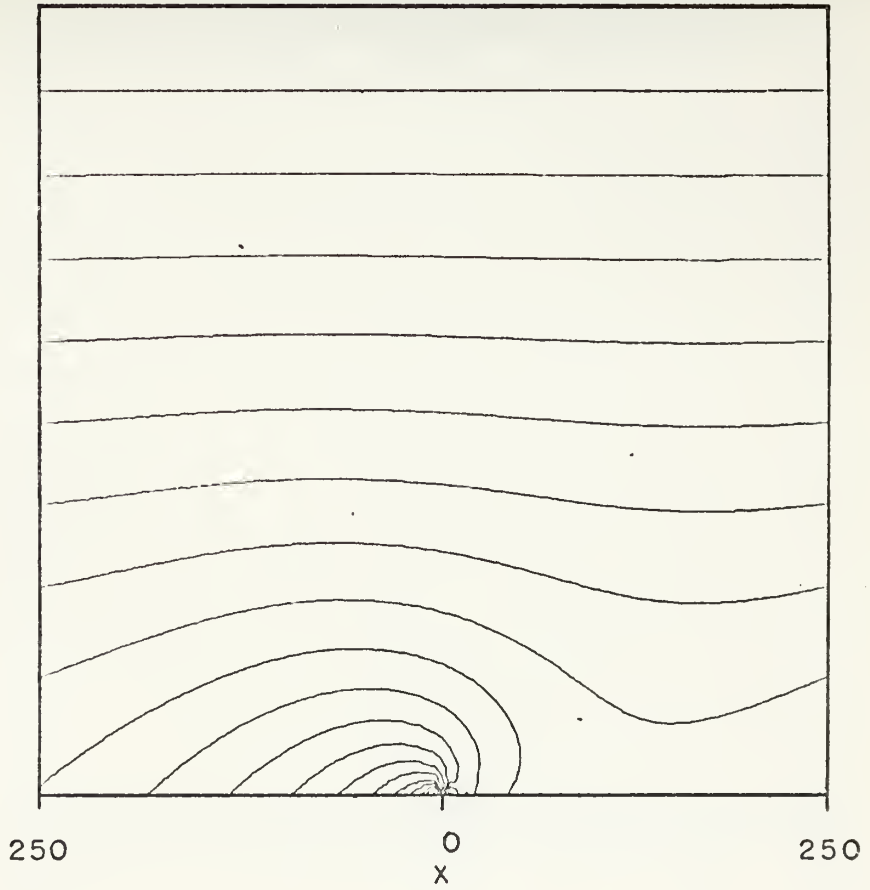

Figure 35. Potential Contour Plot, $\hat{\phi}=5.80$, $\gamma=0$, $\beta=1$, $\hat{n}=10^{-3}$, array size= 500L, 51x51 grid.

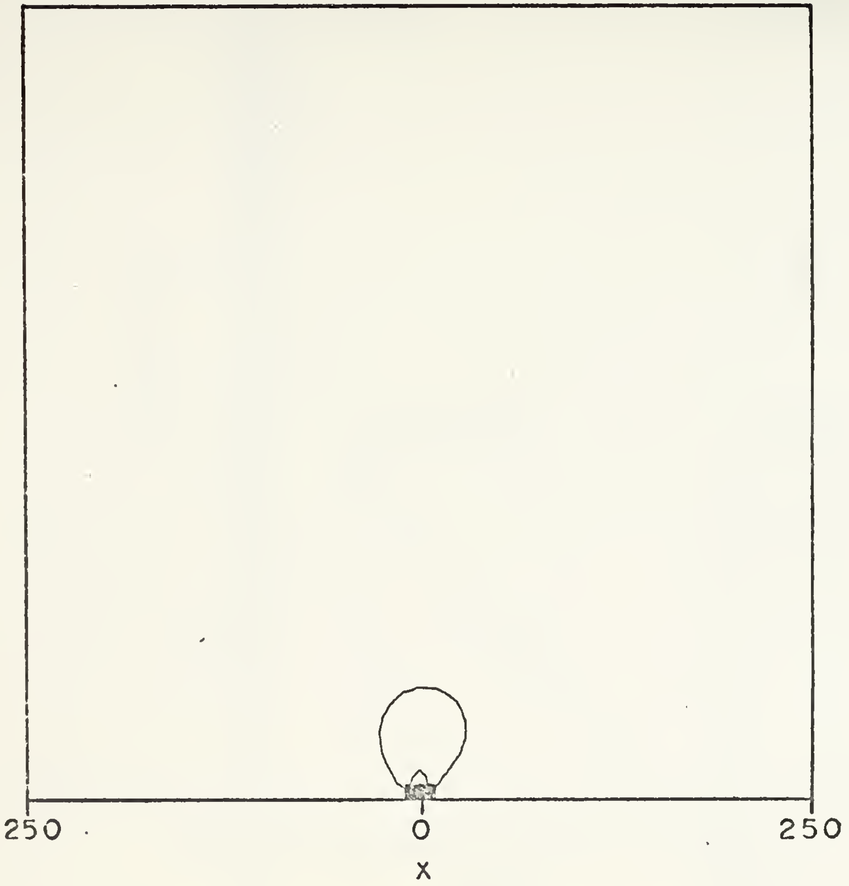

Figure 36. Electron Density Contour Plot, $\hat{\phi}=5.80, \gamma=0, \beta=1, \hat{n}=10^{-3}$, array size=500L, 51x51 grid.

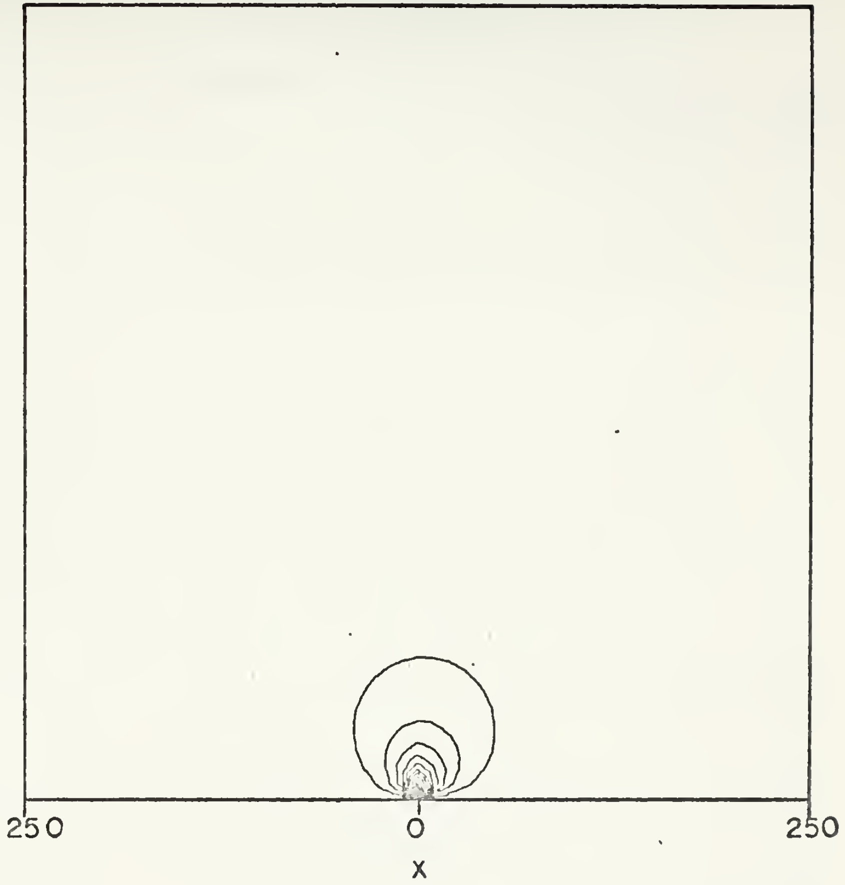

Figure 37. Ion Density Contour Plot, $\hat{\phi}=5.80$, $\gamma=0, \beta=1, \hat{n}=10^{-3}$, array size=500L, 51x51 grid.

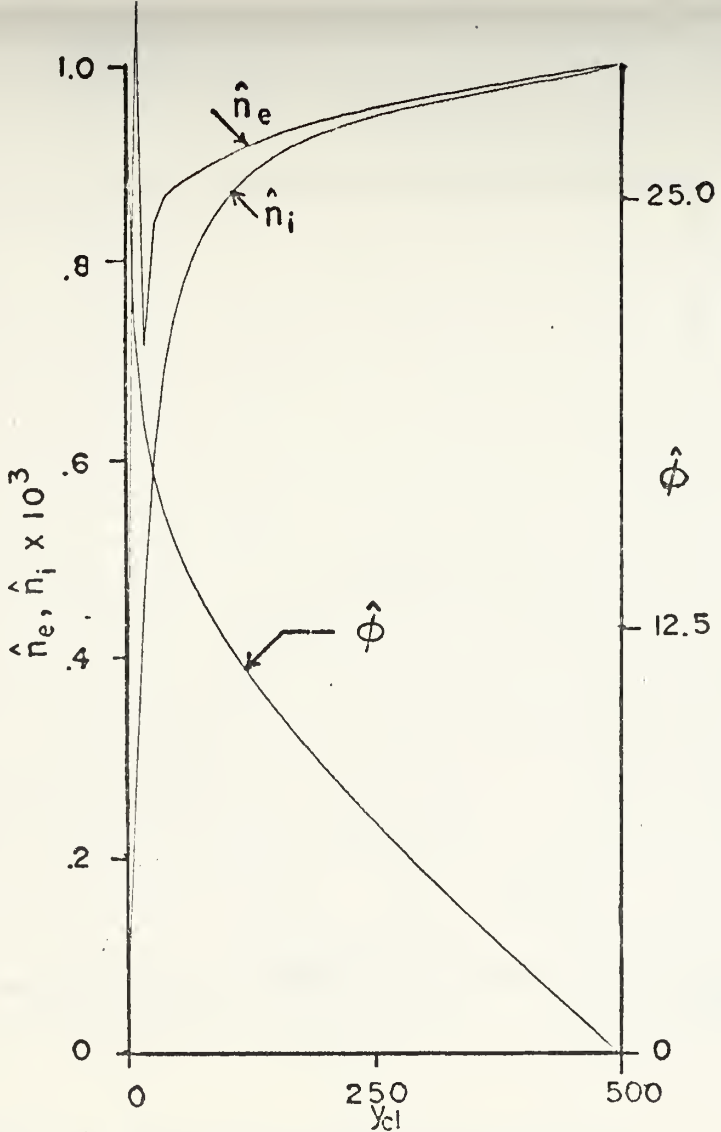

Figure 38. Potential and Charge Density Profile, $\hat{\phi}=29.0$, $\gamma=0$, $\beta=1$, $\hat{n}=10^{-3}$, array size=500L, 51x51 grid.

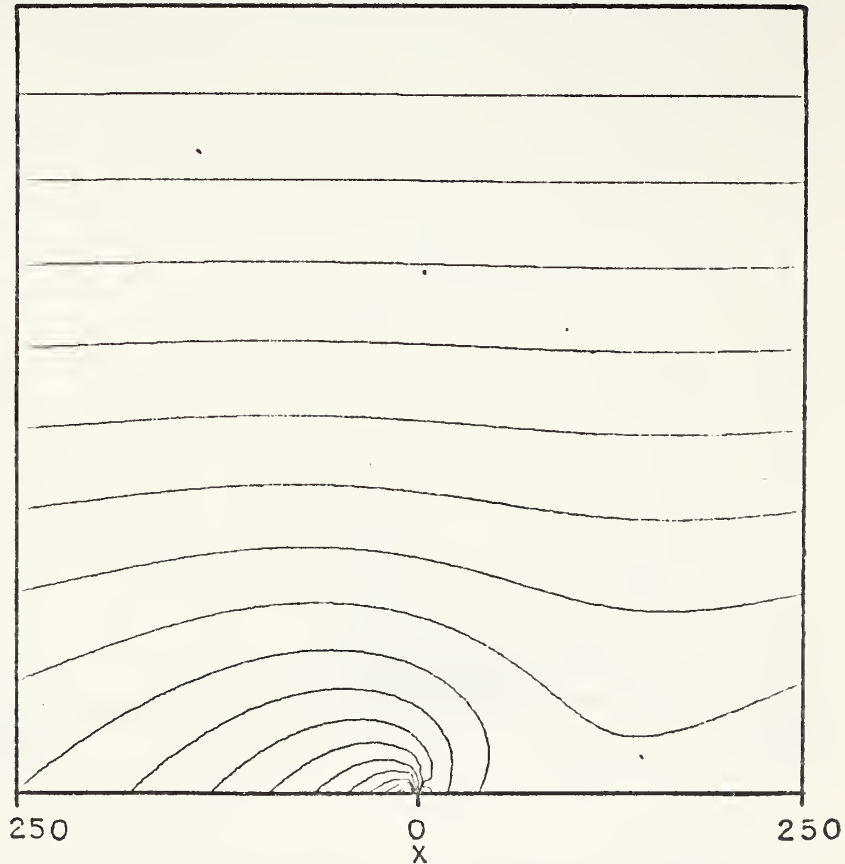

Figure 39. Potential Contour Plot, $\hat{\phi}=29.0$, $\gamma=0$, $\beta=1$, $\hat{n}=10^{-3}$, array size=500L, 51x51 grid.

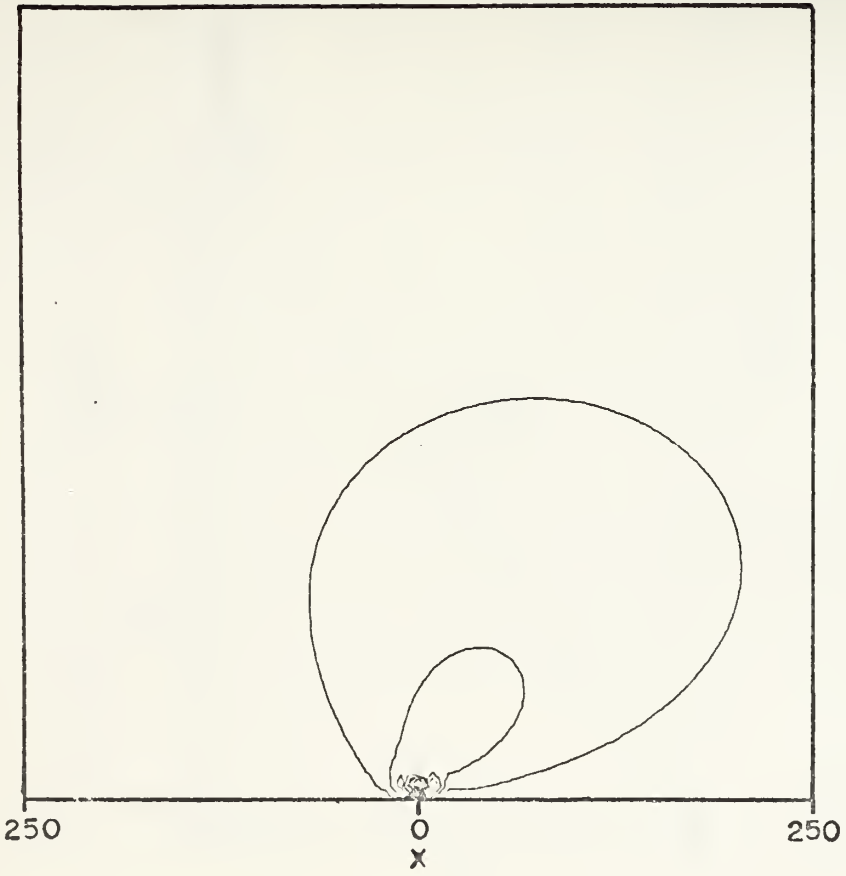

Figure 40. Electron Density Contour Plot, $\hat{\phi}=29.0$, $\gamma=0$, $\beta=1$, $\hat{n}=10^{-3}$, array size=500L, 51x51 grid.

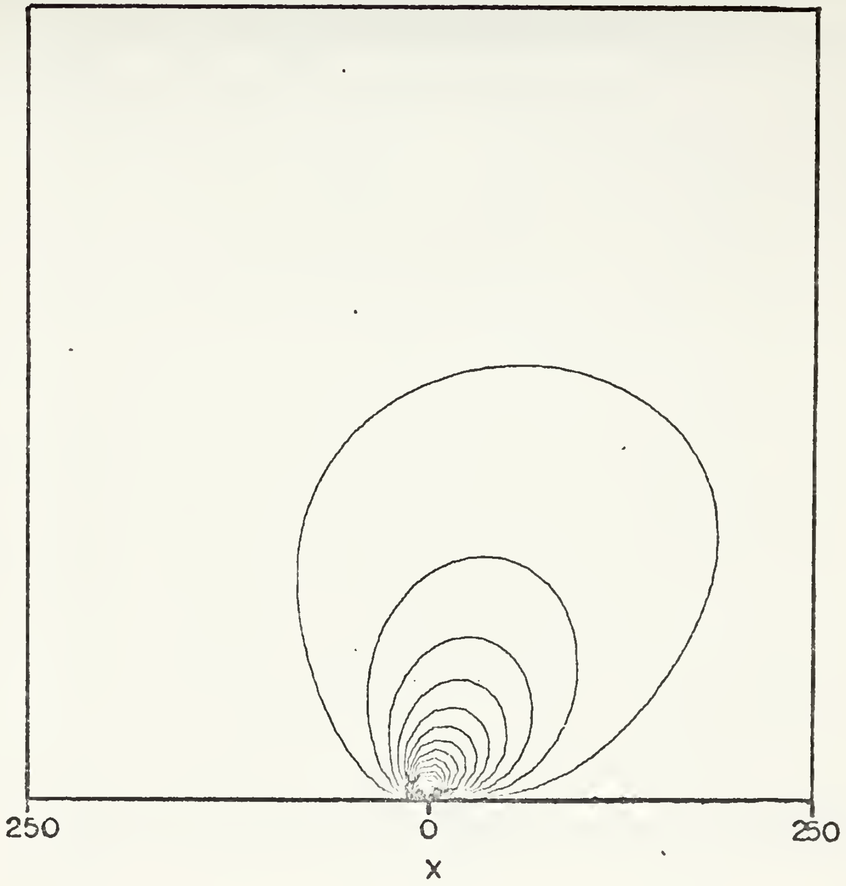

Figure 41. Ion Density Contour Plot, $\hat{\phi}=29.0$, $\gamma=0$, $\beta=1$, $\hat{n}=10^{-3}$, array size=500L, 51x51 grid.

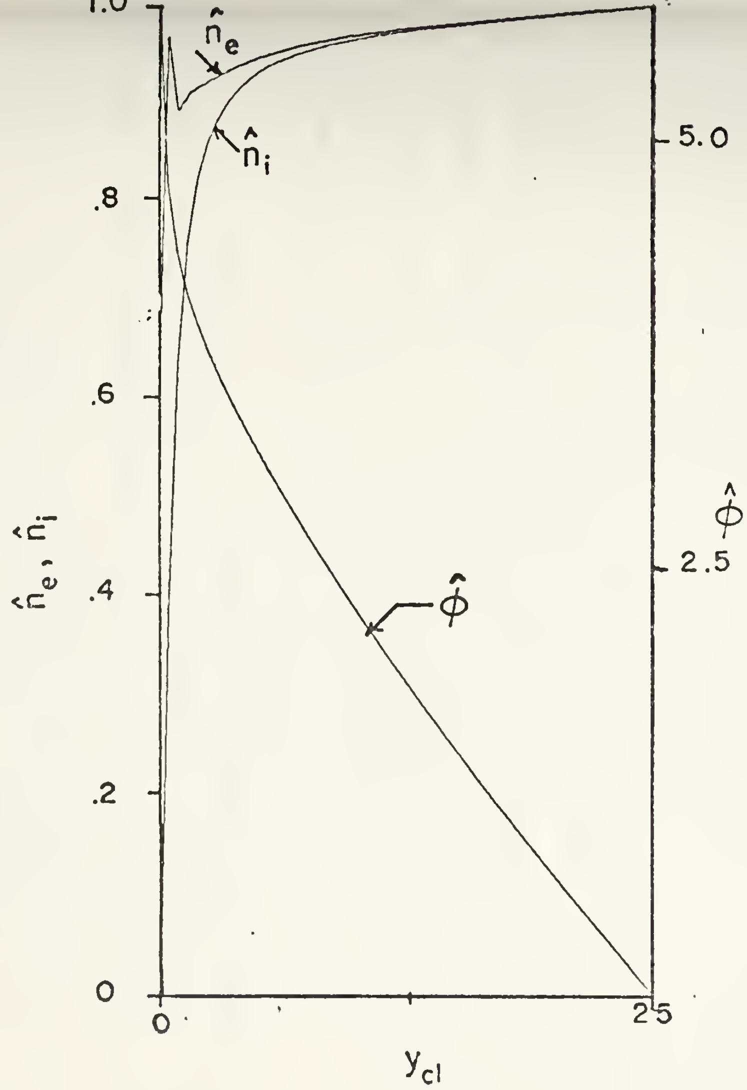

Figure 42. Potential and Charge Density Profile, $\hat{\phi}=5.80$, $\gamma=0$, $\beta=2$, $\hat{n}=1$, array size=25L, 51x51 grid.

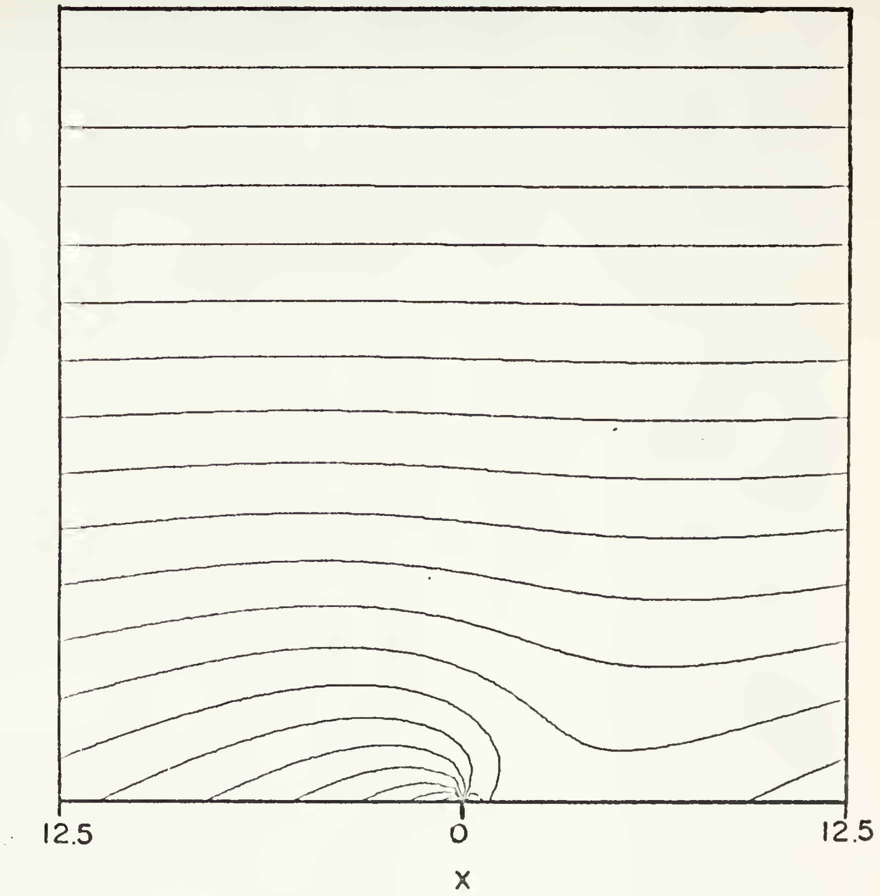

Figure 43. Potential Contour Plot, $\hat{\phi}=5.80$, $\gamma=0$, $\beta=2$, $\hat{n}=1$, array size=25L, 51x51 grid.

As with the runs in the absence of a magnetic field the effects of the presence of a point electrode are dampened as the free boundary is approached. The magnetic field produces little or no distortion to symmetry outside the sheath.

G. CURRENT PROFILES

For each of the previous runs a complete two-dimensional current distribution can be made using the potential and charge density distributions. The current lines make an angle with the potential contour lines approximately equal to the Hall angle and would theoretically be exact except for the effects of diffusion. Figures 44 and 45 show the current streamlines in the field for $\hat{\phi} = 5.80$ and $\beta = 0$ and 1, respectively. These were sketched from numerical data from the "Current Program" which gives the current in vector form. The streamlines entering the field from the right are from the active site that lies periodically to the right of the one in the field.

To determine the total current flowing through the system it is necessary to look some distance from the electrode. Theoretically, for this model the density of the current will vary from some given value at the free stream to infinity at the electrode, however, as explained for the case of charge density a "smearing" takes place due to the numerical approximation.

In terms of the amount of information available, Figs. 46 through 48 are the most important in this work. They are the current-voltage diagrams for the charge densities $\hat{n} = 10^{-3}$ and $\hat{n} = 1$. The dimensionless current density was taken one or two stations from the free boundary (in order to avoid numerical errors at the boundary) and represents

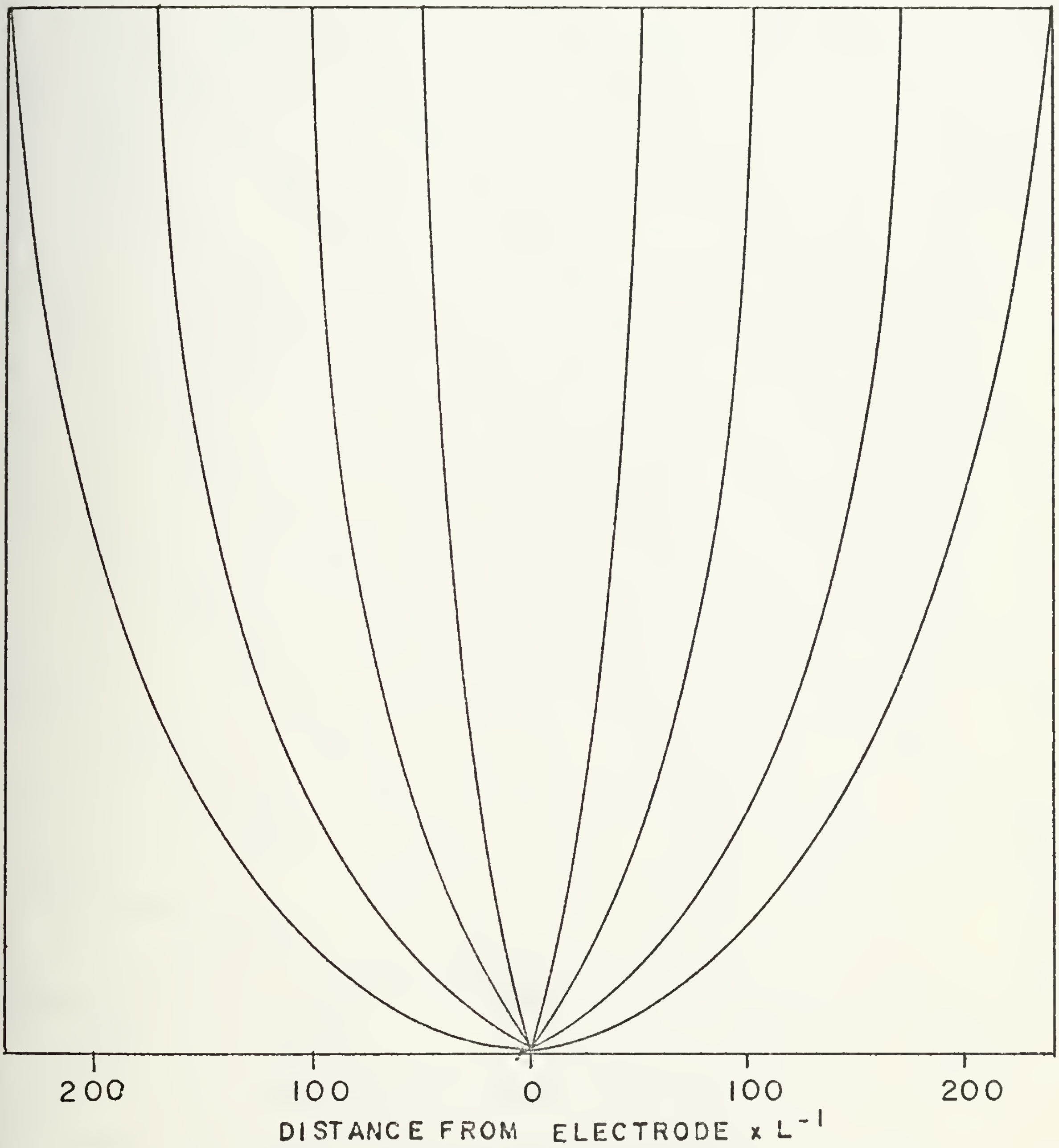

Figure 44. Current Density Contour Plot, $\hat{\phi}=5.80, \gamma=0, \beta=0$, $\hat{n}=10^{-3}$, array size=500L, 51x51 grid.

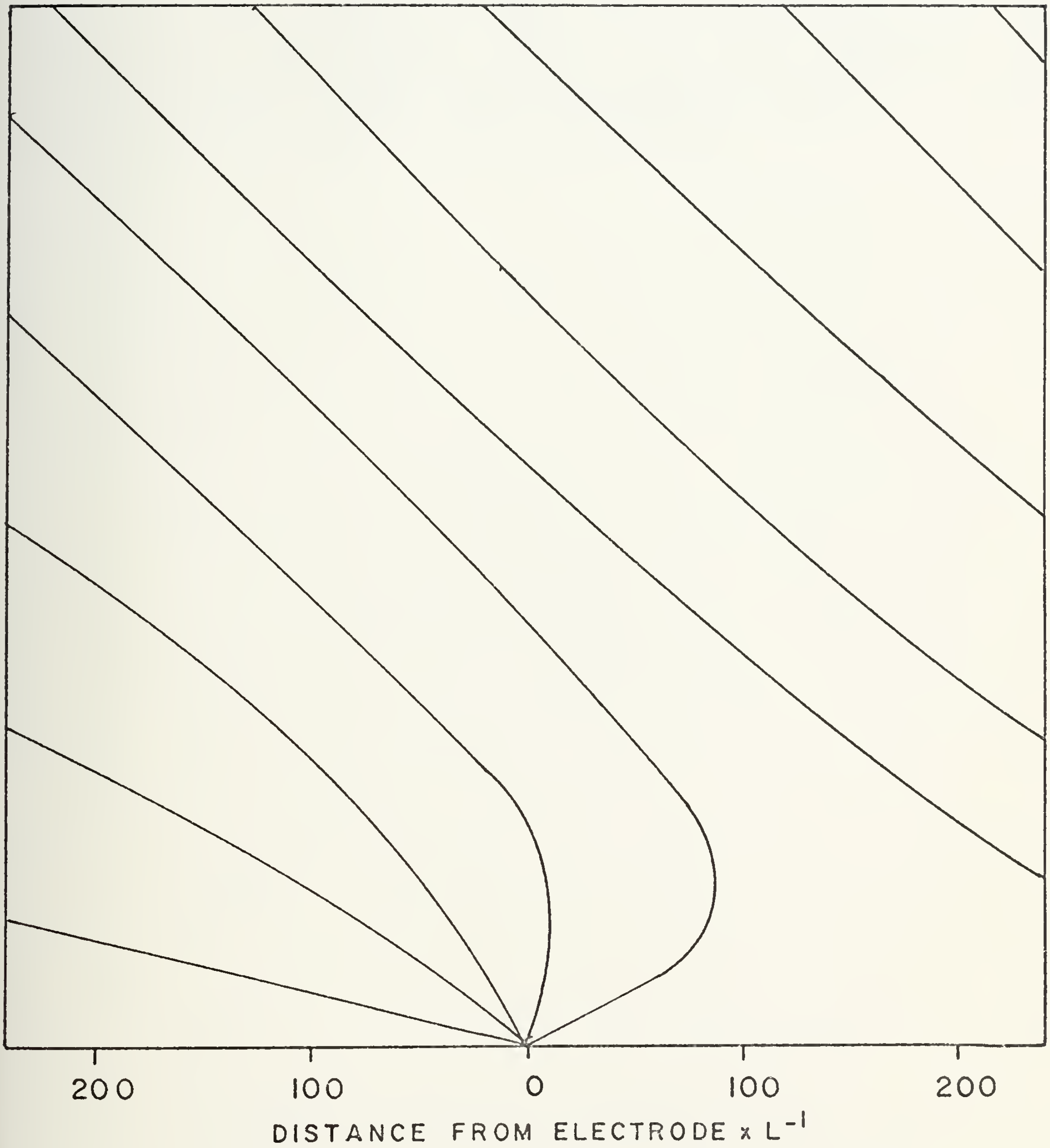

Figure 45. Current Density Contour Plot, $\hat{\phi}=5.80, \gamma=0, \beta=1$, $\hat{n}=10^{-3}$, array size=500L, 51x51 grid.

the macroscopic current that would be observed in a two-dimensional model. The non-dimensionalization of the current was consistent with Eqs. 7 and 11 and contain the term $(1+\beta^2)$. The conductivity was introduced to replace the mobility, and constant terms were collected to give the simplified coefficient shown in the figures. An interpretation of these results as well as examples of their use is given in Section V as conclusions.

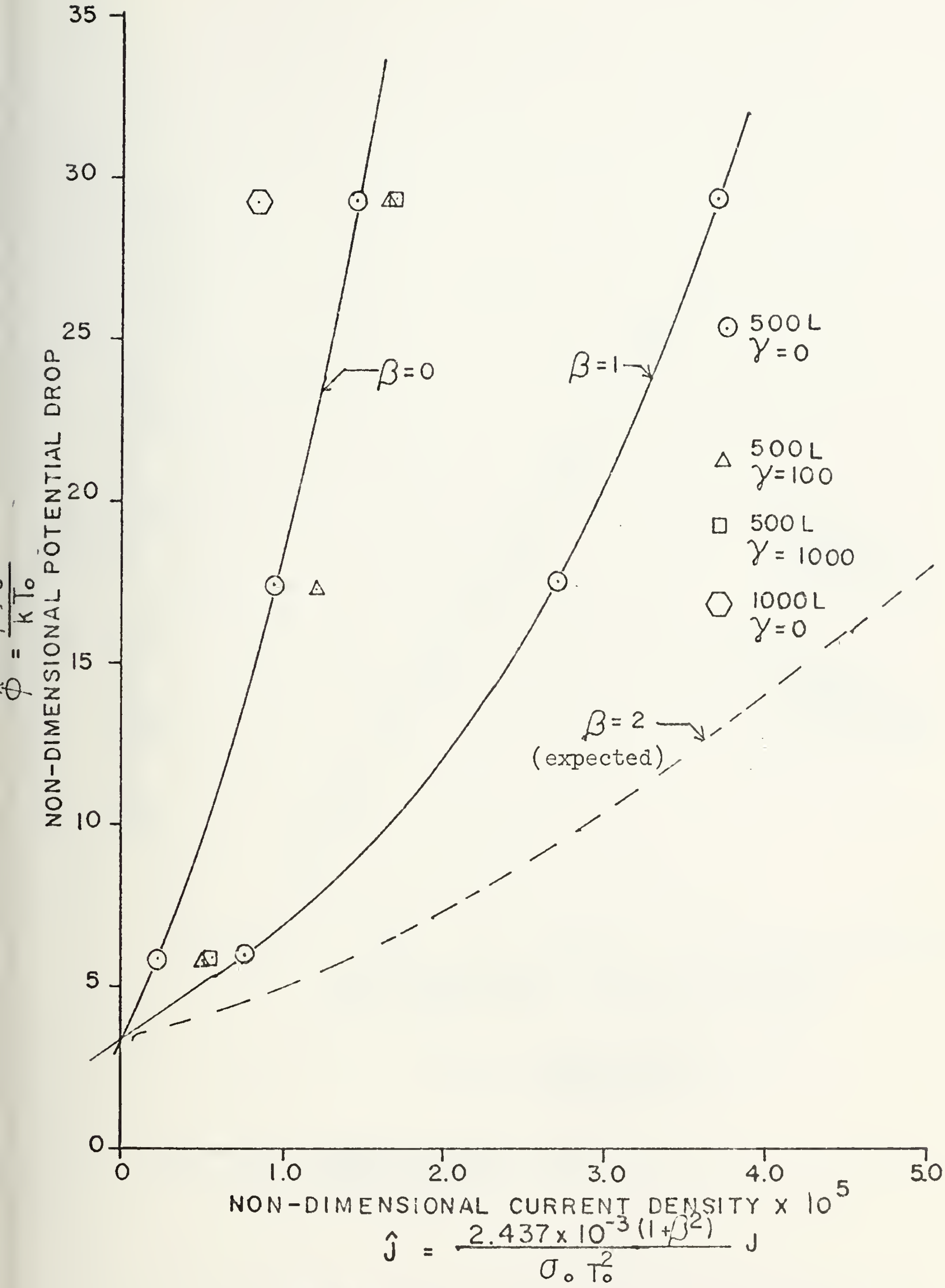

Figure 46. Current-Voltage Diagram, $\hat{n}=10^{-3}$, 51x51 grid.

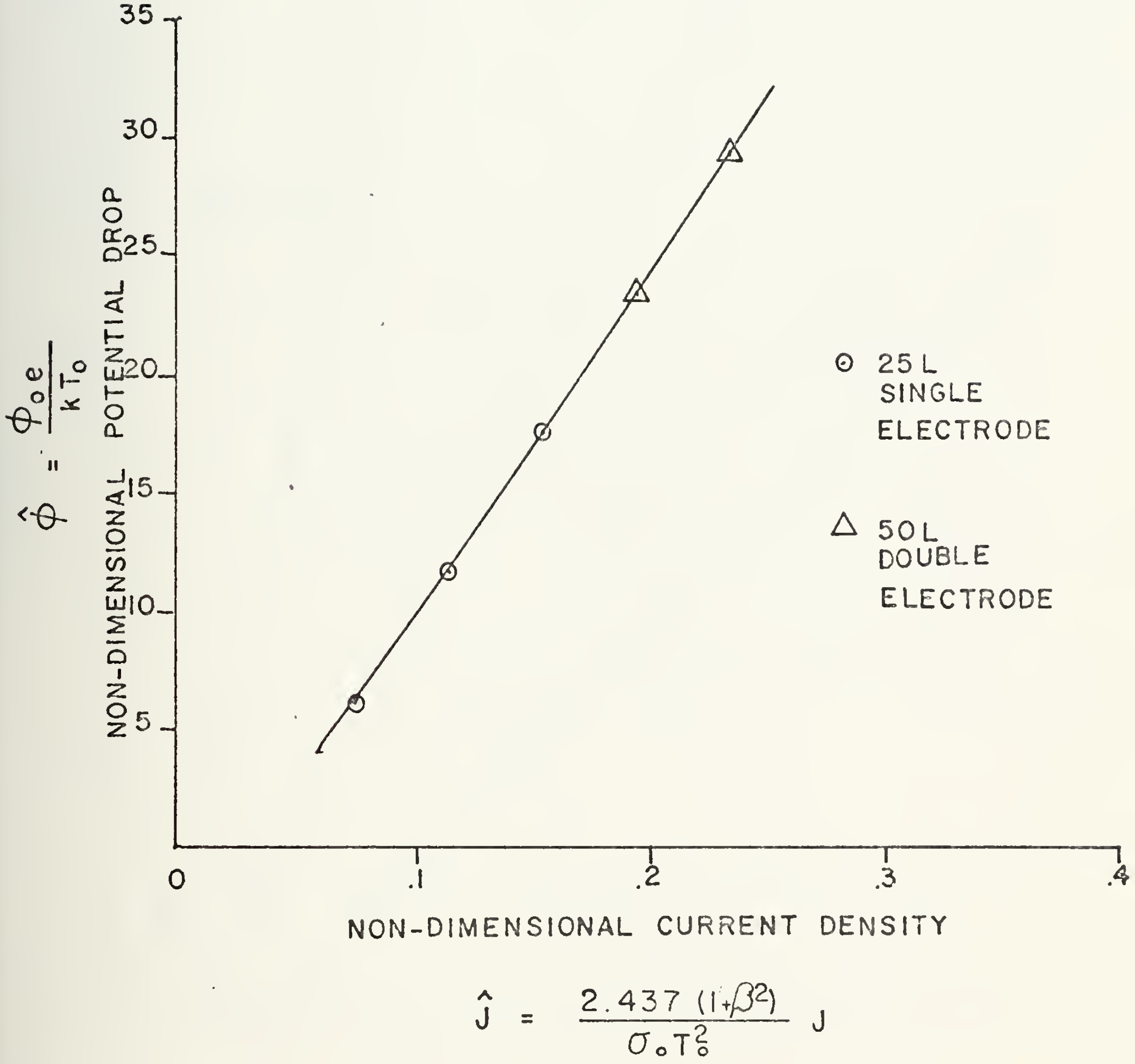

Figure 47. Current-Voltage Diagram, $\hat{n}=1$, 41x41 grid.

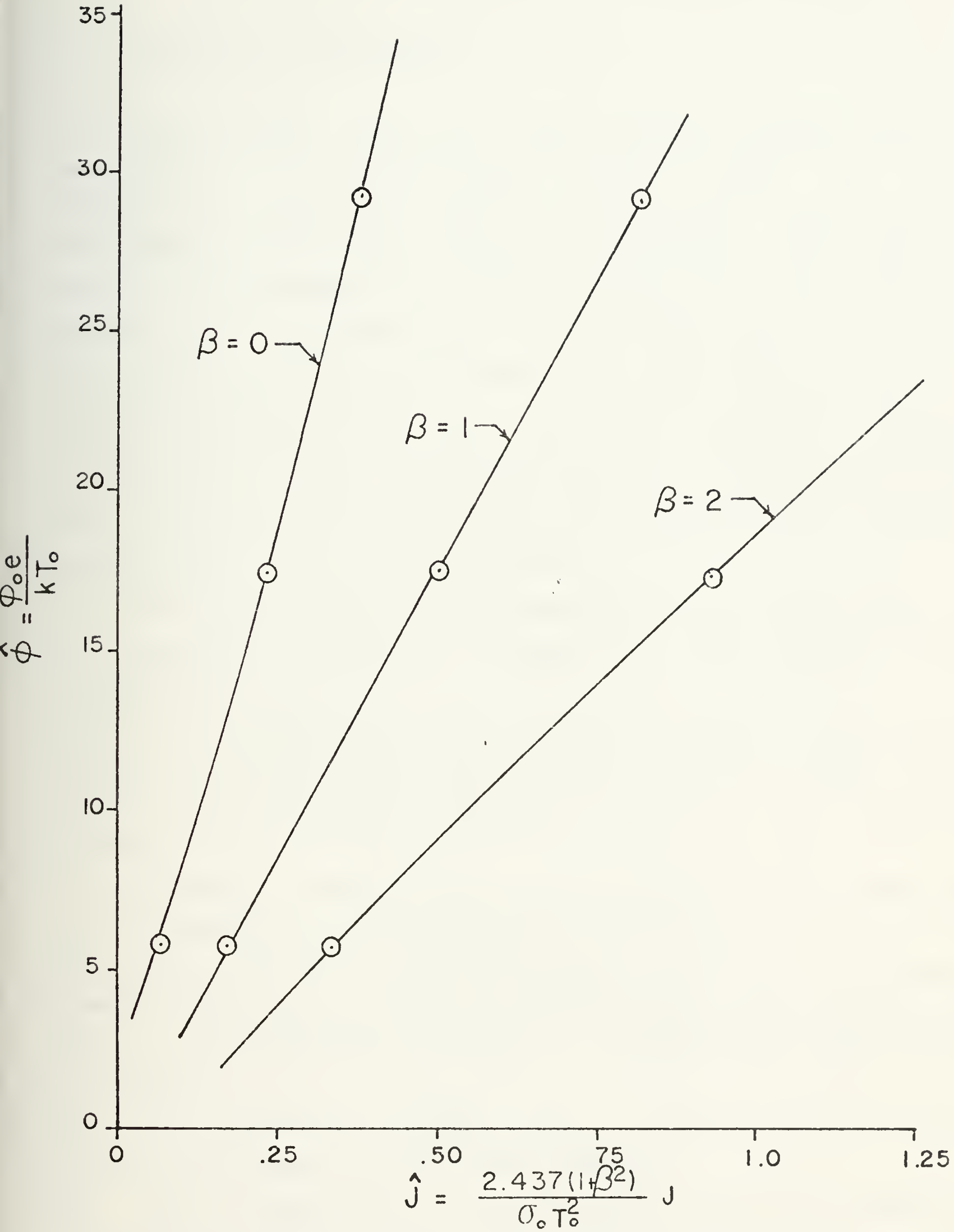

Figure 48. Current-Voltage Diagram, $\hat{n}=1$, 51x51 grid.

V. CONCLUSIONS AND RECOMMENDATIONS

A. PHYSICAL CONCLUSIONS

A successful model of the sheath evolved from the assumptions of steady state, frozen flow, and uniform temperature for neutral and ion particles. Qualitatively, the results of the analysis used in this work offer much insight into voltage drops attributable to electrodes in contact with an MHD plasma. Quantitatively, these results are useful if it is remembered that the model is two-dimensional and does not give the additional degree of freedom for current expansion afforded by three dimensions. A summary of the more basic conclusions which were drawn from the results is presented here. They will be explained individually later in this section.

1. The sheath can be self-generated from a consistent set of equations with or without the use of an energy equation.
2. The electrode node boundary condition for charged particle density has little effect upon the field, while the insulated wall boundary condition has a profound effect.
3. Current constrictions are necessary at the electrode to satisfy the system of equations.
4. The resulting current-voltage diagram has a curvature consistent with theoretical predictions for space-charge in a one-dimensional flow of current and experimental evidence.
5. The current density, for a given potential drop, varies inversely as the node spacing.
6. The conductivity of the plasma within the sheath is critical in determining the sheath voltage drop, and methods to increase this conductivity will result in a

decrease of both sheath and boundary layer drops.

1. Sheath Formation and Charge Density Profiles

The results have shown that a sheath develops consistent with theory. The thickness of the sheath varies with the potential and is approximately that predicted from theory on Debye shielding. In each of the resulting plots presented in the previous section the size of the ambipolar region is essentially of the order of magnitude of the sheath length. No quantitative conclusions have been drawn as to the relative size of the ambipolar region other than to notice that higher voltages showed the tendency of the ambipolar region to increase in length relative to the sheath. It is very possible that at higher voltages the ambipolar region may grow to about the size of the boundary layer thickness. But since the potential drop in this region is low compared to that in the sheath it is not as significant in this analysis. The addition of Joule heating and a magnetic field did not appear to affect the sheath length. For the parameters used in this investigation, the difference between unlike charge densities (space charge) was about 10% of the equilibrium density.

Some of the resulting one-dimensional profiles shown in the previous section exhibit erratic behavior in the first few stations past the electrode node. This is believed to be caused by numerical convergence problems in the procedure arising from steep derivatives near the node and the extreme non-linearity of the equations. This appears to have little or no effect on the rest of the field since, as can be shown, the current distributions derived from these runs are consistent with those from smoother runs. Furthermore, charge densities other than zero were tested as a boundary condition at the electrode with no

change in the overall results. It seems then, that other conditions must be more dominant in the behavior of the potential field.

One very significant factor appears to be the choice for the insulated boundary condition. For example, a catalytic wall was attempted by setting $\hat{n}_i = \hat{n}_e = 0$, but no reasonable results were obtained. The biggest problem with the catalytic condition appeared to be the non-compatability of the wall condition with the free stream boundary conditions, specifically the free stream slopes did not approach zero regardless of the mesh size or characteristic length. Density gradients occurring at a catalytic wall occur in a small region when compared with the sheath, and violate the assumption of a continuous fluid. Numerically this means that the charge densities must go from zero to equilibrium values within one grid space. Physically the majority of the field should not "see" this wall anyway. So the conditions chosen, namely that of an equilibrium wall, are consistent with the rest of the field and yield meaningful results.

2. Current Density Distributions

The current-voltage diagrams in Figs. 46 through 48 show the behavior of the system for various conditions. Figure 46 shows that the non-dimensional current density is inversely proportional to the electrode spacing since the current density for the $\hat{\$} = 29.02$ case with the array size=1000L is approximately half that with the array size=500L. This is shown even more vividly in Fig. 47 where the introduction of multiple electrodes with double the step size (keeping the electrode spacing constant) resulted in a single current line. The significance of this dependancy is that the voltage drop for a given current density becomes a

function of the electrode node density, and is thus a problem which has inputs from surface physics as well as MHD conditions. It must be remembered that for the square arrays used in this work the electrode node spacings are of the same order as the sheath length. The minimum spacing must be of this order to avoid one-dimensional effects that would result from further "crowding" of the active sites. Spacing the nodes much greater than a sheath length makes computation more difficult since a much larger array would be needed to describe the effects. Thus, this work models a minimum spacing resulting in a near maximum current density for a given potential drop. On an actual electrode, the spacing would be random and dependent on empirical factors.

Figure 48 is the current-voltage diagram for the $\hat{n}$ = 1 case using a 51x51 array. It was noticed that for a given potential, the current density for the $\beta = 2$ line was approximately twice that of the $\beta = 1$ line. Using this result a $\beta = 2$ line was sketched in Fig. 46, since no converged solutions were available for this line at $\hat{n} = 10^{-3}$.

The introduction of the magnetic field moves the line to the right as shown in Fig. 46, and appears to cause a smaller potential drop for a given current. But recall that the current is already multiplied by the term $(1+\beta^2)$ due to the effective reduction in conductivity, and this partially offsets the reduction in the potential drop.

The introduction of the energy equation shows that Joule heating increases the current for a given voltage, but only to a slight degree. This is because the region that is affected by the Joule heating is small and very close to the electrode, well within the sheath.

In the absence of a magnetic field the

current-voltage diagram tends to be concave upward, a fact that can be predicted with the following arguments: Cobine (Ref. 27, p. 129) shows that the high pressure space-charge current should go as V^2/y^3 in one dimension. If y is taken to be the sheath length in Eq. C.7 then it can be shown that V goes as J^2. Figures 46 and 47 are nearly parabolic in appearance, and have curvatures consistent with this analysis.

The zero voltage intercept produces an interesting problem since it has different signs for Figs. 46 and 47. It would be expected from Eq. 1 that for zero potential difference in the absence of a magnetic field, the electron current density would be positive because of the diffusion term and the positive charge gradient for the existing boundary conditions. However, recall that the validity of the catalytic electrode depends upon the fact that it is charged. In the absence of a charged electrode, the node should appear the same as the insulated wall, and no density gradient should exist. Therefore, no special significance can be placed on this intercept without further investigation of the boundary conditions.

Reference [31] reports on the beneficial effect that increasing the seed fraction has on lowering the electrode voltage drops. From the behavior of the electron collision cross-sections with temperature, the optimum conductivity[32] is reached at seed fractions higher than in the core because of the lower total temperature at the electrodes. Heretofore, the only benefit would seem to be a higher boundary layer conductivity, but as shown in Figs. 46-48, the local conductivity also affects the sheath drop. Hence, a higher value of σ_o is expected to decrease the voltage loss associated with both the sheath and ambipolar regions.

An example would be appropriate here to show the orders of magnitude of the quantities being dealt with. Suppose it was desired to find the potential drop across the sheath in a plasma where the temperature is 1800°K, the current density is 0.2 amps-cm^{-2}, free-stream conductivity is 0.10 mhos/m, and the charge density is known to be of the order of 10^{18} particles/m^3. Equation 7 shows the characteristic charge density to be 7×10^{20} particles/m^3. Thus Fig. 46 would be the appropriate current-voltage diagram with $\hat{n}=10^{-3}$. The non-dimensional current density in the absence of a magnetic field is 1.50×10^{-5} which gives a dimensionless potential drop of 32.0. This corresponds to 4.9 volts at the given temperature.

3. Comparisons with Experiment

Argyropoulos et al[33] cite the use of a sophistocated computer solution for the boundary layer drop, comparing the results with an experiment on the AVCO-APL channel. Their results show the anode drop to be 101 volts due to the boundary layer. They do not consider sheath effects. Using these data, namely, $T_{wall} = 2000$°K, $J = 3.95\times10^4$ amps/m^2, $\beta = 1.02$ and a chemistry consisting of toluene and oxygen with cesium seed, the conductivity at the electrode is 1.14 mhos/m. Figure 46 shows a non-dimensional current density of 4.307×10^{-5}. Using the $\beta = 1$ line this gives $\hat{\phi} = 35.6$ for an actual drop of 6.13 volts at the given temperature.

Another comparison is from the work of Sonju and Teno[34]. For this experiment they used the same chemical constituents as the previous one. The conductivity at the wall temperature of 1800°K is 0.30 mhos/m and the other parameters are $J = 1.6\times10^4$ amps/m^2 and $\beta = 1.8$. Figure 46 gives $j = 1.7\times10^{-4}$, $\hat{\phi} = 121.3$, and a sheath voltage drop of

18.8 volts.

Caution must be exercised when making these comparisons since several factors have not been considered yet. First, tendencies towards non-equilibrium would increase the conductivity near the electrode resulting in a smaller potential drop. Secondly, nothing has been said about the node density of the experiments as compared to the assumptions made in the numerical solutions, namely that the distance between nodes is of the order of the sheath length. Should the actual node density differ from this it will affect the current-voltage characteristics. Thirdly, the use of a two-dimensional model rather than a three-dimensional one may tend to predict different voltage drops. The following example illustrates these limitations.

An experiment by Kessler and Eustis[6] was conducted using ethanol in oxygen with 1% KOH. Nitrogen was introduced for cooling such that the N_2/O_2 ratio was 0.5. For this run $T_{wall} = 1685^oK$, $T_{core} = 2700^oK$, $J=.75 \times 10^4 amps/m^2$, $\beta = 1.5$, and the electrode conductivity is 0.56 mhos/m. Figure 46 gives $j = 3.697 \times 10^{-4}$, $\hat{\phi} = 490.2$, and $\phi = 71.1$ volts. This is a higher drop than the measured 45 volts that should account for both the sheath and boundary layer contributions.

The primary difference between the above examples appears to be the conductivity at the electrodes. Since the equilibrium conductivity has such a strong dependence on temperature, the electrode temperature is a critical parameter in controlling the sheath losses. A very accurate comparison can only be made using a plot generated from the correct charge density and on precise knowledge of anode temperatures.

It is common practice to predict the losses according to the empirical formula

$$V = A + B\delta \qquad (46)$$

where δ is the boundary layer thickness and A and B are constants to be determined for a particular experiment. Such a scheme might be useful here if A is the sheath drop and B is the boundary layer drop. Using the comparisons above and from Appendix A for the boundary layer drop, the formula would look like

Sonju and Teno $V = 18.8 + 1190\delta$
Argyropoulos et al $V = 6.1 + 1110\delta$

where δ is measured in meters and V is measured in volts.

B. NUMERICAL CONCLUSIONS

The numerical technique is discussed in detail in Section III. Generally it consisted of a finite difference scheme for the solution of a system of three (later four) coupled, non-linear, partial, second-order differential equations. The line iterative method of solution was used. This method allowed a smaller storage requirement, and a choice of a 51x51 array balanced the computer time to converge with a mesh size sufficient to show the detail of a two-dimensional sheath. Convergence required four to six hours of computer time on the IBM 360/67 computer for each potential and/or Hall parameter chosen. The addition of Joule heating reduced the convergence time to one hour because of the damping effect of the temperature term near the electrode.

The use of successive over-relaxation to reduce the convergence time met with only marginal success. Because of numerical instabilites, an over-relaxation parameter greater

than 1.1 usually caused the process to diverge. Consequently, a value of 1.05 was used resulting in less than a 10% improvement in time.

In its present form, the computational procedure outlined in this work is limited as to the size of the parameters describing the system. For example, divergence resulted for non-dimensional potentials exceeding 35, Hall parameters greater than 2, and Joule heating parameters greater than 10^4. It can be observed from Eq. 28 that the Hall parameter weights the relative size of the axial derivatives compared to the cross-channel derivatives, giving rise to numerical instabilities for excessively large values of . The maximum potential attainable seems to be limited by the size of the array since a value of $\hat{\Phi} = 35$ was obtained for a 51x51 array and only 29 was achieved for a 41x41 array.

C. RECOMMENDATIONS FOR FURTHER STUDY

Since the principal limitations to this work arises because of the large storage and time required for calculations, much more could be accomplished with improved numerical techniques. A search by the author for a packaged subroutine capable of solving the computational matrix more efficiently than the one used here proved futile. Improved techniques are needed which will accomodate larger fields of computation.

The validity of these results is limited by the fact that the current density decreases in two dimensions rather than three. A three-dimensional scheme, admittedly a major task to develop, could render more realistic information on the effects of the sheath and on other electrode phenomena. One possible scheme is to model a three-dimensional system

by using an axi-symmetric cylindrical geometry for the point electrodes.

Additional physical effects involving changes in boundary conditions are possible. For example, boundary conditions could change the anode to a cathode by changing the sign of the charge and making the electrode an emitter of electrons.[Ref. 27, p. 106] The addition of convection into the system of equations (should it be deemed appropriate) is expected to accelerate convergence because it would ease the requirements of current density decreasing away from the electrode.

Other effects such as neutral and ion heating may be incorporated into the scheme to investigate thermal instabilities known to exist for such a case. Conduction of heat in the solid walls, ion slip, and frozen flow may be added. It is anticipated that frozen flow would decrease the importance of the boundary layer drop and increase the importance of the sheath drop.

With each additional effect the model rises in complexity and the numerical scheme becomes more unwieldy; therefore, only the principal effects should be reflected in the description of the sheath.

APPENDIX A

A SIMPLIFIED TECHNIQUE FOR DETERMING THE BOUNDARY LAYER VOLTAGE DROP IN MHD GENERATORS

As a complement to the two-dimensional sheath problem, and in order to assist in understanding the overall loss problem, a one-dimensional boundary layer analysis was investigated. The result is a method for determining the voltage drop across the thermal boundary layer which is simpler than most methods in existence today.

The technique balances sophistocation with ease of application. Because of its lack of rigor, many simplifying assumptions have been made which render the results inaccurate for certain cases. These assumptions are detailed in the following paragraphs, and experimental comparisons are shown.

1. Geometry

Figure A1 is a schematic of the voltage drops across a typical channel. the geometry assumes opposing electrodes, but does not preclude the possibility of diagonal construction. This analysis looks at only the ohmic portion of the voltage profile and assumes that the sheath losses can and must be determined separately. The boundary layer may be fully developed and uses the wall conditions as one of the boundaries for ohmic analysis.

2. Boundary Layer Drop

Reconstructing and modifying a formulation by Rosa[35],

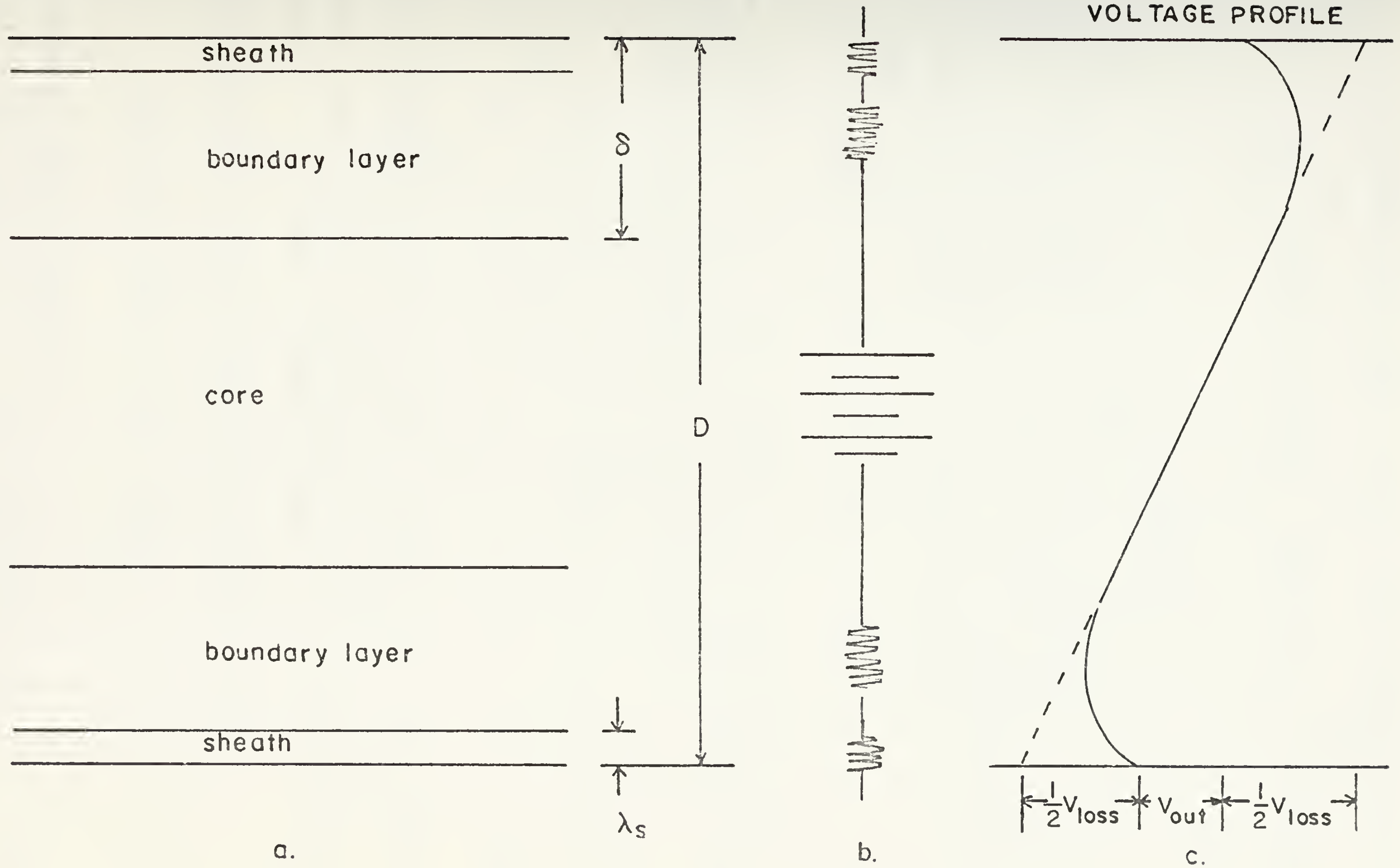

Figure A.1 Three representations of voltage losses in the MHD generator. a) sketch showing regions of loss mechanisms, b) electrical analog, c) voltage profile.

the average resistivity $\overline{(\sigma^{-1})}$ across the channel can be written as

$$\overline{(\sigma^{-1})} = \frac{1}{D}\int_0^D \frac{1}{\sigma}\,dy = \frac{1}{\sigma_c}\frac{1}{D}\left[\int_0^{\delta} \left(\frac{\sigma_c}{\sigma}\right) dy + \int_{\delta}^{D-\delta} \left(\frac{\sigma_c}{\sigma}\right) dy + \int_{D-\delta}^{D} \left(\frac{\sigma_c}{\sigma}\right) dy\right] \qquad (A.1)$$

where δ is the thermal boundary layer thickness and D is the channel width between opposing electrodes. Assuming constant conductivity in the free stream region, symmetric boundary layers at opposing walls, and non-dimensionalizing the integration variable, the equation becomes

$$\overline{(\sigma^{-1})} = \frac{1}{\sigma_c}\left[1 + 2\,\frac{\delta}{D}\int_0^1 \frac{\sigma_c}{\sigma}\, d\left(\frac{y}{\delta}\right) - 2\,\frac{\delta}{D}\right] \qquad (A.2)$$

Rosa [Ref. 32, p. 75] assumed a plasma where the gas properties vary only across the channel, and averaged Ohm's law. The resulting equations for current are

$$J_y = \frac{\bar{\sigma}}{G}\left(\bar{E}_y + \bar{U} \times B\right) - \frac{\beta}{G}\, J_x \qquad (A.3)$$

$$J_x = \bar{\sigma}\, E_x + \beta J_y \qquad (A.4)$$

where $G = \bar{\sigma}\left(\overline{\frac{1+\beta^2}{\sigma}}\right) - \beta^2$ and all terms have been averaged across the channel (y-direction). The x-direction is the direction of flow. Eliminating J_x, assuming β is a constant across the channel, solve for E_y to get

$$\bar{E}_y = \bar{U}B + \frac{J_y}{\sigma}\left(G + \beta^2\right) = \beta E_x \qquad (A.5)$$

The actual output voltage is

$$V_{out} = \int_0^D E_y\, dy = \bar{E}_y D = \bar{U}BD + \frac{J_y}{\sigma_c}\left(G+\beta^2\right) + \beta E_x D \qquad (A.6)$$

The intercept of the voltage profile with the channel wall (see figure A1) is given by

$$\bar{E}_{y_\infty} D = U_o BD + \frac{J_y}{\sigma_c} (1 + \beta^2) D + \beta E_x D \qquad (A.7)$$

Taking the difference and substituting for G the voltage loss is

$$V_{loss} = (U_o - \bar{U}) BD - (1 + \beta^2) [\sigma_c (\overline{\sigma^{-1}}) - 1] \frac{J_y D}{\sigma_c} \qquad (A.8)$$

This loss is Ohmic and is attributed to the two boundary layer temperature drops. For a turbulent boundary layer the first term will be small compared to the second

$$V_{bl} = \frac{J_y D}{2\sigma_c} (1 + \beta^2) [\sigma_c (\overline{\sigma^{-1}}) - 1] \qquad (A.9)$$

3. Conductivity Expression

An expression will now be derived for $\frac{\sigma_c}{\sigma}$ to be used in Eq. A.9. Hurwitz, Kilb, and Sutton[36] have shown that for cases where the current is entirely cross-channel (Faraday mode), the conductivity can indeed be treated as a scalar since for most such channels the magnetic field is approximately uniform between the electrodes. For the case of scalar conductivity we can write[26],[37]

$$\sigma = n_e e^2 / [m_e \bar{c}_e n_n (\sum_k x_k Q_k)] \qquad (A.10)$$

The subscript k denotes the various species present in the plasma, and $x_k = n_k / n_n$. For non-reacting plasmas the sum of the products $x_k Q_k$ will be relatively independent of temperature. We will assume this to be approximately true for reacting plasmas. Taking the ratio of the conductivity at a point to that at free stream, Eq. A.10 leads to

$$\frac{\sigma_c}{\sigma} = \frac{n_{eo}\bar{c}_e n_n}{n_e \bar{c}_{eo} n_{n0}} \tag{A.11}$$

Assuming a locally Maxwellian velocity distribution, quasi-equilibrium (allowing the use of the Saha relation), and constant pressure across the boundary layer, Eq. A.11 becomes

$$\frac{\sigma_c}{\sigma} = \theta^{-7/4}\, e^{\alpha(1/\theta-1)} \tag{A.12}$$

where $\alpha = \frac{\epsilon_I}{2kT_0}$ and $\theta = T/T_o$.

4. Constant Specific Heat

At this point a description of the turbulent boundary layer is needed. For the purpose of this analysis we will use the 1/7th-power law and Reynold's analogy[38] to describe the temperature field. An extensive and detailed study of the heat transfer problem related to these high temperatures was conducted by Brim[39], but in the interest of simplicity the Prandtl Number is assumed to be one. For constant C_p,

$$\frac{y}{\delta} = \left(\frac{T - T_w}{T_o - T_w}\right) = \left(\frac{\theta - \theta_w}{1 - \theta_w}\right)^7 \tag{A.13}$$

so

$$d\left(\frac{y}{\delta}\right) = \frac{7(\phi - \phi_w)^7}{(1 - \phi_w)^6}\, d\theta, \tag{A.14}$$

Now combining Eqs. A.2 and A.12 and changing variables according to Eq. A.14, the result is

$$\overline{(\sigma^{-1})} = \frac{1}{\sigma_c}\left[1 + 2\frac{\delta}{D}\int_{\theta_w}^{1} \theta^{-7/4} e^{\alpha(1/\theta-1)} \frac{7(\theta-\theta_w)^6}{(1-\theta_w)^7}\, d\theta - 2\frac{\delta}{D}\right] \tag{A.15}$$

Putting Eq. A.15 into A.9 for the average resistivity gives

$$V_{bl} = J_y(1+\beta^2)\delta/\sigma_c$$

$$\left[\frac{7}{(1-\theta_w)^7}\int_{\theta_w}^{1} \theta^{-7/4}\, e^{\alpha(1/\theta-1)}\,(\theta-\theta_w)^6\, d\theta - 1\right] \tag{A.16}$$

5. Non-constant Specific Heat

For a plasma with a non-constant C_p the 1/7th-power law is

$$\frac{y}{\delta} = \left(\frac{h-h_w}{h_o-h_w}\right)^7 \tag{A.17}$$

A change of variables would then give

$$V_{bl} = J_y(1+\beta^2)\delta/\sigma_c$$

$$\left[\frac{7C_pT_o}{(h_o-h_w)^7}\int_{\theta_w}^{1} \theta^{-7/4}\, e^{\alpha(1/\theta-1)}\,(h-h_w)^6\, d\theta - 1\right] \tag{A.18}$$

Obviously an enthalpy table or equation is needed to solve Eq. A.18. However, Mollier diagrams are obtainable, and once the enthalpy relation is known, the method shown in this analysis retains its simplicity.

6. Weighting Functions and Voltage Drop Parameters

Figure A2 is a graph of the conductivity from Eq. A.11 for Toluene and pure oxygen with 2% cesium seed at a core temperature of 2600°K. Plotted also is the conductivity from a more sophistocated program provided by AVCO Everett which also assumes quasi-equilibrium, but does not make the other simplifications done above. The agreement at 2600°K results from the "forced" condition in the simplified program.

An examination of Eqs. A.16 and A.18 shows that the

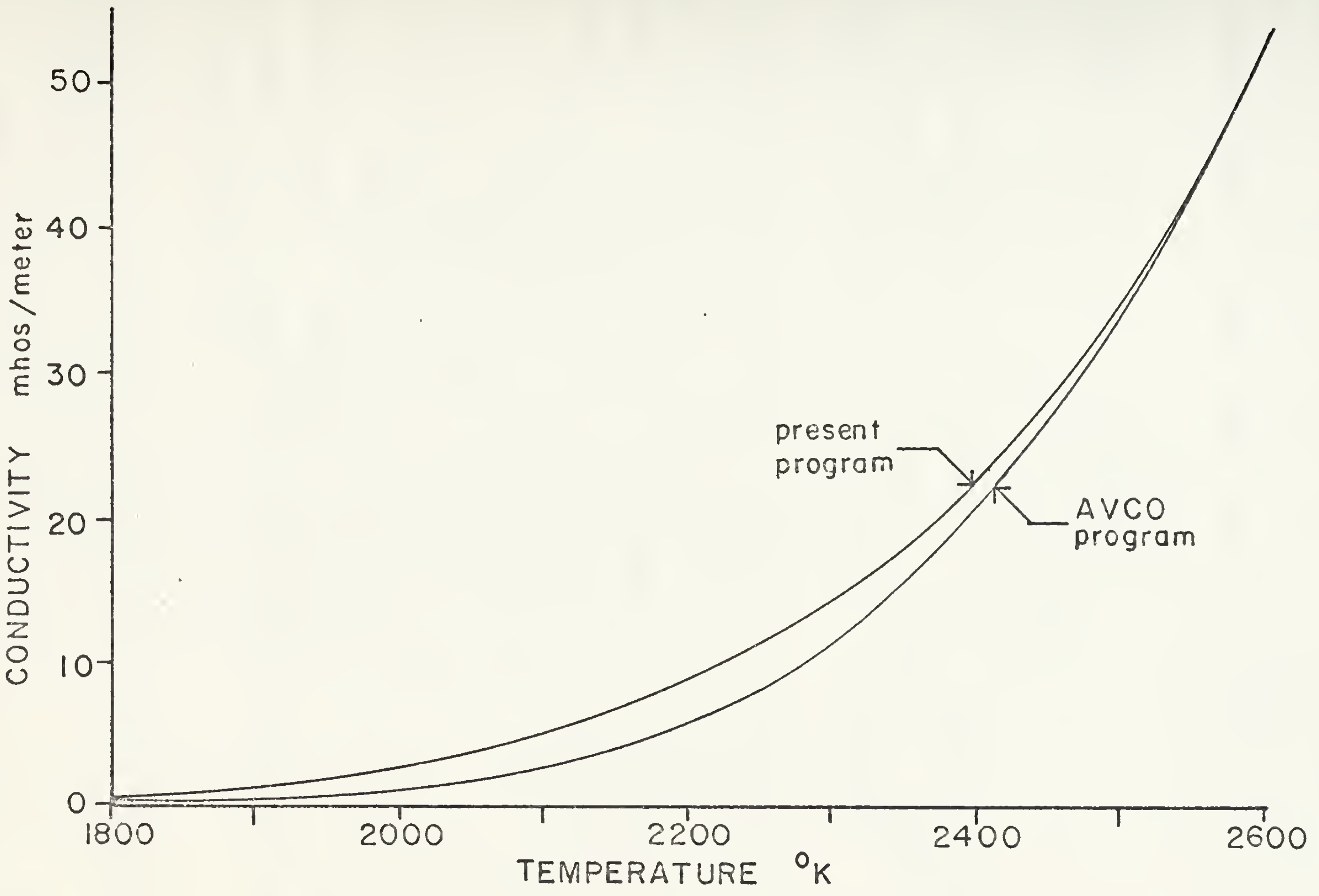

Figure A.2 Conductivity for stochiometric mixture of Toluene and Oxygen with two percent Cesium seed at 0.3 atmospheres. Base temperature = 2600°K.

effect of changing the integration variable was to average the resistivity across the boundary layer in "temperature space" instead of "geometry space". In each case this change generated a weighting function which weights the contribution of the resistivity to the integral according to the temperature. Other weighting functions derived here are:

for constant C_p : $$W = \frac{7(\theta-\theta_w)^6}{(1-\theta_w)^7}$$

for variable C_p : $$W_h = 7C_pT_o\frac{(h-h_w)^6}{(h_o-h_w)^7}$$

Other descriptions are possible, and often desirable. Useful descriptions for laminar boundary layers are available in Cramer and Pai[40] and Kerrebrock[41].

Figure A3 shows the effect that the weighting function has on resistivity. The resistivity (reciprocal of conductivity) is plotted first from the AVCO program and the approximate value from Eq. A.12. Next, the reacting plasma weighting function times the differential $\Delta\theta$ is plotted. Lastly, the product of the first two graphs shows that the effect is to reduce the error considerably, by weighting more heavily those values near the core. In fact the average resistivity from Fig. A3 (area under the right hand graph) is 0.0254 for the AVCO program, and 0.0244 for the simplified program. Obviously, the effect of the boundary layer shape is to smooth out the errors of the approximate resistivity calculations.

From Eqs. A.16 and A.18 a non-dimensional boundary layer voltage parameter can be identified.

$$\phi_{bl} = V_{bl}\sigma_c/[J_y(1+\beta^2)\delta] \qquad (A.19)$$

so that

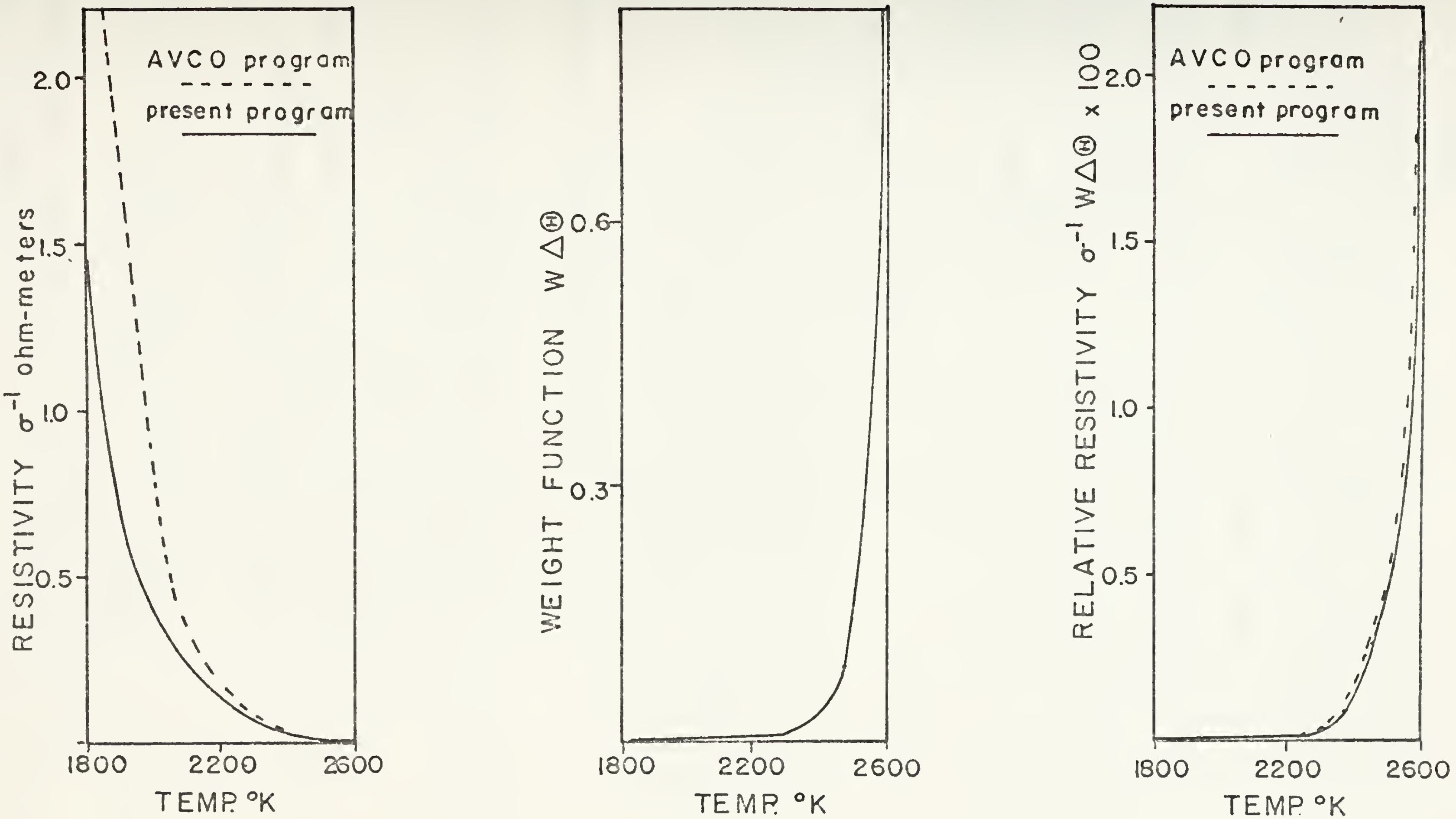

Figure A.3 Effect of weighting function on two programs for resistivity of Toluene/Oxygen/Cesium plasma using 1/7th power law and varying C_p.

$$\phi_{bl} = \int_{\theta_w}^{1} \theta^{-7/4} e^{\alpha(1/\theta-1)} W(\theta)\, d\theta - 1 \tag{A.20}$$

where $W(\theta)$ is the weighting function appropriate to the boundary layer description. Figures A4a and A4b are plots of ϕ_{bl} vs. wall temperature and core temperature for a constant C_p gas and Cesium seed. The former uses the 1/7th-power law while the latter uses a 1/8th-power law. As might be expected the 1/8th-power law predicts less of a voltage loss because the region of lower temperature plasma is thinner. Figures A5a and A5b are similar graphs for the combustion products of Toluene in pure oxygen and 2% cesium seed added.

7. Experimental Comparisons

As with all experimental predictions the accuracy of the results is dependent upon the accuracy of the input data as well as the ability of the model to represent the actual situation. The following examples illustrate the convenience of this method, but at the same time show the importance of an adequate model.

Sonju and Teno[34] report the results of an experimental run on the Viking I generator. Fig. A6 is a reproduction of the voltage profile for one run. Because of burner innefficiencies they found the conductivity of the Toluene/oxygen/cesium plasma to be between 12 and 16 mhos/m, about half the 33 mhos/m that would have been predicted for complete combustion[42]. Using $\beta = 1.8$, $J_y = 1.6\text{x}10^4$ amps/m², σ_c = 12-16 mhos/m, δ = .1m (half the channel width for fully developed flow), T_{core} = 2500°K, T_{wall} = 1800°, The voltage drop parameter is 0.282. This equates to a voltage loss per boundary layer of 119 volts for $\sigma_c = 16$, and 159 volts

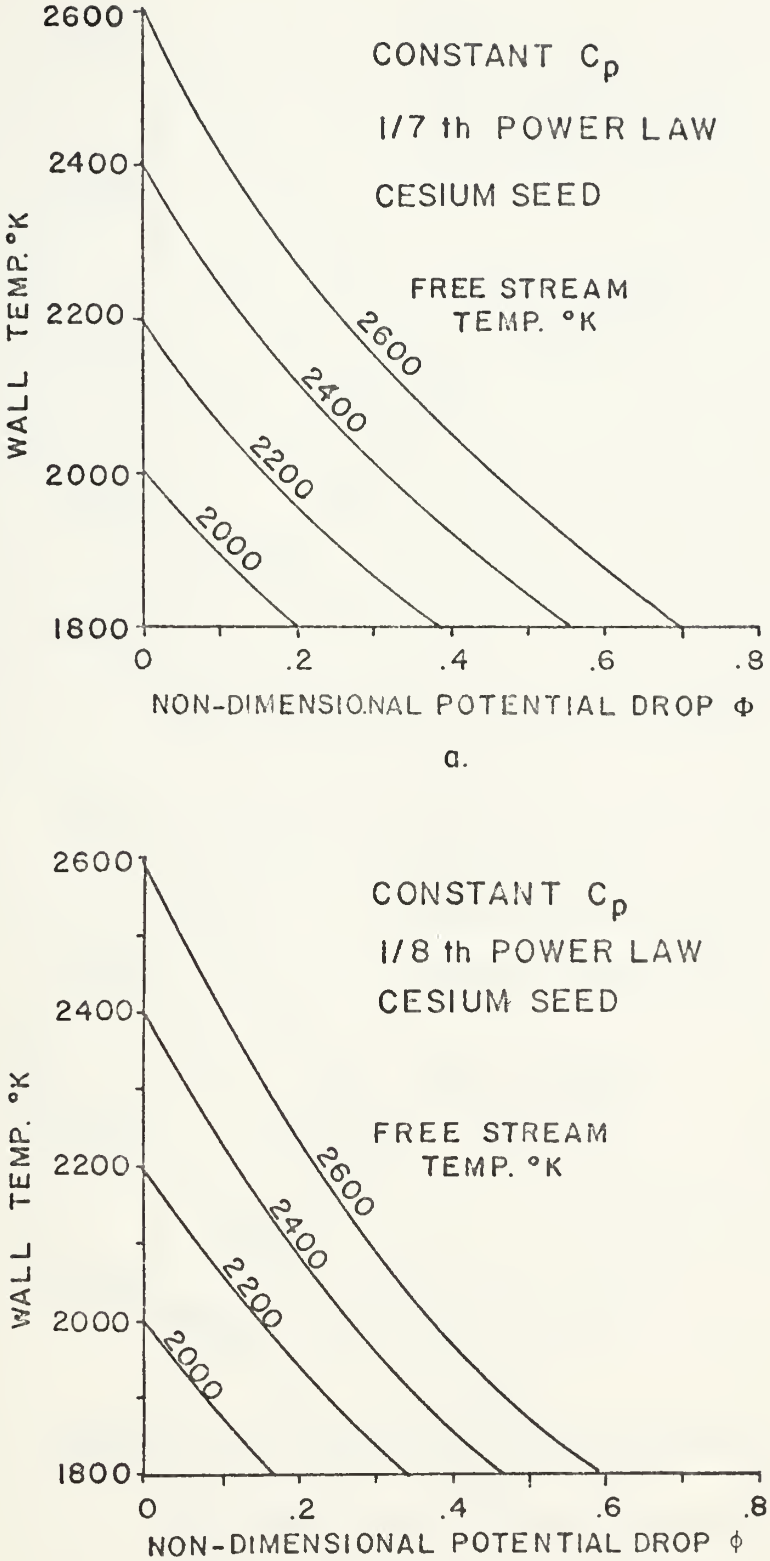

a.

b.

Figure A.4 Non-dimensional voltage drop ϕ versus wall temperature and free stream temperature for Cesium seed, constant C_p.

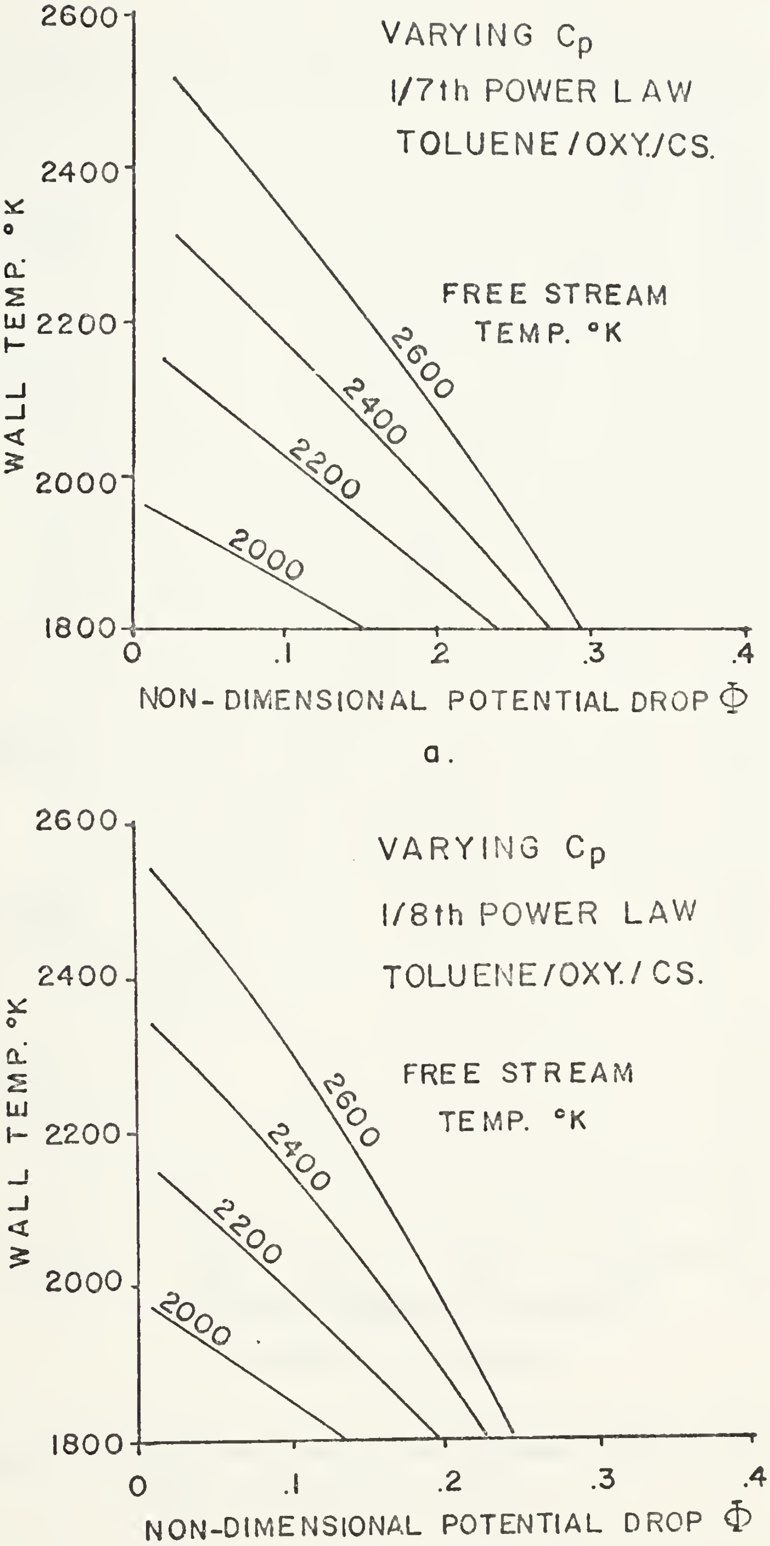

a.

b.

Figure A.5 Non-dimensional voltage drop Φ versus wall temperature and free stream temperature for Cesium seed, varying C_p.

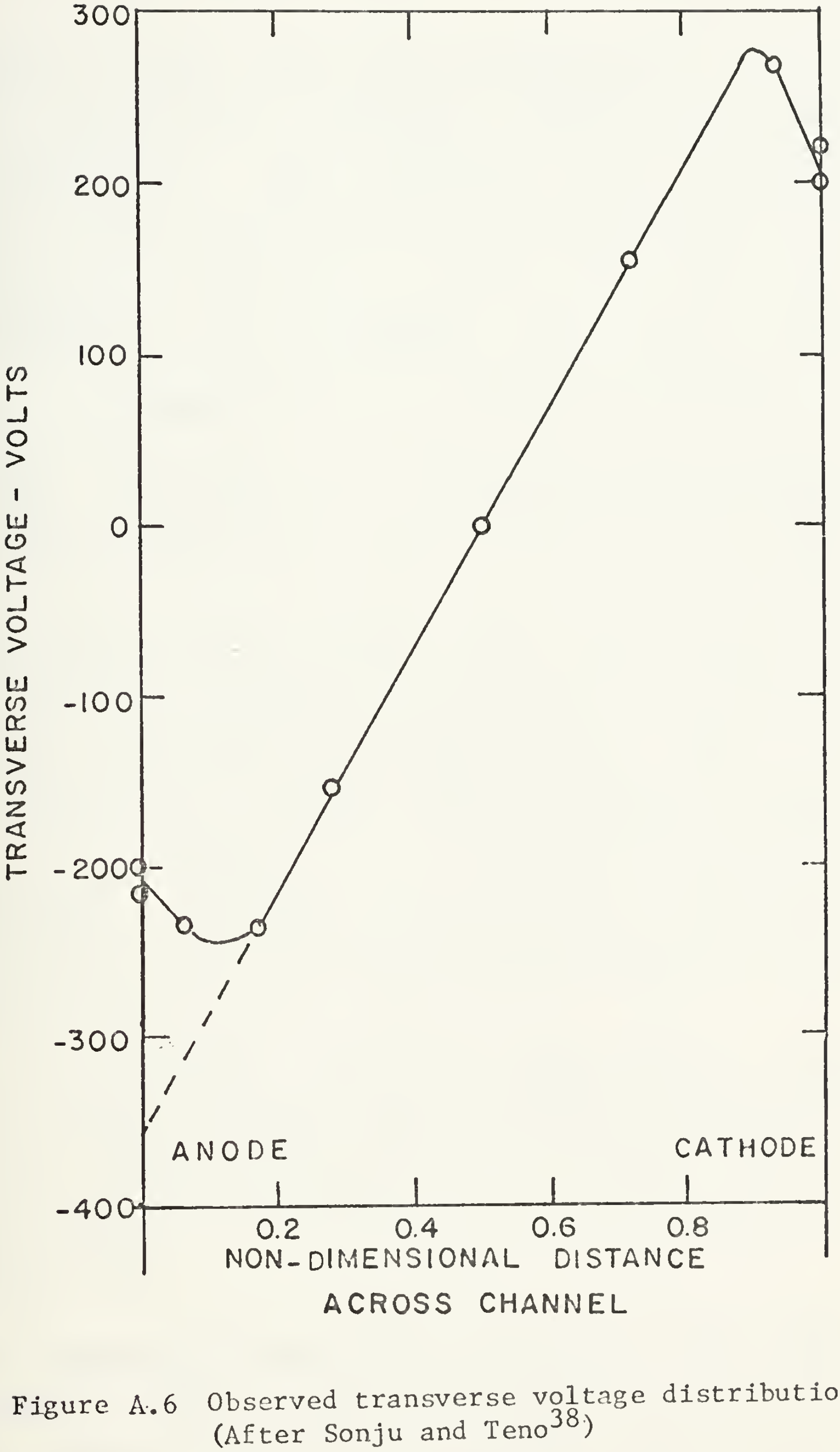

Figure A.6 Observed transverse voltage distribution. (After Sonju and Teno[38])

for σ_c=12. Extending the voltage profile to the channel wall in Fig. A6 shows a V_{bl} of about 150 volts.

Another example comes from Argyropoulos et al[33] who use a sophistocated computer technique to compare theory with experiments. They arrived at a boundary layer potential drop at the anode of 101 volts for an experiment on the AVCO-APL channel. Using the same data, namely T_{core} = 2600°K, T_{wall} = 2000°K, β = 1.02, δ=60 mm, a chemistry of toluene, oxygen and cesium, and the 1/7th-power law, Fig. A.5 gives a non-dimensional potential drop of 0.24. This corresponds to a predicted drop of 110.5 volts.

The next example shows the importance of selecting a proper model for the boundary layer. Fig. A7 is from data of Kessler and Eustis[6]. The parameters for the experiment were: I = 2.75 amps, electrode surface area = 3.68 cm², T_{elec} = 1685°K, T_{core} =2700°K, σ_c= 10 mhos/m, β=1.5. The gas was Ethanol in oxygen with 1% KOH added to increase conductivity. Nitrogen was introduced for cooling such that the N_2/O_2 ratio was 0.5. Using the 1/7th-power law ϕ_{bl} was found to be 0.290. Kessler predicted the boundary layer thickness to be 1.2 cm. The calculated voltage drop is then 8.5 volts falling well below the 46 volts shown in Fig. A7. The difference is too great to be attributed to sheath phenomena alone.

The geometry of this last case is the cause of the discrepency. The channel depth is 3.1 cm while the width between opposing electrodes is 10 cm. This means that the flow does not behave as between two flat plates since the sidewalls have a strong effect on the electrode wall boundary layer. The model used in this comparison is

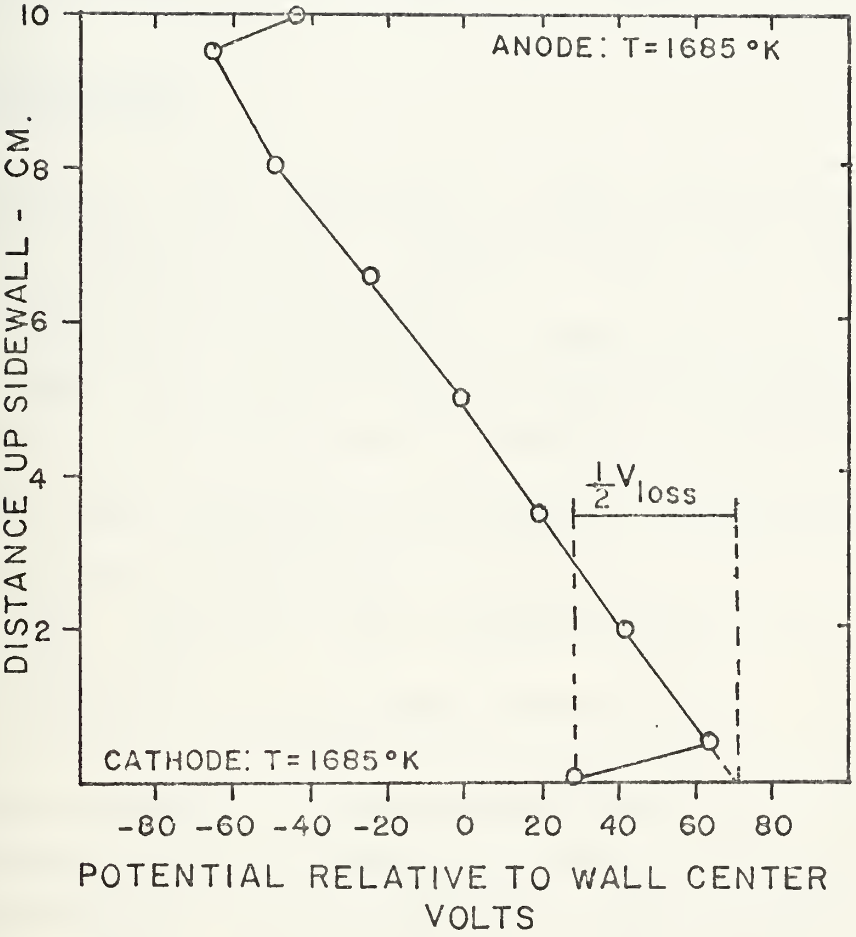

Figure A.7 Sidewall probe potential, core temperature = 2700°K. (After Kessler and Eustis[6])

obviously inappropriate. Schlichting (Ref. 38, p. 575) contains information on the problem of wall interference in non-circular cross-sections and points out the increase in friction and boundary layer size. A gross, but closer approximation for this procedure is to assume fully developed flow (as was suggested by Reseck[43] for this same channel). This results in a voltage drop prediction of 35.5 volts. Kessler attributes 10 volts to the sheath drop for the cathode. When combined with the 35.5 volts predicted above, the entire drop is accounted for more fully.

8. Conclusions

Equation A.20 represents a useful means of determining thermal boundary layer voltage losses as long as the following conditions are met:

1) A function of enthalpy vs. temperature is available, or, for the case of Eq. A.16, the gas has a fairly constant C_p in the range of temperatures of the channel,
2) the core conductivity is known or can be estimated with some degree of accuracy,
3) Hall parameter, core temperature and wall temperature are known, and
4) a suitable boundary layer description is available.

The simplicity of this approach makes it desirable for integration with a computer program which predicts the performance of an MHD generator. Such programs usually already contain free stream and wall temperatures, core conductivity, and Hall parameters. Since these equations are one-dimensional they allow calculations at stations along the channel, eliminating the need to determine properties at points in a two-dimensional field. A sample program applying this method at one station is given in the section "Computer Programs."

APPENDIX B

PROOF OF THE NON-EXISTENCE OF A ONE-DIMENSIONAL SHEATH SOLUTION

A first attempt at solving a complicated set of equations is usually to reduce the problem to one dimension. For the equations which describe the sheath this procedure seems reasonable due to the small thickness of the sheath relative to the electrode dimensions. Such an attempt for a constant temperature plasma with no ionization or recombination will fail because of the nonexistence of such a solution. Results published in Ref. 21 are summarized here along with significant conclusions which were instrumental in shaping the course of the two-dimensional work.

In order to simplify the analysis a change of variables is made.

$$\Gamma = \hat{n}_i - \hat{n}_e \qquad \xi = \hat{n}_i + \hat{n}_e \tag{B.1}$$

The following manipulations are made on Eqs. 26 and 27 in the text:

1) Magnetic field effects are dropped,
2) The equations are considered in only one-dimension,
3) The equations are added to each other and subtracted,
4) The change of variables in Eq. B.1 are applied.

The results, including Eq. 8 are

$$\frac{d^2\phi}{dy^2} = -\Gamma \tag{B.2}$$

$$\frac{d}{dy}\left(\Gamma \frac{d\phi}{dy}\right) + \frac{d^2\xi}{dy^2} = 0 \tag{B.3}$$

$$\frac{d}{dy}\left(\xi \frac{d\phi}{dy}\right) + \frac{d^2\Gamma}{dy^2} = 0 \tag{B.4}$$

If Eqs. B.3 and B.4 above are integrated and $E = -\,d\phi/dy$ is introduced then

$$\frac{dE}{dy} = \Gamma \tag{B.5}$$

$$-\,\Gamma E + \frac{d\xi}{dy} = C_1 \tag{B.6}$$

$$-\,\xi E + \frac{d\Gamma}{dy} = C_2 \tag{B.7}$$

It is not difficult to show that, in the absence of a net ion current

$$C_1 = -C_2 = J_y/(eD_e) \tag{B.8}$$

where J_y is the conventional current flux and D_e is the electron diffusion coefficient. Obviously, since J_y exists, C_1 and C_2 are non-zero constants.

Because the ambipolar region is quasi-neutral, Γ approaches zero away from the anode, reaching a value of zero at the plasma proper. Thus, as y increases:

Γ approaches 0
ξ approaches ξ_∞
E approaches E_∞

Eventually a distance $y = y_o$ would be reached so that for every $y > y_o$

$$|\Gamma E| < C_1/2 \tag{B.9}$$

Hence

$$\frac{d\xi}{dy} \geq C_1/2 \quad \text{for all} \quad y > y_o \tag{B.10}$$

$$\xi(y) \geq \xi(y_o) + (C_1/2)(y - y_o) \tag{B.11}$$

which does not approach a constant as required. Furthermore, since

$$\frac{d\Gamma}{dy} = -C_1 + \xi E \tag{B.12}$$

$$\frac{d\Gamma}{dy} \geq -C_1 + [\xi(y_o) + C_1/2 \times (y - y_o)]\, E \quad , \tag{B.13}$$

for $y > y_c$, which eventually grows at least as fast as

$$E\,\frac{C_1}{4}\,(y - y_o)^2 \tag{B.14}$$

and does not approach zero as required.

These obvious inconsistencies arise because of the constant C_1. The necessary requirement for a solution is that the current density decrease away from the anode giving rise to current constrictions at the surface. Under these conditions, C_1 would decrease at an appropriate rate so that Γ approaches zero and ξ approaches ξ_∞. Mechanisms which allow a proper variation of C_1 are diffusion in two or three dimensions and ionization/recombination. The former negates the applicability of a one-dimensional Cartesian solution while the latter eliminates the frozen flow assumption.

APPENDIX C

DIMENSIONAL AND FRACTIONAL ANALYSES OF THE SHEATH EQUATIONS

Equations 1-6 in the text are cumbersome in that they contain many physical parameters which in their present form must be carried along as the equations are operated on. It is useful to conduct a dimensional analysis or these equations in an attempt to collect the coefficients and variables in such a way as to simplify the appearance of the equations and better understand their nature. Also, before introducing the problem into the computer it is imperative to know the sizes of the quantities that are being dealt with. For this latter reason, a fractional analysis showing the relative significance of certain physical effects is also given in this appendix.

1. Dimensional Analysis

The method outlined by Langhaar[44] is utilized here to determine the non-dimensional parameters relevant to the sheath equations. The significant parameters which appear in Eqs. 1 and 3 are J, ϕ, n_s, y, e, ϵ_o, D_s, μ_s, β, and B, where y represents any coordinate length. An expansion and manipulation of Eq. 1 with Eqs. 3 and 5 will show that the terms D_s and μ_s can be replaced by kT_o. Since k and T_o always appear together, they can be expressed as a single term. Additionally, the Hall parameter β is already non-dimensional and will not be included in this analysis. This leaves ϕ, n_s, y, e, ϵ_o, and kT_o. In the MKS system these parameters are combinations of the units of mass (M), length(L), charge (q) and time (t). The matrix showing the

coefficients of these units for each parameter is:

	Φ	n	L	e	ϵ_o	kT_o
M	1	0	0	0	-1	1
L	2	-3	1	0	-3	2
q	-1	0	0	1	2	0
t	-2	0	0	0	2	-2

At first glance it might be expected that there are 6 - 4 = 2 dimensionless parameters (number of parameters minus the number of units necessary to describe them). However, closer examination shows that the t row is not linearly independent of the M row. In fact the rank of this matrix is three not four. Thus there are 6 - 3 = 3 independent dimensionless parameters (number of parameters minus the rank of the matrix) which describe the system of equations. This result would also have arisen if k and T_o had been considered separately.

Disregarding the t row, the homogeneous linear algebraic equations whose coefficients are the numbers in the rows of the dimensional matrix are

$$\begin{aligned} a_1 - a_5 + a_6 &= 0 \\ 2a_1 - 3a_2 + a_3 - 3a_5 + 2a_6 &= 0 \qquad \text{(C.1)} \\ -a_1 + a_4 + 2a_5 &= 0 \end{aligned}$$

Solving for a_4, a_5, and a_6 in terms of the other three gives

$$a_4 = a_1 + 6a_2 - 2a_3$$

$$a_5 = -3a_2 + a_3 \qquad (C.2)$$

$$a_6 = -a_1 - 3a_2 + a_3$$

Now setting the values $a_1=1$, and $a_2=a_3=0$, the result is: $a_4=1$, $a_5=0$, and $a_6=-1$.

Continuing by assigning a value of one successively to a_2 and a_3 with the other two of that set equal to zero, the solution matrix is generated.

	ϕ	n	L	e	ϵ_o	kT_o
$\hat{\phi}$	1	0	0	1	0	-1
$\hat{n}$	0	1	0	6	-3	-3
$\hat{y}$	0	0	1	-2	1	1

The resulting non-dimensional parameters are then

$$\hat{\phi} = \frac{e\phi}{kT_o} \qquad \hat{n} = \left(\frac{e^2}{kT_o\varepsilon_o}\right)^3 n \qquad \hat{y} = \frac{\varepsilon_o kT_o}{e^2}\, y \qquad (C.3)$$

These terms are all independent since $\hat{\phi}$, $\hat{n}$ and $\hat{y}$ appear in only one of each. In numerical form they look like

$$\hat{\phi} = \phi/\phi_o = 1.16\text{x}10^4\ T_o^{-1}\ \phi$$

$$\hat{n} = n/n_o = 9.26\text{x}10^{-12}\ T_o^{-3}\ n \qquad (C.4)$$

$$\hat{y} = y/L = 4.76\text{x}10^3\ T_o\ y$$

2. Estimate of the Sheath Size

The sheath size can be estimated by a technique called fractional analysis or approximation theory[45]. Eq. 3 is

$$\nabla^2\phi = -(n_i - n_e)e/\varepsilon_o \tag{C.5}$$

Now "characteristic" parameters ϕ_o, λ_s, and n_o are factored out of the equation for each variable.

$$\frac{\phi_o}{\lambda_s^2}\,\hat{\nabla}^2\hat{\phi} = -\frac{n_o e}{\varepsilon_o}\,(\hat{n}_i - \hat{n}_e) \tag{C.6}$$

where ϕ_o and n_o are the maximum value of the potential and charge concentration respectively, and λ_s is a sheath charactersitic length. Since in the sheath all the variables are of order unity, for the equation to be consistent the term $\frac{n_o e\lambda^2}{\phi_o}$ must also be of order unity. Setting this term equal to one and solving for λ_s, the result is

$$\lambda_s \approx \frac{\phi_o\varepsilon_o}{n_o e} \tag{C.7}$$

This gives an order of magnitude for the characteristic sheath length. For example, for a sheath drop of 10 volts in a plasma ionized to 10^{18} electrons/m^3 the characteristic sheath length is 2.4×10^{-5}m.

3. Characteristic Current from Conduction

From Eq. 10 the conduction current is

$$J_e = -\mu_e e n_e \nabla\phi \tag{C.8}$$

Working in one-dimension and identifying a characteristic current J_o, a fractional analysis gives the equation

$$\frac{J_o \lambda_s}{\phi_o \mu_e e n_o} \simeq 1 \tag{C.9}$$

Notice that in order to be consistent the characteristic length in the potential derivative must again be λ_s, the sheath length. Solving for J_o when $n_o = 10^{18} m^{-3}$, $\mu_e = 1$ $m^2(\text{volt-sec})^{-1}$, and $\phi_o = 10$, gives $J_o = 6.8 \times 10^4$ amps/m². The value for μ_e comes from Eq. 16 for electrons colliding with CO_2 molecules at 1000°K.

4. Diffusion Length

The potential is a monotonic positive function which is suitable for approximation theory, however the charge density profiles have many inflection points in the sheath and are not well suited. Nevertheless, it is possible to consider profiles beyond the sheath where characteristic lengths can be defined.

If diffusion is to play a significant role in current production then

$$J_o \simeq \mu_e k T_e \frac{\partial n}{\partial y} \tag{C.10}$$

Again, using fractional analysis, the following approximation is made:

$$\frac{J_o L_d}{n_o \mu_e k T_e} \simeq 1 \tag{C.11}$$

Solving for L_d with the same parameters as above gives $L_d = 2.03 \times 10^{-7}$. Since $L_d < \lambda_s$ it can be concluded that any role played by the mechanism of diffusion should be visible within the sheath.

5. Ionization/Recombination Length

From Hinnov and Hirschberg[46] the three-body recombination rate of electrons and ions is given by

$$\frac{dn_e}{dt} = \alpha n_e^2 \tag{C.12}$$

where

$$\alpha = 5.6\text{x}10^{-33} \left(\frac{kT}{e}\right)^{-4.5} n_e \tag{C.13}$$

Using the technique outlined previously,

$$\frac{n_o}{\tau_r} \frac{dn_e}{dt} = 5.6\text{x}10^{-33} \left(\frac{kT}{e}\right)^{-4.5} n_o^3 \hat{n}_e^3 \tag{C.14}$$

where τ_r is the characteristic recombination time. Let the term $5.6\text{x}10^{-39}(kT/e)^{-4.5}n_o^2$ be of the order of unity and solve for τ_r.

$$\tau_r = \left[(5.6\text{x}10^{-33}) \left(\frac{kT}{e}\right)^{-4.5} (n_o^2)\right]^{-1} \tag{C.15}$$

At $T=1000^oK$ and $n_o = 10^{18}m^{-3}$, the characteristic time becomes $2.9\text{x}10^{-3}$sec.

In order to change the characteristic time to a characteristic length the mean thermal velocity is used since this is the transport mechanism for ionization and recombination. Thus

$$L_r = \tau_r\bar{c} = \tau_r \sqrt{\frac{8kT_e}{\pi m_e}} \tag{C.16}$$

Using the same conditions as above $L_r = 5.7\text{x}10^2$ m. Since $L_r >> \lambda_s$ it can be concluded that ionization and recombination

do not have time to occur within the sheath for the conditions used in this analysis. Since the results of this work show that the ambipolar region is of the same order as the sheath length, ionization/recombination is not expected to play a part in that region either.

6. Convection Time

At atmospheric pressure and temperatures around 1000°K sonic velocity is of the order of 10^3 m/sec. This is the order of velocity of the flows of MHD generators. A rough characteristic time relevant to the sheath could be established by comparing the flow velocity with the size of the sheath.

$$\tau_c = \lambda_s/U_c \qquad (C.17)$$

Using $\phi_o = 10$ volts and $n_o = 10^{18}\ m^{-3}$, $\tau_c = 2.4\times10^{-8}$sec.

A characteristic sheath time can be defined from

$$\tau_s = \lambda_s/\bar{c} \qquad (C.18)$$

for comparison with τ_c. Using representative values for λ_s and $\bar{c}$, $\tau_s = 1.2\times10^{-10}$ sec. Thus, any effects occuring from convective phenomena such as mixing and boundary layer effects do not have sufficient time to affect the sheath.

COMPUTER PROGRAMS

The principal program used in this work is the one that calculates the potential and charge density distributions for the sheath and ambipolar regions. This program is explained in Part 1 of this section and reproduced there.

Auxiliary programs are those that calculate the current distribution and produce the outputs used in this work. Part 2 shows the auxiliary programs.

Part 3 is a reproduction of the program used in the calculation of the boundary layer in Appendix A. A sample enthalpy table is provided in data format for the Toluene/oxygen/cesium mixture.

1. Sheath Program

The sheath program begins with an assumed solution and operates on the field of parameters to replace the assumed solution with a more accurate one. Theoretically, the more iterations that are used, the more accurate the result is. An example of an initial assumed solution is P(I,J)=0, G(I,J)=BZ, SI(I,J)=BZ, and TH(I,J)=1.0 throughout the field. (see the program comment cards for definitions) These three arrays are operated on and a more accurate solution is stored for later analysis or further iterations.

The following pages are a reprint of this program, and an explanation of the parameters and subroutines is included.

```
C**              SHEATH COMPUTATION PROGRAM                         **
C
C
C  THIS PROGRAM IS DESIGNED TO CALCULATE A TWO-DIMENSIONAL
C  SHEATH FIELD GIVEN THE FOLLOWING INITIAL PARAMETERS:
C     P     POTENTIAL DISTRIBUTION
C     G     ELECTRON DENSITY DISTRIBUTION
C     SI    ION DENSITY DISTRIBUTION
C     TH    ELECTRON TEMPERATURE DISTRIBUTION
C     BET   HALL PARAMETER
C     GAM   JOULE HEATING PARAMETER
C     ZL    STEP SIZE MULTIPLE
C     PHI   ELECTRODE POTENTIAL
C     W     SUCCESSIVE OVER-RELAXATION PARAMETER
C     BZ    CHARGE DENSITY BOUNDARY VALUE
C     MAX   NUMBER OF ITERATIONS PER CYCLE
C     MM    NUMBER OF CYCLES
C     JMIN  MINIMUM PRINTOUT PARAMETER (BEGINS PRINTOUT AT
C        END OF ITERATION JMIN WITHIN EACH CYCLE)
C     NROWS ARRAY WIDTH
C     NCOLS ARRAY LENGTH
C     NCEN  ELECTRODE LOCATION ON WALL
C  THIS ROUTINE USES ASSUMED VALUES FOR ARRAYS P,G,SI AND TH
C  AND UPDATES THESE VALUES.  THE PROGRAM USES THE FOLLOWING
C  SUBROUTINES:
C     MAIN...CONTROLS INPUT AND OUTPUT AND DEFINES MOST
C        CONSTANTS AND PARAMETERS
C     LOAD...LOADS THE COMPUTATIONAL MATRIX AND CONTROLS
C        THE SWEEP MODE
C     DERV...DERIVES INTERMEDIATE DERIVATIVES FOR USE IN
C        LOAD
C     ROTAT..ROTATES ARRAY FOR CROSS-COORDINATE SWEEPS
C     TMP....SOLVES ENERGY EQUATION FOR USE IN LOAD
C     WRITER..PRINTER OUTPUT SUBROUTINE
C     DGELB..IBM PACKAGED SUBROUTINE FOR THE SOLUTION OF
C        NON-SYMMETRIC SIMULTANEOUS ALGEBRAIC EQUATIONS WITH
C        BANDED STRUCTURE.
      IMPLICIT REAL*8(A-H,O-Z)
      COMMON/BL1/P(51,51),G(51,51),SI(51,51)
      COMMON/BL2/BET,GAM,H,PHI,BZ,NCOLS,NROWS,NCEN,MAX
      COMMON/BL3/BMAX,W,JMIN,JMAX
      COMMON/BL4/PP(51),PPP(51),GXP(51),GXPP(51),SP(51),SPP(
         51)
      COMMON/BL5/NLFT,NRIT
      COMMON/BL6/TH(51,51),DTX(51)
C  READ CONSTANTS
      READ(5,200) PHI,ZL,BET,W,GAM,BZ
      READ(5,300) MAX,MM,JMIN,NCEN
      WRITE(6,201) PHI,ZL,BET,W,GAM,BZ,MAX,MM,JMIN,NCEN
      JMAX=MAX
      BMAX=1.0D-08
      TEMP=2.0D 03
      NROWS=51
      NCOLS=51
      H=ZL/DFLOAT(NROWS-1)
      PHI=PHI*1.1609D 04/TEMP
      DO 1 J=1,NCOLS
      DTX(J)=0.0
      PP(J)=0.0
      GXP(J)=0.0
    1 SP(J)=0.0
      DO 11 J=1,NCOLS
      DO 11 I=1,NROWS
      TH(I,J)=1.D 00
   11 CONTINUE
C  READ STORED ARRAYS
      READ(2) P
      READ(2) G
      READ(2) SI
      REWIND 2
C  OPERATE ON ARRAYS
      DO 2 KK=1,MM
```

```
      CALL LOAD
    2 CONTINUE
C  OUTPUT AND STORE RESULTS
      WRITE(2) P
      WRITE(2) G
      WRITE(2) SI
      WRITE(6,100)
  100 FORMAT(3X,'DATA HAS BEEN READ INTO FILE')
  200 FORMAT(6D10.0)
  300 FORMAT(4I4)
  201 FORMAT(3X,6D12.3,4I4)
      STOP
      END



      SUBROUTINE LOAD
      IMPLICIT REAL*8(A-H,O-Z)
      REAL*4 EPS
      COMMON/BL1/P(51,51),G(51,51),SI(51,51)
      COMMON/BL2/BET,GAM,H,PHI,BZ,NCOLS,NROWS,NCEN,MAX
      COMMON/BL3/BMAX,W,JMIN,JMAX
      COMMON/BL4/PP(51),PPP(51),GXP(51),GXPP(51),SP(51),SPP(
     1   51)
      COMMON/BL5/NLFT,NRIT
      COMMON/BL6/TH(51,51),DTX(51)
      DIMENSION T(153),A(10,153),B(1505)
      EQUIVALENCE (A(1,1),B(1))
      HS=1.0D 00/(H*H)
      HR=.5D 00/H
      H4=HS/4.D 00
      BETR=BET*HR/2.D 00
      NCOM=NCOLS-1
      NFLAG=1
      NCOLS3=10
      NROWS3=NROWS*3
      MUD=4
      MLD=5
C  BEGIN ITERATIONS
      DO 99 JCNT=1,MAX
      ND=2
C  ROTATION PARAMETERS
      IN=NFLAG-(NFLAG/4)*4
      IF(IN.EQ.0.OR.IN.EQ.3) ND=1
      IF(GAM.LT.1.D 00) GO TO 30
      CALL TMP(ND)
C  SWEEP IN I DIRECTION
   30 DO 1 IX=1,NROWS
      I=IX
      IF(IN.EQ.0.OR.IN.EQ.2) I=NROWS-IX+1
      DO 90 M=1,NROWS3
      DO 90 L=1,NCOLS3
      A(L,M)=0.0
   90 CONTINUE
      IF(I.NE.1.AND.I.NE.NROWS) CALL DERV(I,2)
      DO 2 J=1,NCOLS
C  INTRODUCE TEMPERATURE PARAMETERS
      TT=TH(I,J)
      THS=TT*TT*HS
C  LOAD COMPUTATIONAL MATRIX
      DO 2 K=1,3
      M=3*(J-1)+K
      GO TO (50,51),ND
   50 IF(J.EQ.1.AND.I.EQ.NCEN) GO TO (76,21,21),K
      IF(J.EQ.NCOLS) GO TO (21,19,19),K
      IF(I.EQ.1) GO TO 91
      IF(I.EQ.NROWS) GO TO (96,97,98),K
      IF(J.EQ.1) GO TO (40,19,19),K
      DTY=TH(I,J+1)-TH(I,J-1)
      TS=.5D 00*TT*DTY*H4-BET*TT*HR*(PP(J)+.5D 00*DTX(J))
      GO TO (5,6,7),K
   51 IF(I.EQ.1.AND.J.EQ.NCEN) GO TO (76,21,21),K
```

```
      IF(I.EQ.NROWS) GO TO 1
      IF(J.EQ.1) GO TO 91
      IF(J.EQ.NCOLS) GO TO 86
      IF(I.EQ.1) GO TO (41,19,19),K
      DTY=TH(I,J+1)-TH(I,J-1)
      TS=.5D 00*TT*DTY*H4
      GO TO (5,6,7),K
C    INTERNAL FIELD COEFFICIENTS
    5 A(7,M)=-1.D 00
      A(8,M)=1.D 00
      A(3,M)=HS
      A(9,M)=HS
      A(6,M)=-4.D 00*HS
      T(M)=-PPP(J)
      GO TO 2
    6 A(3,M)=THS-TS
      A(6,M)=-4.D 00*THS
      A(9,M)=THS+TS
      A(2,M)=TT*(G(I,J+1)-G(I,J-1))*H4-.5D 00*G(I,J)*DTY*H4-
     1     BET*HR*(TT*GXP(J)-.5D 00*G(I,J)*DTX(J))
      A(8,M)=-A(2,M)
      T(M)=TT*(-TT*GXPP(J)+GXP(J)*PP(J)-
     1     .5D 00*DTX(J)*GXP(J)+G(I,J)*(G(I,J)-SI(I,J)))-
     2     .5D 00*G(I,J)*DTX(J)*PP(J)-
     3     .5D 00*BET*DTY*HR*(G(I,J)*PP(J)+
     4     TT*GXP(J))
      GO TO 2
    7 A(3,M)=HS
      A(6,M)=-4.D 00*HS
      A(9,M)=HS
      A(1,M)=-(SI(I,J+1)-SI(I,J-1))*H4
      A(7,M)=-A(1,M)
      T(M)=SI(I,J)*(SI(I,J)-G(I,J))-PP(J)*SP(J)-SPP(J)
      GO TO 2
C    BOUNDARY CONDITIONS
   76 T(M)=PHI
      GO TO 85
   91 I1=I
      J1=J
      IF(ND.EQ.1) I1=NROWS
      IF(ND.EQ.2) J1=NCOLS
      GO TO (92,93,94),K
   92 T(M)=P(I1,J1)
      GO TO 85
   93 T(M)=G(I1,J1)
      GO TO 85
   94 T(M)=SI(I1,J1)
      GO TO 85
   96 T(M)=P(2,J)-P(1,J)+P(NCOM,J)
      GO TO 85
   97 T(M)=G(2,J)-G(1,J)+G(NCOM,J)
      GO TO 85
   98 T(M)=SI(2,J)-SI(1,J)+SI(NCOM,J)
      GO TO 85
   86 A(3,M)=-1.D 00
      GO TO (87,88,89),K
   87 T(M)=P(I,2)-P(I,1)
      GO TO 85
   88 T(M)=G(I,2)-G(I,1)
      GO TO 85
   89 T(M)=SI(I,2)-SI(I,1)
      GO TO 85
   21 T(M)=0.0
      GO TO 85
   19 T(M)=BZ
      GO TO 85
   40 A(6,M)=3.D 00*BZ
      A(9,M)=-4.D 00*BZ
      A(7,M)=-3.D 00
      A(10,M)=4.D 00
      T(M)=-BZ*P(I,3)+G(I,3)+BET*BZ*(P(I+1,1)-P(I-1,1))
      GO TO 2
```

```
   41 T(M)=P(I,J)
   85 A(6,M)=1.D 00
    2 CONTINUE
C  MODIFY MATRIX FOR USE IN SUBROUTINE DGELB
      KMAX=NROWS3-4
      MB=0
      MK=6
      DO 200 KA=1,KMAX
      MK=MK-1
      IF(KA.LT.6) MB=MB+MK
      DO 200 KB=1,10
      IF(KA.LT.6.AND.KB.LE.MK) GO TO 200
      M=10*(KA-1)+KB
      MA=M-MB
      B(MA)=A(KB,KA)
  200 CONTINUE
      KMM=KMAX+1
      MK=0
      DO 202 KA=KMM,NROWS3
      MB=MK+MB
      MK=MK+1
      MP=10-MK
      DO 202 KB=1,10
      IF(KB.GT.MP) GO TO 202
      M=10*(KA-1)+KB
      MA=M-MB
      B(MA)=A(KB,KA)
  202 CONTINUE
C  SOLVE MATRIX
      CALL DGELB(T,B,NROWS3,1,MUD,MLD,EPS,IER)
      IP=I+1
      IF(IN.EQ.0.OR.IN.EQ.2) IP=I-1
      IF(IP.GT.1.AND.IP.LT.NROWS) CALL DERV(IP,1)
C  SUCCESSIVE OVER-RELAXATION FEATURE
      DO 13 J=1,NCOLS
      M=3*(J-1)
      HINT1=T(M+1)-P(I,J)
      HINT2=T(M+2)-G(I,J)
      HINT3=T(M+3)-SI(I,J)
      P(I,J)=P(I,J)+W*HINT1
      G(I,J)=G(I,J)+W*HINT2
   13 SI(I,J)=SI(I,J)+W*HINT3
    1 CONTINUE
C  PRINTER OUTPUT
      WRITE(6,103) JCNT
      IF(JCNT.LT.JMIN.OR.JCNT.GT.JMAX) GO TO 43
      WRITE(6,100) JCNT
      CALL WRITER(P,NROWS,NCOLS)
      WRITE(6,101) JCNT
      CALL WRITER(G,NROWS,NCOLS)
      WRITE(6,102) JCNT
      CALL WRITER(SI,NROWS,NCOLS)
   43 IF(IN.EQ.1.OR.IN.EQ.3) GO TO 99
      CALL ROTAT(P,NROWS,NCOLS)
      CALL ROTAT(G,NROWS,NCOLS)
      CALL ROTAT(SI,NROWS,NCOLS)
      CALL ROTAT(TH,NROWS,NCOLS)
   99 NFLAG=NFLAG+1
      RETURN
  100 FORMAT(//,3X,'POTENTIAL PLOT',I4,/)
  101 FORMAT(//,3X,'ELECTRON PLOT',I4,/)
  102 FORMAT(//,3X,'ION PLOT',I4,/)
  103 FORMAT(3X,I4)
  104 FORMAT(//,3X,'TEMPERATURE PROFILE',I4,/)
      END
```

```
      SUBROUTINE DERV(I,NF)
      IMPLICIT REAL*8(A-H,O-Z)
      COMMON/BL1/P(51,51),G(51,51),SI(51,51)
      COMMON/BL2/BET,GAM,H,PHI,BZ,NCOLS,NROWS,NCEN,MAX
      COMMON/BL4/PP(51),PPP(51),GXP(51),GXPP(51),SP(51),SPP(
     1 51)
      COMMON/BL6/TH(51,51),DTX(51)
      LM=NROWS-1
      I1=I+1
      I2=I-1
      IF(I.EQ.1) I2=LM
      IF(I.EQ.NROWS) I1=2
      IF(NF.EQ.2) GO TO 4
C   FIRST DERIVATIVES
      H2=.5D 00/H
      DO 1 J=1,NCOLS
      DTX(J)=(TH(I1,J)-TH(I2,J))*H2
      PP(J)=(P(I1,J)-P(I2,J))*H2
      GXP(J)=(G(I1,J)-G(I2,J))*H2
    1 SP(J)=(SI(I1,J)-SI(I2,J))*H2
      RETURN
C   SECOND DERIVATIVES
    4 HS=1.0D 00/(H*H)
      DO 2 J=1,NCOLS
      PPP(J)=(P(I1,J)+P(I2,J))*HS
      GXPP(J)=(G(I1,J)+G(I2,J))*HS
    2 SPP(J)=(SI(I1,J)+SI(I2,J))*HS
      RETURN
      END


      SUBROUTINE WRITER(Z,NCOLS,NROWS)
      IMPLICIT REAL*8(A-H,O-Z)
      DIMENSION Z(NROWS,NCOLS)
      J1=1
      J2=11
   10 IF(J2.GE.NCOLS) J2=NCOLS
      DO 15 I=1,NROWS
   15 WRITE(6,220) I,(Z(I,J),J=J1,J2)
      WRITE(6,240)
      IF(J2.EQ.NCOLS) RETURN
      J1=J1+11
      J2=J2+11
      GO TO 10
  220 FORMAT(' ',I3,11E11.4)
  240 FORMAT(/)
      END
```

```
      SUBROUTINE ROTAT(A,NROWS,NCOLS)
      IMPLICIT REAL*8 (A-H,O-Z)
      DIMENSION A(NROWS,NCOLS),B(51,51)
      DO 1 I=1,NROWS
      DO 1 J=1,NCOLS
    1 B(I,J)=A(I,J)
      DO 2 I=1,NROWS
      DO 2 J=1,NCOLS
    2 A(I,J)=B(J,I)
      RETURN
      END
```

```
      SUBROUTINE TMP(ND)
      IMPLICIT REAL*8(A-H,O-Z)
      COMMON/BL1/P(51,51),G(51,51),SI(51,51)
      COMMON/BL2/BET,GAM,H,PHI,BZ,NCOLS,NROWS,NCEN,MAX
      COMMON/BL6/TH(51,51),DTX(51)
      NROM=NROWS-1
      NCOM=NCOLS-1
      G1=GAM*.25D 00/(H*H)
      G2=GAM/(H*H)
      DO 2 I=2,NROM
      DO 2 J=2,NCOM
      EL=G(I,J)
      DPX=P(I+1,J)-P(I-1,J)
      DPY=P(I,J+1)-P(I,J-1)
      DNX=G(I+1,J)-G(I-1,J)
      DNY=G(I,J+1)-G(I,J-1)
      ARG=G1*(DNX*DPX+DNY*DPY)/EL-1.D 00
      ARG2=G2*(DPX*DPX+DPY*DPY)
      TH(I,J)=(-ARG+DSQRT(ARG*ARG+ARG2))/2.D 00
    2 CONTINUE
      IF(ND.EQ.1) GO TO 5
      TF=(1.D 00+DSQRT(1.D 00+4.D 00*GAM*P(NROM,NCEN)**2))/2
     1.D 00
      DO 3 J=1,NCOLS
      TH(NROWS,J)=TF
    3 TH(1,J)=1.D 00
      DO 4 I=2,NROM
      TH(I,NCOLS)=TH(I,1)
    4 TH(I,1)=TH(I,2)-TH(I,NCOLS)+TH(I,NCOM)
      RETURN
    5 TF=(1.D 00+DSQRT(1.D 00+4.D 00*GAM*P(NCEN,NCOM)**2))/2
     1.D 00
      DO 6 I=1,NROWS
      TH(I,1)=1.D 00
    6 TH(I,NCOLS)=TF
      DO 7 J=2,NCOM
      TH(NROWS,J)=TH(1,J)
    7 TH(1,J)=TH(2,J)-TH(NROWS,J)+TH(NROM,J)
      RETURN
      END
```

2. Auxiliary Programs

Several auxiliary programs were used to process the results of the sheath program. The first calculates the non-dimensional current from the potential, charge density and temperature profiles. The second program creates a graphical display of the potential and charge distributions along a cut perpendicular to the electrode and through it. The third program uses the same cut to regenerate the electron temperature in a one-dimensional plot. The fourth program is a modification of one by Biblarz[47] which produces a two-dimensional display or contour map of the potential and charge density fields.

These programs are reproduced in the following pages and include explanations of their parameters and use.

```
C**                         CURRENT PROGRAM                              **
C
C
C   THIS PROGRAM IS DESIGNED TO CALCULATE THE CURRENT
C   DISTRIBUTION GIVEN THE POTENTIAL AND CHARGE DENSITY
C   FIELDS.  IT OUTPUTS USING SUBROUTINE WRITER FROM THE
C   SHEATH PROGRAM.  AS WITH THE SHEATH PROGRAM IT USES A
C   DATA CELL FOR VARIABLE STORAGE.  IT REQUIRES THE
C   FOLLOWING PREDETERMINED PARAMETERS:
C      P        POTENTIAL DISTRIBUTION
C      G        ELECTRON DENSITY DISTRIBUTION
C      SI       ION DENSITY DISTRIBUTION
C      GAM      JOULE HEATING PARAMETER
C      BET      HALL PARAMETER
C      ZL       STEP SIZE MULTIPLE
C      NROWS ARRAY WIDTH
C      NCOLS ARRAY LENGTH
      IMPLICIT REAL*8(A-H,O-Z)
      DIMENSION P(51,51),G(51,51),SI(51,51),XJ(51,51),YJ(51,
     1   51),SX(51,51),ZI(51),TH(51,51)
      READ(1) P
      READ(1) G
      READ(1) SI
      GAM=0.0
      ZL=5.D 02
      BET=1.D 00
      NROWS=51
      NCOLS=51
      NROM=NROWS-1
      NCOM=NCOLS-1
      NB=NCOLS-1
      NC=NB-1
      H=ZL/DFLOAT(NROWS-1)
      HR=5.0D-01/H
      G1=GAM*.25D 00/(H*H)
      G2=GAM/(H*H)
      DO 10 I=1,NROWS
      DO 10 J=1,NCOLS
   10 TH(I,J)=1.D 00
      IF(GAM.LE.1.D-04) GO TO 20
C   CALCULATE DERIVATIVES AND ELECTRON TEMPERATURE
      DO 2 I=2,NROM
      DO 2 J=2,NCOM
      EL=G(I,J)
      DPX=P(I+1,J)-P(I-1,J)
      DPY=P(I,J+1)-P(I,J-1)
      DNX=G(I+1,J)-G(I-1,J)
      DNY=G(I,J+1)-G(I,J-1)
      ARG=G1*(DNX*DPX+DNY*DPY)/EL-1.D 00
      ARG2=G2*(DPX*DPX+DPY*DPY)
      TH(I,J)=(-ARG+DSQRT(ARG*ARG+ARG2))/2.D 00
    2 CONTINUE
C   CALCULATE CROSS-CHANNEL CURRENT DENSITY
   20 DO 3 I=1,NROWS
      SI(I,1)=-3.*G(I,1)+4.*G(I,2)-G(I,3)-G(I,1)*(-
     1   3.*P(I,1)+4.*P(I,2)-P(I,3))
      SI(I,NCOLS)=G(I,NC)-4.*G(I,NB)+3.*G(I,NCOLS)-
     1   G(I,NCOLS)*(P(I,NC)-4.*P(I,NB)+
     2   3.*P(I,NCOLS))
      DO 3 J=2,NB
    3 SI(I,J)=TH(I,J)*(G(I,J+1)-G(I,J-1))-G(I,J)*(P(I,J+1)-
     1   P(I,J-1))
C   CALCULATE AXIAL CURRENT DENSITY
      DO 4 J=1,NCOLS
      SX(1,J)=-3.*G(1,J)+4.*G(2,J)-G(3,J)-G(1,J)*(-
     1   3.*P(1,J)+4.*P(2,J)-P(3,J))
      SX(NROWS,J)=G(NC,J)-4.*G(NB,J)+3.*G(NROWS,J)-
     1   G(NROWS,J)*(P(NC,J)-4.*P(NB,J)+
     2   3.*P(NROWS,J))
      DO 4 I=2,NB
    4 SX(I,J)=TH(I,J)*(G(I+1,J)-G(I-1,J))-G(I,J)*(P(I+1,J)-
     1   P(I-1,J))
```

```
C   APPLY HALL PARAMETER
      DO 5 I=1,NROWS
      DO 5 J=1,NCOLS
      YJ(I,J)=(SI(I,J)-BET*SX(I,J))*HR
      XJ(I,J)=(SX(I,J)+BET*SI(I,J))*HR
    5 CONTINUE
C   INTEGRATE FOR NET CURRENT
      FAC=1.D 00/(3.D 00*DFLOAT(NB))
      DO 7 I=1,NROWS
      SUM1=0.0
      SUM2=0.0
      SUM=XJ(I,1)+XJ(I,NCOLS)
      DO 8 J=2,NB,2
    8 SUM1=SUM1+XJ(I,J)
      DO 9 J=3,NC,2
    9 SUM2=SUM2+XJ(I,J)
      ZI(I)=(SUM+4.D 00*SUM1+2.D 00*SUM2)*FAC
    7 CONTINUE
C   OUTPUT
      WRITE(6,101)
      CALL WRITER(XJ,NROWS,NCOLS)
      WRITE(6,102)
      CALL WRITER(YJ,NROWS,NCOLS)
      WRITE(6,104) (I,ZI(I),I=1,NROWS)
      STOP
  101 FORMAT(//,3X,'X-CURRENT',/)
  102 FORMAT(//,3X,'Y-CURRENT',/)
  104 FORMAT(//,51(3X,I4,1PD12.5,/))
      END
```

```
C**.      ONE-DIMENSIONAL POTENTIAL AND CHARGE DISPLAY        **
C
C
C   THIS PROGRAM DISPLAYS THE POTENTIAL AND CHARGE DENSITY
C   DISTRIBUTIONS ALONG A CUT PERPENDICULAR TO THE WALL
C   AND THROUGH THE ELECTRODE.  IT DISPLAYS THE RESULT AS A
C   GRAPH ON THE CALCOMP PLOTTER USING A NAVAL POSTGRADUATE
C   SCHOOL SUBROUTINE DRAWP.  IT REQUIRES THE FOLLOWING
C   PREDETERMINED PARAMETERS:
C      P      POTENTIAL DISTRIBUTION
C      G      ELECTRON DENSITY DISTRIBUTION
C      SI     ION DENSITY DISTRIBUTION
C      RAT    CHARGE DENSITY BOUNDARY VALUE
C      NM     ARRAY LENGTH
C      NC     ELECTRODE LOCATION
C      ZL     STEP SIZE MULTIPLE
C      TITLE DESIRED GRAPH LEGEND
C   OTHER PARAMETERS ARE EXPLAINED IN SUBROUTINE DRAWP.
      IMPLICIT REAL*8 (A-H,O-Z)
      INTEGER*4 ITB(12)/12*0/
      REAL*4 RTB(28)/28*0.0/
      REAL*4 LABL(3)/'POT ','POS ','NEG '/
      DIMENSION X(51),Y(51),Z(51),W(51)
      DIMENSION A(51,51)
      EQUIVALENCE (TITLE,RTB(5))
      REAL*8 TITLE(12)
      READ(5,101) TITLE
C   SET CONSTANTS
      RAT=1.D-03
      NM=51
      NC=26
      ZL=5.D 02
      H=ZL/DFLOAT(NM-1)
      ITB(4)=10
      RTB(2)=.125
      ITB(5)=1
      ITB(6)=1
      ITB(8)=2
      DO 12 I=1,NM
   12 X(I)=H*DFLOAT(I-1)
C   INPUT DATA
      READ(1) A
      AA=A(1,26)
      DO 1 I=1,NM
    1 Y(I)=A(I,NC)/AA
      READ(1) A
      DO 2 I=1,NM
    2 Z(I)=A(I,NC)
      READ(1) A
      DO 3 I=1,NM
    3 W(I)=A(I,NC)
      NFLAG=1
   10 GO TO (4,5,6,7),NFLAG
    5 DO 8 I=1,NM
    8 Y(I)=W(I)/RAT
      GO TO 4
    6 DO 9 I=1,NM
    9 Y(I)=Z(I)/RAT
    4 RTB(3)=LABL(NFLAG)
      ITB(1)=NFLAG
C   OUTPUT
      CALL DRAWP(NM,X,Y,ITB,RTB)
      NFLAG=NFLAG+1
      GO TO 10
    7 STOP
  101 FORMAT(6A8)
      END
```

```
C**             ELECTRON TEMPERATURE PROFILE                             **
C
C
C  THIS PROGRAM CALCULATES THE ELECTRON TEMPERATURE RATIO
C  ALONG A CUT PERPENDICULAR TO THE WALL AND THROUGH THE
C  ELECTRODE.  IT DISPLAYS THE RESULT AS A GRAPH ON THE
C  CALCOMP PLOTTER USING THE NAVAL POSTGRADUATE SCHOOL
C  SUBROUTINE DRAWP.  IT REQUIRES THE FOLLOWING
C  PRE-DETERMINED PARAMETERS:
C     P      POTENTIAL DISTRIBUTION
C     G      ELECTRON DENSITY DISTRIBUTION
C     SI     ION DENSITY DISTRIBUTION
C     GAM    JOULE HEATING PARAMETER
C     Z      STEP SIZE MULTIPLE
C     NM     ARRAY LENGTH
C     NC     ELECTRODE LOCATION
C     TITLE DESIRED LEGEND ON GRAPH
C  OTHER PARAMETERS ARE EXPLAINED IN SUBROUTINE DRAWP
      IMPLICIT REAL*8 (A-H,O-Z)
      INTEGER*4 ITB(12)/12*0/
      REAL*4 RTB(28)/28*0.0/
      DIMENSION P(51,51),G(51,51),SI(51,51),TH(51),X(51)
      EQUIVALENCE (TITLE,RTB(5))
      REAL*8 TITLE(12)
      READ(5,101) TITLE
C  SET CONSTANTS
      GAM=1.0D 03
      Z=5.0D 02
      NM=51
      NROM=50
      H=Z/DFLOAT(NROM)
      NC=26
      NCM=NC-1
      NCP=NC+1
      G1=GAM*.25D 00/(H*H)
      G2=GAM/(H*H)
      ITB(4)=10
      ITB(5)=1
      ITB(6)=1
      ITB(8)=2
      READ(1) P
      READ(1) G
      READ(1) SI
      DO 12 I=1,NM
   12 X(I)=H*DFLOAT(I-1)
      TH(1)=1.D 00
      TH(NM)=1.D 00
C  CALCULATE ELECTRON TEMPERATURE RATIO
      DO 1 I=2,NROM
      EL=G(I,NC)
      DPX=P(I+1,NC)-P(I-1,NC)
      DPY=P(I,NCP)-P(I,NCM)
      DNX=G(I+1,NC)-G(I-1,NC)
      DNY=G(I,NCP)-G(I,NCM)
      ARG=G1*(DNX*DPX+DNY*DPY)/EL-1.D 00
      ARG2=G2*(DPX*DPX+DPY*DPY)
      TH(I)=(-ARG+DSQRT(ARG*ARG+ARG2))/2.D 00
    1 CONTINUE
C  OUTPUT RESULTS
      WRITE(6,100) (TH(I),I=1,NM)
      CALL DRAWP(NM,X,TH,ITB,RTB)
      STOP
  100 FORMAT(51(3X,F12.3,/))
  101 FORMAT(6A8)
      END
```

```
C**                         CONTOUR PROGRAM                            **
C
C
C  THIS PROGRAM PLOTS THE CONTOURS OF THE POTENTIAL AND
C  CHARGE DISTRIBUTIONS USING THE CALCOMP PLOTTER.  IT USES
C  THE SAME DATA CELL AS THE SHEATH PROGRAM.  THE
C  FOLLOWING PARAMETERS MUST BE PREDETERMINED:
C     AD     POTENTIAL OR CHARGE DENSITY ARRAY
C     NROWS ARRAY LENGTH
C     NCOLS ARRAY WIDTH
C     NL     NUMBER OF POTENTIAL CONTOURS TO BE PLOTTED < 21
C     NL1    NUMBER OF CHARGE DENSITY CONTOURS TO BE PLOTTED
C     IW     DESIRED OUTPUT WIDTH IN INCHES < 10
C     IH     DESIRED OUTPUT HEIGHT IN INCHES < 16
C     TABL  6 FORMATTED VARIABLES
C        (1) JOULE HEATING PARAMETER
C        (2) TEMPERATURE
C        (3) ELECTRODE POTENTIAL
C        (4) CHARGE DENSITY BOUNDARY CONDITION
C        (5) HALL PARAMETER
C        (6) CHARACTERISTIC LENGTH
C     LTG   3 GRID SELECTIONS TRUE/FALSE
C        (1) TRUE...ALL EXTERIOR CONTOUR SEGMENTS AND
C                   INTERNAL MAXIMUMS WILL BE LABELED.
C        (2) TRUE...REQUEST TIC MARKS AND CORRESPONDING
C                   SCALE VALUES ONE INCH APART ON EXTERIOR
C                   FRAME OF THE CONTOUR GRAPH
C            FALSE..OMIT TIC OPTION
C        (3) TRUE...REQUEST A ONE INCH BY ONE INCH STRAIGHT
C                   LINE GRID SUPERIMPOSED ON THE CONTOUR
C                   GRAPH
C            FALSE..OMIT GRID
C  THE PROGRAM HAS THE FOLLOWING SUBROUTINES:
C        MAIN...GENERAL COORDINATION AND PREPARATION OF
C               OUTPUT
C        FLCF...ORIENTS ARRAYS TO CORRESPOND WITH OUTPUT
C               LABELLING CONVENTION
C        CLVL...DETERMINES LINES OF CONSTANT VALUE TO BE
C               PLOTTED
C        CONTUR...LABELLING AND PLOTTING COORDINATION,
C               ALLOWS SUPERPOSITION OF 3 CONTOURS ON ONE
C               PLOT.  IT UTILIZES ADDITIONAL SUBROUTINES
C               SUCH AS RESTOF, SCAN, TRACE, CALC AND PLOTT
C               AND IS A MODIFICATION OF AN NPS PROGRAM.
      COMMON/BL6/NROWS,NCOLS,IW,IH,N1
      COMMON/BL11/XLIN(100),YLIN(100)
      REAL*8 TITLE(30)/'        ','        ','        ',
     1'        ','        ','        ','GAM     ',
     2'        ','        ','DENSITY ','        ',
     3'        ','TEMP    ','        ','        ',
     4'VOLTAGE ','        ','        ','BET     ',
     5'        ','        ','LENGTH  ','        ',
     6'        ',' R. DOLS','ON      ',' POTENTI',
     7'AL MAP  ','        ','BOX 1219'/
      REAL*8 TITLEA(4)/'ELECTRON',' CHARGE ','ION CHAR','GE
      REAL*8 TABLE(6)
      REAL*8 AD(51,51)
      LOGICAL*1 LTG(3)
      DIMENSION A(81,61)
      DIMENSION CL(30)
      NAMELIST/TABL/TABLE,LTG
      NAMELIST/DOLL/NROWS,NCOLS,NL,NL1,IW,IH
      READ(5,TABL)
      READ(5,DOLL)
      XVAL=(IW*1.)/(NCOLS*1.-1.)
      YVAL=(IH*1.)/(NROWS*1.-1.)
      N1=0
      DO 10 I=1,1
      N1=N1+1
      XLIN(N1)=XVAL*(20)
   10 YLIN(N1)=0.0
      DO 1 K=1,3
```

```
C   INPUT ARRAY
      READ(2) AD
      DO 19 I=1,NROWS
      DO 19 J=1,NCOLS
   19 A(I,J)=AD(I,J)
      CALL FLOP(A,NROWS,NCOLS)
C     FIRST FIGURE CONTOUR LEVELS TO BE PLOTTED FOR MATRIX A
   11 CALL CLVL(A,CL,NL)
      WRITE(6,210)
      DO 3 I=1,NL
    3 WRITE(6,215) I,CL(I)
   12 TITLE(8)=TABLE(1)
      TITLE(11)=TABLE(4)
      TITLE(14)=TABLE(2)
      TITLE(17)=TABLE(3)
      TITLE(20)=TABLE(5)
      TITLE(23)=TABLE(6)
      CALL CONTUR(A,NROWS,NCOLS,81,CL,NL,TITLE,LTG)
C     NOW PLOT CHARGE FIELD CONTOURS
      IF(K.EQ.3) STOP
      KL=2*K-1
      KP=KL+1
      TITLE(27)=TITLEA(KL)
      TITLE(28)=TITLEA(KP)
    1 CONTINUE
  210 FORMAT(' ',T26,'THE LEVELS PLOTTED')
  215 FORMAT(' ',T33,'CL(',I2,')=',F8.4)
      STOP
      END


      SUBROUTINE FLOP(Z,NROWS,NCOLS)
      DIMENSION Z(81,61)
      IIVRT=NROWS/2
      DO 3 I=1,IIVRT
      M=NROWS-(I-1)
      DO 3 J=1,NCOLS
      SAVE=Z(I,J)
      Z(I,J)=Z(M,J)
    3 Z(M,J)=SAVE
      RETURN
      END


      SUBROUTINE CLVL(CM,CLM,NUML)
      COMMON/BL6/NROWS,NCOLS,IW,IH,N1
      DIMENSION CM(81,61),CLM(NUML)
      CMIN=CM(1,1)
      CMAX=CMIN
      DO 5 J=1,NCOLS
      DO 5 I=1,NROWS
      IF(CM(I,J).LT.CMIN) CMIN=CM(I,J)
      IF(CM(I,J).GT.CMAX) CMAX=CM(I,J)
    5 CONTINUE
C     NOW DETERMINE CONTOUR LEVELS TO BE PLOTTED.
      J=NUML
      I=NUML-1
      ANL=I*1.
      PLINT=(CMAX-CMIN)/ANL
C     NOW FILL THE CONTOUR LEVEL VECTOR
      DO 6 I=1,J
    6 CLM(I)=CMIN+(I-1)*PLINT
      RETURN
      END


      SUBROUTINE CONTUR(AM,M,N,MX,CL,NL,TITLE,LTG)
      COMMON /INTFAC/ X,Y
      COMMON /DAYHOF/ MT,NT,NI,IX,IY,IDX,IDY,ISS,IT,IV,NP,
```

```
      COMMON/TABL/ TABC(20,6),JC
      COMMON/DITS/XMIN,YMIN,SLOPEX,SLOPEY,DITSDX,DITSDY,
      COMMON/BL6/NROWS,NCOLS,IW,IH,N1
      COMMON/BL11/XLIN(100),YLIN(100)
      COMMON/BL13/NSCN
      REAL*8 TITLE(1)
      REAL*8 WIDTH/'WIDTH'/,HEIGHT/'HEIGHT'/,WHICH
      DIMENSION AM(MX,1),CL(1)
      DIMENSION             REC(900),  X(1800), Y(1800)
      DIMENSION IPT(3,3),INX(8),INY(8)
      DIMENSION DITSX(5),DITSY(5)
      LOGICAL*1 LTG(1),MINUS,LABL
      JC=0
      LABL=LTG(1)
C     CHECK IW PARAMETER
      WHICH=WIDTH
      IF(IW) 1,1,2
    1 WRITE(6,60) WHICH
   60 FORMAT('0',T7,A8,'OF CONTOUR GRAPH ILLEGAL.')
   71 WRITE(6,64)
   64 FORMAT('0',T7,'NO GRAPH WILL BE PRODUCED.')
      RETURN
C     CHECK IF IW IS TOO WIDE
    2 IF(IW-9) 3,3,40
   40 WRITE(6,61)
   61 FORMAT('0',T7,'IW PARAMETER GREATER THAN 9. CONTUR
      IW=9
C     NOW CHECK IH PARAMETER
    3 IF(IH) 4,4,5
    4 WHICH=HEIGHT
      GO TO 1
    5 DITSDX=(N-1.0)/IW
      DITSDY=(-1.0+M)/IH
      XMIN=1.0
      YMIN=-M
      SLOPEX=1.0/DITSDX
      SLOPEY=1.0/DITSDY
      DITSX(1)=1.0
      DITSX(4)=1.0
      DITSX(5)=1.0
      DITSX(2)=N
      DITSX(3)=N
      DITSY(1)=-1.0
      DITSY(2)=-1.0
      DITSY(5)=-1.0
      DITSY(3)=-M
      DITSY(4)=-M
      DO 2011 I=1,5
      DITSX(I)=SLOPEX*(DITSX(I)-XMIN)
 2011 DITSY(I)=SLOPEY*(DITSY(I)-YMIN)
      STARTP=(9.0-IW)/2.0
      CALL PLOTS
      CALL PLOT(STARTP,0.0,-3)
      CALL LINE(DITSX,DITSY,5,1,1)
      DITSX(1)=DITSX(1)-.5
      DITSX(5)=DITSX(1)
      DITSX(4)=DITSX(4)-.5
      DITSX(2)=DITSX(2)+.5
      DITSX(3)=DITSX(3)+.5
      DITSY(1)=DITSY(1)+.5
      DITSY(5)=DITSY(1)
      DITSY(2)=DITSY(2)+.5
      DITSY(3)=DITSY(3)-.5
      DITSY(4)=DITSY(4)-.5
      CALL LINE(DITSX,DITSY,5,1,1)
      SLOPEX=1.0/DITSDX
      SLOPEY=1.0/DITSDY
      IENDX=SLOPEX*N+1
      IENDY=SLOPEY*M+1
      IF(.NOT.LTG(2)) GO TO 34
C     DRAW TIC MARKS ON OUTER FRAME
C     START ON LEFT EDGE GOING DOWNWARD
```

```
      IFLAG=0
      ZINGX=-.1
      ZINGY=0.0
      ZX=0.0
      ZY=-.9
      CX=DITSX(1)
      CY=DITSY(1)-.5
      IEND=11
 2222 IFLAG=IFLAG+1
      DO 2022 I=1,IEND
      CALL PLOT(CX,CY,3)
      COORDX=CX+ZINGX
      COORDY=CY+ZINGY
      CALL PLOT(COORDX,COORDY,2)
      CX=CX+ZX
 2022 CY=CY+ZY
      GO TO (21,22,23,24),IFLAG
C     NOW DO THE RIGHT EDGE GOING DOWNWARD
   21 ZINGX=.1
      CX=DITSX(2)
      CY=DITSY(2)-.5
      GO TO 2222
C     NOW DO TOP EDGE
   22 ZINGX=0.0
      ZINGY=.1
      ZX=.9
      ZY=0.0
      CX=DITSX(1)+.5
      CY=DITSY(1)
      IEND=11
      GO TO 2222
C     NOW DO THE BOTTOM EDGE
   23 ZINGY=-.1
      CX=DITSX(4)+.5
      CY=DITSY(4)
      ZINGY=-.1
      GO TO 2222
C     NOW LABEL TIC MARKS
C     DO X-DIRECTION FIRST, TOP EDGE
C     POSITION PEN
   24 DELTAX=.1
      IFLAG=0
      ZX=.9
      ZY=0.0
      CX=DITSX(1)+.35
      CY=DITSY(1)+.12
 3033 IFLAG=IFLAG+1
      XZERO=0.0
      DO 3333 I=1,11
      CALL NUMBER(CX,CY,.14,XZERO,0.0,2)
      CX=CX+ZX
      CY=CY+ZY
 3333 XZERO=XZERO+DELTAX
      GO TO (31,32,33,34),IFLAG
C     LABEL BOTTOM EDGE TIC MARKS
   31 CX=DITSX(4)+.35
      CY=DITSY(4)-.19
      GO TO 3033
C     LABEL LEFT EDGE OF TIC MARKS
   32 CX=DITSX(4)-.4
      CY=DITSY(4)+.46
      DELTAX=.1
      IEND=IENDY
      ZX=0.0
      ZY=.9
      GO TO 3033
C     NOW LABEL RIGHT EDGE TIC MARKS
   33 CX=DITSX(3)+.12
      CY=DITSY(3)+.46
      GO TO 3033
C     CHECK IF GRID DESIRED
   34 CALL RESTOF(LTG,IENDX,IENDY,NL,AM,M,N,MX,CL,STARTP,TIT
```

```
         LE,DITSX,    DITSY)
      RETURN
      END
      SUBROUTINE RESTOF(LTG,IENDX,IENDY,NL,AM,M,N,MX,CL,STAR
         TP,TITLE,    DITSX,DITSY)
      REAL*8 TITLE(1)
      DIMENSION AM(MX,1),CL(1)
      DIMENSION DITSX(5),DITSY(5)
      LOGICAL*1 LTG(1),MINUS,LABL
      COMMON/TABL/TABC(20,6),JC
      COMMON/DITS/XMIN,YMIN,SLOPEX,SLOPEY,DITSDX,DITSDY,
      COMMON/BL6/NROWS,NCOLS,IW,IH,N1
      COMMON/BL11/XLIN(100),YLIN(100)
      COMMON/BL13/NSCN
      IF(.NOT.LTG(3)) GO TO 35
C     DRAW INCH BY INCH GRID
      IEND=IENDX-2
C     POSITION PEN
      IFLAG=0
      CX=DITSX(1)+.5
      CY=DITSY(1)-.5
      COORDX=0.0
      COORDY=-IH
      DX=1.0
      DY=0.0
 4044 DO 4444 I=1,IEND
      CX=CX+DX
      CY=CY+DY
      CALL PLOT(CX,CY,3)
      ZX=CX+COORDX
      ZY=CY+COORDY
 4444 CALL PLOT(ZX,ZY,2)
      IF(IFLAG) 35,42,35
   42 IFLAG=1
      IEND=IENDY-2
      CY=DITSY(4)+.5
      CX=DITSX(4)+.5
      COORDX=IW
      COORDY=0.0
      DX=0.0
      DY=1.0
      GO TO 4044
   35 CONTINUE
      CALL LINE(XLIN,YLIN,N1,1,-6)
      DO 20 I=1,NL
   20 CALL SCAN(AM,M,N,MX,CL(I))
      NSCN=1
      IF(.NOT.LABL) GO TO 778
      IF(JC.EQ.0) GO TO 778
      DO 777 I=1,JC
      COORDX=TABC(I,4)
      COORDY=TABC(I,5)
      CLEV=TABC(I,6)
      CALL NUMBER(COORDX,COORDY,.07,CLEV,0.0,3)
  777 CONTINUE
  778 CALL SYMBOL(-STARTP,IH+1.0,.21,TITLE(25),0.0,48)
      CALL SYMBOL(-STARTP,IH+1.5,.21,TITLE(19),0.0,48)
      CALL SYMBOL(-STARTP,IH+2.0,.21,TITLE(13),0.0,48)
      CALL SYMBOL(-STARTP,IH+2.5,.21,TITLE(7),0.0,48)
      CALL SYMBOL(-STARTP,IH+3.0,.21,TITLE(1),0.0,48)
      CALL PLOT(-STARTP,IH+6.5,-3)
      CALL PLOTE
      RETURN
  779 CALL SYMBOL(-STARTP,IH+1.0,.21,TITLE(25),0.0,48)
      CALL PLOT(-STARTP,IH+4.5,-3)
      CALL PLOTE
      RETURN
      END
      SUBROUTINE SCAN(AM,M,N,MX,CL)
      DIMENSION AM(MX,1 ),REC(900),   X(1800), Y(1800)
      DIMENSION IPT(3,3),INX(8),INY(8)
      COMMON /DAYHOF/ MT,NT,NI,IX,IY,IDX,IDY,ISS,IT,IV,NP,NQ
```

```
         ,JT,                      PY,REC,CV,     IFT,INX,
         INY,DL,RA,THE
      COMMCN /INTFAC/ X,Y
      LOGICAL *1 LABL,MINUS
      COMMON/DITS/XMIN,YMIN,SLOPEX,SLOPEY,DITSDX,DITSCY,
      COMMON/BL13/NSCN
      D=0.
      R=1.
      TH = 1.570796
      NP=0
      DL=D
      RA=R
      THE=TH
      MT=N
      NT=M
      CV=CL
      IF(NSCN.EQ.1) IZW=0
      IF(IZW-120631) 1,3,1
    1 IPT(1,1)=8
      IPT(1,2)=1
      IPT(1,3)=2
      IPT(2,1)=7
      IPT(2,3)=3
      IPT(3,1)=6
      IPT(3,2)=5
      IPT(3,3)=4
      INX(1)=-1
      INX(2)=-1
      INX(3)=0
      INX(4)=1
      INX(5)=1
      INX(6)=1
      INX(7)=0
      INX(8)=-1
      INY(1)=0
      INY(2)=1
      INY(3)=+1
      INY(4)=+1
      INY(5)=0
      INY(6)=-1
      INY(7)=-1
      INY(8)=-1
      IZW=120631
    3 XT=MT
      DO 58 J=1,900
   58 REC(J)=0
      ISS=0
    2 MT1=MT-1
      IDIR=1
      DO 110 I=1,MT1
      IF(AM(1,I)-CV) 55,110,110
   55 IF(AM(1,I+1)-CV) 110,57,57
   57 IX=I+1
      IY=1
      IDX=-1
      IDY=0
      CALL TRACE (AM,MX)
  110 CONTINUE
      NT1=NT-1
      IDIR=2
      DO 20 I=1,NT1
      IF(AM(I,MT)-CV) 15,20,20
   15 IF(AM(I+1,MT)-CV) 20,17,17
   17 IX=MT
      IY=I+1
      IDX=0
      IDY=-1
      CALL TRACE (AM,MX)
   20 CONTINUE
      IDIR=3
   22 DO 30 I=1,MT1
      MT2=MT+1-I
```

```
      IF(AM(NT,MT2)-CV) 25,30,30
   25 IF(AM(NT,MT2-1)-CV) 30,27,27
   27 IX=MT2-1
      IY=NT
      IDX=1
      IDY=0
      CALL TRACE (AM,MX)
   30 CONTINUE
      IDIR=4
      DO 40 I=1,NT1
      NT2=NT+1-I
      IF(AM(NT2,1)-CV) 35,40,40
   35 IF(AM(NT2-1,1)-CV) 40,37,37
   37 IX=1
      IY=NT2-1
      IDX=0
      IDY=1
      CALL TRACE (AM,MX)
   40 CONTINUE
      IDIR=5
      ISS=1
      NT1=NT-1
      MT1=MT-1
      DO 10 J=2,NT1
      DO 10 I=1,MT1
      IF(AM(J,I)-CV)5,10,10
    5 IF(AM(J,I+1)-CV) 10,7,7
    7 COM=100*(I+1)+J
      IF (NP) 12,11,12
   12 DO 9 ID= 1,NP
      IF (REC(ID)-COM) 9,10,9
    9 CONTINUE
   11 IX= I+1
      IY=J
      IDX=-1
      IDY=0
      CALL TRACE (AM,MX)
   10 CONTINUE
      RETURN
      END
      SUBROUTINE TRACE (AM,MY)
      DIMENSION AM(MY,1 ),REC(900),   X(1800), Y(1800)
      DIMENSION IPT(3,3),  INX(8),INY(8)
      COMMON /DAYHOF/ MT,NT,NI,IX,IY,IDX,IDY,ISS,IT,IV,NP,
      COMMON /INTFAC/ X,Y
      PY=0.0
      RC=  COS (THE)*RA
      RS=  SIN (THE)*RA
  501 JT=0
      N=0
      IXO=IX
      IYO=IY
      ISX=IDX+2
      ISY=IDY+2
      IS=IPT(ISX,ISY)
      JTB=0
      ISO=IS
      IF(ISO-8)18,18,17
   17 ISO=ISO-8
   18 IT=0
    5 CONTINUE
      CALL CALC  (AM,MY)
      NZ=N
      N=NZ
      IF (IT+JT-1) 49,49,47
   47 XS=X(N-1)
      YS=Y(N-1)
      X(N-1)=X(N)
      Y(N-1)=Y(N)
      X(N)=XS
      Y(N)=YS
   49 IS=IS+1
```

```
    JT=IT
  9 IF (IS-9) 8,7,7
  7 IS=IS-8
  8 IDX=INX(IS)
    IDY=INY(IS)
    IX2=IX+IDX
    IY2=IY+IDY
    JTB=JTB+1
    IF (JTB-1799) 51,51,308
308 PRINT                  103,CV,X(N),Y(N)
103 FORMAT(1H0,23HA CONTOUR LINE AT LEVEL,E12.5,
    RETURN
 51 CONTINUE
    IF (ISS) 10,10,20
 20 IF(IX-IXO) 12,21,12
 21 IF(IY-IYO) 12,22,12
 22 IF(IS-ISO) 12,23,12
 23 CONTINUE
    CALL CALC (AM,MY)
    GO TO 73
 10 IF(IX2) 13,50,13
 13 IF (IX2-MT) 19,19,50
 19 IF (IY2) 11,50,11
 11 IF (IY2-NT) 12,12,50
 12 IF(CV-AM( IY2,IX2)) 206,206,5
206 IF (IDX**2+IDY**2-1) 213,6,213
213 DCP=(AM(IY,IX)+AM(IY,IX2)+AM(IY2,IX)+AM(IY2,IX2))/4.0
    IF (DCP-CV) 5,217,217
217 IF (INX(IS-1)) 214,215,214
214 IX=IX+IDX
    IDX=-IDX
    PY=2.0
    CALL CALC  (AM,MY)
    IX=IX+IDX
    GO TO 6
215 IY=IY+IDY
    IDY=-IDY
    PY=2.0
    CALL CALC  (AM,MY)
    IY=IY+IDY
  6 IF(AM(IY,IX-1)-CV) 306,16,16
306 NP=NP+1
    REC(NP)=100*IX+IY
 16 IS=IS+5
    IX=IX2
    IY=IY2
    GO TO 9
 50 XT=MT
    IF(AM(IY,IX-1)-CV) 307,73,73
307 NP=NP+1
    REC(NP)=100*IX+IY
 73 DO 74 I=1,N
    X(I)=X(I)+RC*Y(I)
 74 Y(I)=RS*Y(I)
    CALL PLOTT(N,CV)
    RETURN
    END
    SUBROUTINE CALC(AM,MY)
    DIMENSION AM(MY,1 ),REC(900),  X(1800), Y(1800)
    DIMENSION IPT(3,3),INX(8),INY(8)
    COMMON /DAYHOF/ MT,NT,NI,IX,IY,IDX,IDY,ISS,IT,IV,NP,N,
    COMMON /INTFAC/ X,Y
    IT=0
    N=N+1
    IF (IDX**2 + IDY**2 -1) 20,1,20
  1 IF (IDX) 10,2,10
  2 X(N)=IX
    Z=IY
    IY2=IY+IDY
    DY=IDY
 41 Y(N)=((AM(IY,IX)-CV)/(AM(IY,IX)-AM(IY2,IX)))*DY+Z
    RETURN
```

```
   10 Y(N)=IY
      W=IX
      DX=IDX
      IX2=IX+IDX
   44 X(N)=((AM(IY,IX)-CV)/(AM(IY,IX)-AM(IY,IX2)))*DX+W
      RETURN
   20 IX2=IX+IDX
      IY2=IY+IDY
      W=IX
      Z=IY
      DX=IDX
      DY=IDY
      DCP=(AM(IY,IX)+AM(IY,IX2)+AM(IY2,IX)+AM(IY2,IX2))/4.0
      IF (PY-2.0) 24,21,24
   24 IF (DCP-CV) 21,21,25
   21 AL=AM(IY,IX)-DCP
   23 V=.5*(AL+DCP -CV)/AL
   27 X(N)=V*DX+W
      Y(N)=V*DY+Z
      PY=0.0
      RETURN
   25 IT=1
      AL=AM(IY2,IX2)-DCP
   33 V=.5*(AL+DCP-CV)/AL
   28 X(N)=-V*DX+W  + DX
      Y(N)=-V*DY+Z  + DY
      Y(N)=-V*DY+Z  + DY
      RETURN
      END
      SUBROUTINE PLOTT(NP,CV)
      COMMON/INTFAC/X(1800),Y(1800)
      LOGICAL*1 MINUS,LABL
      COMMON/TABL/ TABC(20,6),JC
      COMMON/DITS/XMIN,YMIN,SLOPEX,SLOPEY,DITSDX,DITSDY,
C     SCALE POINTS FOR PLOT ROUTINE
      DO 100 I=1,NP
      X(I)=SLOPEX*(X(I)-XMIN)
  100 Y(I)=SLOPEY*(-Y(I)-YMIN)
      CALL LINE(X,Y,NP,1,1)
      IF(.NOT.LABL) RETURN
      DIR=0.0
      GO TO (1,2,3,4,6), IDIR
    1 DIR=90.
    2 COORDX=X(1  )
      COORDY=Y(1  )
    5 CALL NUMBER(COORDX,COORDY,.07,CV,DIR,3)
      RETURN
C     MOVE PEN DOWN ONE HALF INCH
    3 DIR=90.
      COORDX=X(1  )
      COORDY=Y(1  )-.3
      GO TO 5
C     MOVE PEN TO THE LEFT
    4 COORDX=X(1  )-.3
      COORDY=Y(1  )
      GO TO 5
C     SEARCH FOR XMAX,XMIN,YMAX,YMIN,AND SAVE YMINX
    6 XMAX=X(1)
      SMIN=XMAX
      YMINX=Y(1)
      YMAX=YMINX
      VMIN=YMINX
      DO 200 I=2,NP
      IF(X(I).GT.XMAX) XMAX=X(I)
      IF(Y(I).LT.VMIN) VMIN=Y(I)
      IF(Y(I).GT.YMAX) YMAX=Y(I)
      IF(X(I).GE.SMIN) GO TO 200
      SMIN=X(I)
      YMINX=Y(I)
  200 CONTINUE
C     JC=NUMBER OF ENTRIES IN TABC
      IF(JC) 400,500,400
```

```
  400 DO 900 I=1,JC
      IF(XMAX.LT.TABC(I,1).AND.YMAX.LT.TABC(I,2).AND.VMIN.
  900 CONTINUE
C     DID NOT FIND THIS CONTOUR TO BE INTERIOR TO ANOTHER
C     CHECK IF EXTERIOR
      DO 1000 I=1,JC
      IF(XMAX.GT.TABC(I,1).AND.YMAX.GT.TABC(I,2).AND.VMIN.
 1000 CONTINUE
  500 IF (JC.EQ.20) RETURN
      JC=JC+1
      MC=JC
  600 TABC(MC,1)=XMAX
      TABC(MC,2)=YMAX
      TABC(MC,3)=VMIN
      TABC(MC,4)=SMIN
      TABC(MC,5)=YMINX
      TABC(MC,6)=CV
      RETURN
C     CHECK IF THIS INTERIOR ONE IS OF HIGHER LEVEL
  700 IF(CV.LE.TABC(I,6) ) RETURN
 2000 MC=I
      GO TO 600
C     CHECK IF LEVEL OF THIS EXTERIOR ONE IS HIGHER
  800 IF(CV.LT.TABC(I,6)) RETURN
      GO TO 2000
      END
```

3. Boundary Layer Program

The program which solves equation A.18 from Appendix A is shown in the following pages. It calculates the solution to the boundary layer voltage drop for a varying C_p. It therefore requires an enthalpy table for the calculation, and such a table is provided in data format following the program. This particular table is for a Toluene/oxygen/cesium mixture at temperatures from 1500°K to 2640°K. An explanation on the use of the program is included.

```
**                    BOUNDARY LAYER ROUTINE                       **
C   THIS ROUTINE IS DESIGNED TC CALCULATE THE BOUNDARY
C   LAYER VCLTAGE DROP IN AN MHD CHANNEL.  IT USES A
C   SIMPSCN'S RULE INTEGRATION TECHNIQUE AND REQUIRES AN
C   ENTHALPY TABLE FOR THE RANGE OF TEMPERATURES CONSICERED.
C   THE FCLLCWING PARAMETERS ARE REQUIRED:
C      POT=SEED IONIZATION POTENTIAL IN EV'S
C      TFREE=FREE STREAM TEMPERATURE
C      TWALL=WALL TEMPERATURE
C      TTCP=MAX TEMPERATURE IN ENTHALPY TABLE. TTOP MUST BE
C         GREATER THAN OR EQUAL TO TFREE.
C      TBCT=LCWEST TEMPERATURE IN ENTHALPY TABLE.  MUST BE
C         EQUAL TO OR SMALLER THAN TWALL.
C      NPTS=NUMBER OF POINTS USED IN INTEGRATION ROUTINE
C      MAX=NUMBER CF POINTS IN ENTHALPY TABLE
C   ENTHALPY TABLE MUST BE EQUALLY INCREMENTED
      COMMCN/BL1/DEL,TFREE,TWALL,TBOT,ALPH,ENTZ,TTOP,MAX,N,E
         NTH(100)
      READ(5,101) POT,TFREE,TWALL,NPTS,N
      WRITE(6,100) POT,TFREE,TWALL,NPTS,N
      READ(5,102) TTCP,TBOT,MAX
      READ(5,103) (ENTH(J),J=1,MAX)
      WRITE(6,105)
      MAX1=MAX-1
      NN=N-1
      NM=N-2
      ALPH=PCT*5.8054E 03/TFREE
      DEL=(TTOP-TBOT)/FLCAT(MAX-1)
      THWALL=TWALL/TFREE
      DELM=(TWALL-TBOT)/DEL
      M=DELM
      ENTZ=ENTH(M+1)+(ENTH(M+2)-ENTH(M+1))*(TWALL-M*DEL-
         TBCT)/DEL
      DELM=(TFREE-TBOT)/DEL
      M=CELM
      IF(M.LT.MAX1) GO TO 4
      ENTF=ENTH(MAX)
      GO TO 5
    4 ENTF=ENTH(M+1)+(ENTH(M+2)-ENTH(M+1))*(TFREE-M*DEL-
         TBCT)/DEL
    5 ENTHM1=ENTF-ENTZ
      FAC=ENTHM1**N
      COEF2=FLCAT(N)*TFREE/FAC
      C=FCTN(1.0)
      DELTA=(1.0-THWALL)/FLOAT(NPTS-1)
C   SIMPSCN'S RULE INTEGRATION PATTERN 1,4,2,4,1
      SUM1=0.0
      SUM2=C.0
      NPT1=NPTS-1
      NPT2=NPTS-2
C   COMPUTATICN FOR LAST POINT. FIRST POINT IS ZERO.
      SUM=C
C   COMPUTATICN FOR EVEN POINTS...THOSE MULTIPLIED BY 4
      THETA=THWALL+DELTA
      DO 10 J=2,NPT1,2
      SUM1=SUM1+FCTN(THETA)
      THETA=THETA+2.*DELTA
   10 CONTINUE
C   COMPUTATICN FOR ODD POINTS...THOSE MULTIPLIED BY 2
      THETA=THWALL+2.*DELTA
      DO 20 J=3,NPT2,2
      SUM2=SUM2+FCTN(THETA)
      THETA=THETA+2.*DELTA
   20 CONTINUE
      VOLT=DELTA*(SUM+4.*SUM1+2.*SUM2)/3.
      VOLT=CCEF2*VOLT-1.0
      WRITE(6,104) TWALL,TFREE,THWALL,VOLT
      STOP
  101 FORMAT(3F9.0,2I9)
  102 FCRMAT(2E9.0,I9)
  100 FORMAT(3X,'IONIZATION POTENTIAL=',F7.3,3X,'FREE STREAM
           TEMP=',F6.1,3X,'WALL TEMP=',F6.1,3X,'NPTS=',I4,'
```

```
  103 FORMAT(7E9.0)
  104 FORMAT(3X,2F9.0,F9.3,E12.4)
  105 FORMAT(/,7X,'TWALL',4X,'TFREE',3X,'THWALL',8X,'VOLT')
      END
C
C   FUNCTION THETA
C
      FUNCTION FCTN(THETA)
      COMMON/BL1/DEL,TFREE,TWALL,TBOT,ALPH,ENTZ,TTOP,MAX,N,E
         NTH(100)
      MAX1=MAX-1
      MAXM=MAX-3
      NN=N-1
      A=THETA**(-1.75)
      B=EXP(ALPH*(1.0/THETA-1.0))
      TEMP=THETA*TFREE
      DELM=(TEMP-TBOT)/DEL
      M=DELM
      IF(M.LT.MAX1) GO TO 4
      ENT=ENTH(MAX)
      GO TO 5
    4 ENT=ENTH(M+1)+(ENTH(M+2)-ENTH(M+1))*(TEMP-M*DEL-
         TBOT)/DEL
    5 ENT1=ENT-ENTZ
      C=ENT1**NN
      IF(M.LT.2) GO TO 1
      IF(M.GT.MAXM) GO TO 2
      CP=(ENTH(M-1)-8.*ENTH(M)+8.*ENTH(M+2)-ENTH(M+
         3))/(12.*DEL)
      GO TO 3
    1 CP=(-50.*ENTH(M+1)+96.*ENTH(M+2)-72.*ENTH(M+3)+
         32.*ENTH(M+4)-6.*ENTH(M+
         5))/(24.*DEL)
      GO TO 3
    2 CP=(6.*ENTH(M-3)-32.*ENTH(M-2)+72.*ENTH(M-1)-
         96.*ENTH(M)+50.*ENTH(M+
         1))/(24.*DEL)
    3 FCTN=A*B*C*CP
      RETURN
      END
C   DATA
3.87      2600.     2000.            401         4
2640.     1500.             58
 -1745.28 -1738.22 -1731.14 -1724.04 -1716.91 -1709.76 -
         1702.58
 -1695.36 -1688.10 -1680.79 -1673.41 -1665.93 -1658.34 -
         1650.61
 -1642.70 -1634.59 -1626.26 -1617.69 -1608.85 -1599.73 -
         1590.33
 -1580.62 -1570.59 -1560.23 -1549.51 -1538.42 -1526.95 -
         1515.05
 -1502.72 -1489.93 -1476.65 -1462.85 -1448.52 -1433.61 -
         1418.11
 -1401.98 -1385.18 -1367.71 -1349.51 -1330.56 -1310.83 -
         1290.29
 -1268.90 -1246.64 -1223.48 -1199.38 -1174.32 -1148.27 -
         1121.20
 -1093.09 -1063.90 -1033.61 -1002.21  -969.66  -935.94  -
         901.04
  -864.93  -827.60
```

BIBLIOGRAPHY

1. Gillette, P. R., "Energy for Naval Operations: a Critical R & D Problem," *Naval Research Reviews*, p. 19-28, August 1975.

2. "Breakthrough in Electric Power Research," *Naval Research Reviews*, p. 25-27,November 1974.

3. High, M. D. and Felderman, E. J., "Turbulent MHD Boundary Layers with Electron Thermal Nonequilibrium and Finite Rate Ionization," *AIAA Journal*, v. 10, p. 98-103, January 1972.

4. Argyropoulos, G. S., Demetriades, S. T., and Lackner, K., "Compressible Turbulent Magnetohydrodydamic Boundary Layers," *Physics of Fluids*, v. 11, p. 2559-2566, December 1968.

5. Doss, E. D., Dwyer H. A., and Hoffman, "Influence of Segmentation and Ambipolar Diffusion on MHD Nonequilibrium Boundary Layers," *AIAA Journal*, v. 12, p. 155-162, February 1974.

6. Kessler, R. and Eustis, R. H., "Effects of Electrode and Boundary Layer Temperature on MHD Generator Performance," *AIAA Journal*, v. 6, p. 1640-1646, September 1968.

7. Rubin, E. S. and Eustis, R. H., "Effects of Electrode Size on the Performance of a Combustion-Driven MHD Generator," *AIAA Journal*, v. 9, p. 1162-1169, June 1971.

8. Wu, Y. C. L., and others, *Current Distribution in MHD Channels with Nonuniform Gas Properties*, paper presented at the 10th Symposium on the Engineering Aspects of MHD, Cambridge, Mass., March 1969.

9. Oliver, D. A. and Mitchner, M., "Nonuniform Electrical Conduction in MHD Channels," *AIAA Journal*, v. 5, p.1424-1432, August 1967.

10. Lam, S. H., "A General Theory for the Flow of Weakly Ionized Gases," *AIAA Journal*, v. 2, p. 256-262, February 1964.

11. Stahl, N. and Su, C. H., "Theory of Continuum Flush Probes," *Physics of Fluids*, v. 14, p. 1366-1376, July 1971.

12. Cohen, I. M., "Asymptotic Theory of Spherical Electrostatic Probes in a Slightly Ionized Collision-Dominated Gas," *Physics of Fluids*, v. 6, October 1963.

13. McKee, H. B. and Mitchner, M., "Electrostatic Probes for Diagnostics in a Collision-Dominated Weakly Ionized Plasma," *Electricity from MHD* (International Atomic Energy Agency, Vienna), v. 1, p. 107, 1966.

14. Bailey, P. B. and Touryan, K. J., "Continuum Electrostatic Probes in the Presence of Negative Ions: A Numerical Solution," AIAA Journal, v. 11, p. 1225-1226, September 1973.

15. Kiel, R. E., "Continuum Electrostatic Probe Theory for Large Sheaths on Spheres and Cylinders," *Journal of Applied Physics*, v. 40, p. 3668-3673, August 1969.

16. Barad M. S. and Cohen, I. M., "Continuum Theory of Spherical Electrostatic Probes in a Stationary, Moderately Ionized Plasma," *Physics of Fluids*, v. 17, p. 724-734, April 1974.

17. Su, C. H. and Lam, S. H., "Continuum Theory of Spherical Electrostatic Probes," *Physics of Fluids*, v. 6, October 1963.

18. Lengyel, L. L., "Current and Potential Distributions in Nonequilibrium MHD Plasmas at High Magnetic Field Strengths," *AIAA Journal*, v. 9, p. 1957-1962, October 1971.

19. Chung, P. M., Talbot, L. and Touryan, K. J., "Electric Probes in Stationary and Flowing Plasmas. Part 2: Continuum Probes," *AIAA Journal*, v. 12, p. 144-153, February 1974.

20. Naval Postgraduate School Report 57Zi75052, AFOSR-TR 75-1383, *Electrode Loss Mechanisms in MHD Generators (Interim Report)*, by O. Biblarz and R. C. Dolson, p. 5, May 1975.

21. Biblarz, O., Dolson, R. C., and Shorb, A. M., "Anode Phenomena in a Collision-Dominated Plasma," *Journal of Applied Physics*, v. 46, p. 3342-3346, August 1975.

22. Chen, F. F., "Electric Probes," published in the book *Plasma Diagnostic Techniques*, p. 159-162, Academic Press, 1965.

23. Biblarz, O., unpublished

24. Kimblin, C. W., "Anode Voltage Drop and Anode Spot Formation in dc Vaccuum Arcs," *Journal of Applied Physics*, v. 40, p. 1744, March 1969

25. Hsu, M. S. S., "Thermal Instabilities and Arcs in the MHD Boundary Layers," Thirteenth Symposium on Engineering Aspects of MHD, Stanford, March 1973.

26. Sutton, G. W. and Sherman, A., *Engineering Magnetohydrodynamics*, p. 225-227, 154-156, McGraw-Hill, 1965.

27. Cobine, J. D., *Gaseous Conductors*, p. 44, Dover, 1958.

28. Blue, E. and Ingold, J. H., "Diffusion Theory for the Spherical Langmuir Probe," *Plasma Physics*, v. 10, p. 899-901, 1968.

29. Ketter, R. L. and Prowel, S. P., *Modern Methods of Engineering Computation*, p. 84, McGraw-Hill, 1969.

30. *Methods in Computational Physics*, v. 9, p. 164-166, Academic Press, 1970.

31. Marston, C., Tate, E., and Zauderer, B., "Large Enthalpy Extraction Results in a Non-Equilibrium MHD Generator,", Sixth International Conference on MHD Electrical Power Generation, Washington, D. C., June 1975.

32. Rosa, R. J., *Magnetohydrodynamic Energy Conversion*, ch. 2, McGraw-Hill, 1965.

33. Argyroupolos, G. S. and others, "Results of Numerical Modelling of Some Recent MHD Generator Channel Designs," Thirteenth Symposium on Engineering Aspects of MHD," Stanford, March 1973.

34. Air Force Aero Propulsion Laboratory Report TR-74-47, Part 1, *Experimental and Analytical Research on a Two Megawatt, High Performance MHD Generator*, by O. K. Sonju and J. Teno, p. 61-94, June 1974.

35. Rosa, R. J., private communication

36. Hurwitz, H., Kilb, R. W., and Sutton, G. W., "Influence of Tensor Conductivity on Current Distribution in a MHD Generator," *Journal of Applied Physics*, v. 32, p. 205-216, February 1961.

37. Mitchner, M. and Kruger, C. H., *Partially Ionized Gases*, Ch. 8, Wiley, 1973.

38. Schlichting, H., *Boundary Layer Theory*, 6th Ed., Ch. 12, McGraw-Hill, 1968.

39. Stanford University Institute for Plasma Research Report 291, *Turbulent Heat Transfer in a Circular Tube at High Bulk-to-Wall Temperature Ratio: An Experimental Study*, by L. H. Brim, May 1969.

40. Cramer, K. R. and Pai, S., *Magnetofluid Dynamics for Engineers and Applied Physicists*, p. 148, McGraw-Hill, 1973.

41. Kerrebrock, J. L., "Similar Solutions for Boundary Layers in Constant Temperature Magneto-Gasdynamic Channel Flow," *Journal of the Aerospace Sciences*, v. 27, February 1960.

42. Kessler, R., private communication

43. Reseck, K. G., *Performance Characteristics of a Combustion-Driven Magnetogasdynamic Power Generator*, Ph.D. Thesis, Stanford University, 1966.

44. Langhaar, H. L., *Dimensional Analysis and Theory of Models*, p. 29-38, Wiley, 1951.

45. Kline, S. J., *Similitude and Approximation Theory*, p. 101-118, McGraw-Hill, 1965.

46. Hinnov, E. and Hirschberg, J. G., "Electron-Ion Recombination in Dense Plasmas," *Physical Review*, v. 125, p. 795-801, February 1962.

47. Naval Postgraduate School Report 57Zi73021A, *Electrohydrodynamics (EHD) Research*, by O. Biblarz, p. 36-82, February 1973.

INITIAL DISTRIBUTION LIST

		No. Copies
1.	Defense Documentation Center Cameron Station Alexandria, Virginia 22314	2
2.	Library, Code 0212 Naval Postgraduate School Monterey, California 93940	2
3.	Department Chairman, Code 57 Department of Aeronautics Naval Postgraduate School Monterey, California 93940	2
4.	Assoc. Professor O. Biblarz, Code57Zi Department of Aeronautics Naval Postgraduate School Monterey, California 93940	2
5.	Professor A. E. Fuhs, Code 59Fu Department of Mechanical Engineering Naval Postgraduate School Monterey, California 93940	1
6.	Professor F. D. Faulkner, Code 53Fa Department of Mathematics Naval Postgraduate School Monterey, California 93940	1
7.	Assoc. Professor G. E. Schacher, Code 61Sq Department of Physics and Chemistry Naval Postgraduate School Monterey, California 93940	1
8.	Assoc. Professor R. E. Ball, Code 57Bp Department of Aeronautics Naval Postgraduate School Monterey, California 93940	1
9.	LT R. C. Dolson, USN Strike Aircraft Task Directorate Naval Air Test Center Patuxent River, Maryland 20670	1
10.	Dr. R. Kessler AVCO Everett Research Laboratory 2385 Revere Beach Parkway Everett, Massachussetts 02149	1
11.	Professor P. M. Chung College of Engineering University of Illinois at Chicago Circle Box 4348 Chicago, Illinois 60680	1

12.	Dr. B. Wolfson AFOSR/SREP 1400 Wilson Blvd Arlington, Virginia 22046	1
13.	John A. Satkowski Office of Naval Research, Power Program, Code 473 Washington, D.C. 20360	1

DUDLEY KNOX LIBRARY
NAVAL POSTGRADUATE
MONTEREY. CALIFORNIA

Thesis 163772
D6423
c.1

Dolson

A computer analysis for the determination of electrode voltage losses in magnetohydrodynamic-generator plasmas.

thesD6423
A computer analysis for the determinatio
3 2768 001 89463 7
DUDLEY KNOX LIBRARY